

UNIVERSITY OF STRATHCLYDE

DOCTORAL THESIS

---

# On the Physics of Diffraction Information in the Scanning Electron Microscope

---

*Author:*

Elena PASCAL

*Supervisor:*

Dr. Ben HOURAHINE

Dr. Carol TRAGER-COWAN

*A thesis submitted in fulfilment of the requirements  
for the degree of Doctor of Philosophy*

*in the*

Semiconductor Spectroscopy and Devices Group  
Department of Physics

August 3, 2018

## Declaration of Authorship

I, Elena PASCAL, declare that this thesis titled, "On the Physics of Diffraction Information in the Scanning Electron Microscope" and the work presented in it are my own. I confirm that:

- This work was done wholly or mainly while in candidature for a research degree at this University.
- Where any part of this thesis has previously been submitted for a degree or any other qualification at this University or any other institution, this has been clearly stated.
- Where I have consulted the published work of others, this is always clearly attributed.
- Where I have quoted from the work of others, the source is always given. With the exception of such quotations, this thesis is entirely my own work.
- I have acknowledged all main sources of help.
- Where the thesis is based on work done by myself jointly with others, I have made clear exactly what was done by others and what I have contributed myself.

Signed:

---

Date:

---



*"The way the creative process works is that you first say something, and later, sometimes years later, you understand what you said."*

Daniel Kahneman



UNIVERSITY OF STRATHCLYDE

*Abstract*

Science  
Department of Physics

Doctor of Philosophy

**On the Physics of Diffraction Information in the Scanning Electron Microscope**

by Elena PASCAL

The Thesis Abstract is written here (and usually kept to just this page). The page is kept centered vertically so can expand into the blank space above the title too...



# Contents

|   |            |
|---|------------|
| <b>Declaration of Authorship</b>                                      | <b>iii</b> |
| <b>Abstract</b>   | <b>vii</b> |
| <b>1 Introduction</b>   | <b>1</b>   |
| 1.1 Science as an incremental process . . . . .                       | 1          |
| 1.2 Motivation . . . . .  | 2          |
| 1.3 Implementations . . . . .   | 2          |
| 1.4 Thesis structure . . . . .  | 3          |
| <b>2 Background and Basics</b>  | <b>5</b>   |
| 2.1 Primer . . . . .  | 5          |
| 2.1.1 Crystal structure . . . . .                                     | 5          |
| 2.1.2 Debye-Waller correction factor . . . . .                        | 6          |
| 2.1.3 $hP$ Bravais lattice and the hexagonal crystal system . . . . . | 8          |
| 2.1.4 Lattice planes and directions in the hexagonal system . . . . . | 11         |
| Miller indices . . . . .  | 11         |
| Miller-Bravais indices . . . . .                                      | 12         |
| 2.1.5 The reciprocal space . . . . .                                  | 14         |
| The reciprocal hexagonal lattice . . . . .                            | 16         |
| 2.1.6 Wavefunction as physical observable . . . . .                   | 17         |
| 2.1.7 Plane waves . . . . .   | 18         |
| 2.1.8 Fourier analysis . . . . .                                      | 20         |
| 2.2 Crystallographic computations in the hexagonal system . . . . .   | 22         |
| 2.2.1 The direct metric tensor . . . . .                              | 22         |
| 2.2.2 The reciprocal metric tensor . . . . .                          | 24         |
| 2.2.3 The interplanar spacing . . . . .                               | 25         |
| 2.2.4 To the reciprocal space and back . . . . .                      | 26         |
| 2.2.5 Rotations in Cartesian frame . . . . .                          | 27         |
| 2.2.6 Crystal to Cartesian frame and the structure matrix . . . . .   | 30         |

|   |   |           |
|---|---|-----------|
| 2.2.7   | Metric tensor implementations . . . . .       | 32        |
| 2.3   | Symmetry in crystallography . . . . .         | 33        |
| 2.3.1   | Symmetry operations . . . . .                 | 34        |
| Operation of first kind: pure rotation . . . . .                                      | 34  |           |
| Operation of first kind: pure translation . . . . .                                   | 37  |           |
| Operation of second kind: pure reflection . . . . .                                   | 39  |           |
| Combination of rotation and translation . . . . .                                     | 39  |           |
| 2.3.2   | Point groups . . . . .                        | 42        |
| 6mm point group from generators . . . . .   | 43  |           |
| 2.3.3   | Space groups . . . . .                        | 46        |
| The International Tables for Crystallography, Volume A . . . . .                      | 46  |           |
| The P6 <sub>3</sub> mc space group . . . . .  | 50  |           |
| 2.4   | Wurtzite crystal structure . . . . .          | 52        |
| 2.5   | Electron scattering . . . . .                 | 53        |
| 2.5.1   | Elastic scattering . . . . .                  | 53        |
| 2.5.2   | Inelastic scattering . . . . .                | 53        |
| 2.5.3   | The rest of the story . . . . .               | 53        |
| 2.6   | The scanning electron microscope . . . . .    | 54        |
| <b>3</b>  | <b>Diffraction</b> . . . . .                  | <b>55</b> |
| 3.1   | A word on <i>channelling</i> . . . . .        | 55        |
| 3.2   | Introduction . . . . .                        | 57        |
| 3.3   | Short historical overview . . . . .           | 58        |
| 3.4   | Kinematical versus dynamical theory . . . . . | 62        |
| 3.5   | Applications and limitations . . . . .        | 63        |
| 3.6   | Diffraction geometry . . . . .                | 63        |
| 3.6.1   | Bragg's law in real space . . . . .           | 63        |
| 3.6.2   | Bragg's law in reciprocal space . . . . .     | 65        |
| 3.7   | Diffraction intensity . . . . .               | 65        |
| 3.7.1   | Electrostatic lattice potential . . . . .     | 65        |
| X-ray scattering by electron charge density and the X-ray scattering factor . . . . . | 65  |           |
| Electron scattering by individual atom and the electron scattering factor . . . . .   | 68  |           |
| Scattering by the unit cell and the structure factor . . . . .                        | 69  |           |
| Scattering by an infinite crystal . . . . .   | 69  |           |
| 3.7.2   | The structure factor . . . . .                | 71        |

|  |           |
|--|-----------|
| Numerical computation of the Fourier coefficients of the lattice potential . . . . . | 71        |
| Symmetry . . . . .   | 71        |
| systematic absences . . . . .  | 71        |
| 3.8 General derivation of the Darwin-Howie-Whelan equations . . . . .                | 71        |
| 3.9 The two beam case: DHW formalism . . . . .                                       | 74        |
| 3.10 Electron channelling modelling . . . . .  | 74        |
| <b>Bibliography</b>  | <b>79</b> |



# List of Figures

|      |  |    |
|------|--|----|
| 2.1  | A periodic structure (c) showing copies of a 2D motif (a) at every lattice point on a 2D lattice. The translation vector $t_{uv}$ moves the lattice to a position indistinguishable from the original one. . . . .   | 6  |
| 2.2  | Hexagonal 2D lattice with basis vectors $\{\mathbf{a}_1, \mathbf{a}_2, \mathbf{c}\}$ . The lattice parameters can be chosen to be $\{a, a, 2\pi/3\}$ or $\{a, a, \pi/3\}$ . . . . .  | 9  |
| 2.3  | 3D hexagonal crystal system with lattice parameters $\{a, a, c, 90^\circ, 90^\circ, 120^\circ\}$ (a) and the 3D hexagonal primitive lattice (b). . . . .   | 10 |
| 2.4  | Hexagonal prism unit cell and the Miller-Bravais basis vectors $\{\mathbf{A}_1, \mathbf{A}_2, \mathbf{A}_3, \mathbf{C}\}$ . . . . .  | 12 |
| 2.5  | Directions belonging to the $\langle 2\bar{1}\bar{1}0 \rangle$ family. The yellow line shows the formation of the vector $\mathbf{t}_{[11\bar{2}0]}$ . . . . .   | 12 |
| 2.6  | Common planes in hexagonal crystal structures. . . . .   | 14 |
| 2.7  | Reciprocal 2D hexagonal lattice with basis vectors $\{\mathbf{a}_1^*, \mathbf{a}_2^*\}$ and lattice parameters $\{a^*, a^*, 60^\circ\}$ (a) and the 3D reciprocal hexagonal crystal system with lattice parameters $\{a^*, a^*, c^*, 60^\circ, 90^\circ, 90^\circ\}$ over-imposed on the real space one while keeping the same origin (b). . . . . | 16 |
| 2.8  | Relationship between real and reciprocal space hexagonal system basis sets. . . . .  | 17 |
| 2.9  | Schematic drawing of plane waves and the vectors considered in this section. . . . .   | 19 |
| 2.10 | Rendered 3D graphical representations of a) three-fold and b) six-fold pure rotations. The circles in the bottom right of the images represent the stereographic projections of the operators. . . . .   | 35 |
| 2.11 | Three-fold rotation around the third axis of a hexagonal basis set. . . . .  | 37 |
| 2.12 | $m(x, -x, z)$ mirror plane operation in a hexagonal basis set. . . . .   | 39 |
| 2.13 | Rendered 3D graphical representations and (sequentially numbered) operations involved in the construction of screw axis a) $2_1$ and b) $6_3$ . Standard 2D graphical projections are included at the bottom. . . . .  | 40 |
| 2.14 | $2_1$ screw axis operation in a hexagonal basis set. . . . .   | 41 |

|  |    |
|--|----|
| 2.15 Graphical 3D representation of <b>6mm</b> point group together with its stereographic projection in the bottom corner right. . . . .  | 44 |
| 2.16 Pages 584-585 (compressed here) of <i>International Tables for Crystallography, Volume A</i> [Hah96] describing the space group <b>P6<sub>3</sub>mc</b> . . . . .   | 48 |
| 2.17 Graphical 3D representation of the <b>6<sub>3</sub>mc</b> symmetry combination together with the 2D projection in the bottom right corner (filled circles indicate the object is in the plane of the drawing, open circles indicate the object is above the plane at the indicated height). . . . .   | 50 |
| 2.18 Top view construction of space group <b>P6<sub>3</sub>mc</b> from the Bravais lattice <i>hP</i> combined with the symmetry combination <b>6<sub>3</sub>mc</b> . [Right image taken taken from Fig. 2.16.] . . . . .   | 51 |
| 2.19 3D render of wurtzite crystal structure hexagonal unit cell, together with the hexagonal primitive cell ( <i>hP</i> ) enclosed by blue edges and the tetrahedral asymmetric unit cell enclosed by glass faces. . . . .  | 52 |
| <br>3.1 a) Open “channels” between rows of atoms along the main direction [001] in GaN – <i>not</i> responsible for what is sometimes called electron “channelling”. b) Artist’s impression of channelling of heavy charged particles, from [Bra68] . . . . .  | 56 |
| 3.2 Geometrical representation of Bragg’s equation in real space. The path difference of the reflected plane wave (2) with respect to (1) is shown in orange. . . . .  | 63 |
| 3.3 Schematic diagram of a) forward scattering and b) scattering by an angle $\theta$ . Note the pathway difference marked by thick blue line in b). . . . .   | 66 |
| 3.4 Atomic X-ray scattering factors for In, Ga, Al, N with superimposed coloured lines indicating the most common planes for InN, GaN and AlN. Each coloured line reaches to the group III element which makes up the compound for which the computation was carried out. For instance, the first vertical line (orange), reaching the In line, represent the <i>s</i> value for the c-plane in InN. . . . . | 67 |
| 3.5 Atomic electron scattering factors for In, Ga, Al, N with superimposed coloured lines indicating the most common planes for InN, GaN and AlN (see Fig. 2.6). The scattering factor units are $\text{V}\text{\AA}^3$ . . . . .  | 70 |
| 3.6 Diagram of incident and diffracted wave vector geometry. . . . .   | 73 |
| 3.7 Dynamical profile of thickness fringes as seen in transmission mode with absorption ignored from a wedge crystal. Profile is calculated in bright field condition[Hir+65]. . . . .   | 75 |

# List of Tables

|      |   |    |
|------|---|----|
| 2.1  | Debye-Waller fitting parameters for cubic elemental crystal from [GP99] and the calculated DW values at 300K. . . . .   | 7  |
| 2.2  | Static correction functions for N in wurtzite materials from DFT LDA calculations [Sch+09] at 300K and the predicted DW factor. . . . .                       | 8  |
| 2.3  | Some common directions in hexagonal system given in Miller and Miller-Bravais notation. . . . .   | 13 |
| 2.4  | Common planes in hexagonal system given in Miller and Miller-Bravais notation. . . . .  | 14 |
| 2.5  | Calculated interplanar distances in wurtzite nitrides. . . . .  | 26 |
| 2.7  | Examples of pure rotation symbols. . . . .  | 35 |
| 2.8  | Example of pure reflection symbols. . . . .   | 39 |
| 2.9  | Examples of screw axis symbols. . . . .   | 41 |
| 2.10 | Primary, secondary and tertiary symmetry directions (Miller-Bravais) of the point group notation for the hexagonal crystal. . . . .                           | 43 |
| 2.11 | The <b>P6<sub>3</sub>mc</b> space group with its corresponding number and crystallographic point group. . . . .   | 51 |
| 3.1  | Particles used in diffraction experiments together with their scattering properties. . . . .  | 57 |
| 3.2  | Partial chronology of the history of diffraction. . . . .   | 60 |
| 3.3  | Kinematical vs. dynamical diffraction theories. . . . .   | 62 |
| 3.4  | Bragg angles for the most common planes in wurtzite materials for 20 keV incident electrons. . . . .  | 64 |
| 3.5  | Doyle & Turner atomic scattering parameters [DT68] for a few elements. These values were calculated assuming that s is expressed in Å <sup>-1</sup> . . . . . | 68 |



# List of Abbreviations

|               |   |
|---------------|---|
| <b>EBSB</b>   | Electron Backscattered Diffraction              |
| <b>EBSP</b>   | Electron Channelling Pattern                    |
| <b>ECCI</b>   | Electron Backscattering Pattern                 |
| <b>ECP</b>    | Electron Channelling Contrast Imaging           |
| <b>SEM</b>    | Scanning Electron Microscopy                    |
| <b>TEM</b>    | Transmission Electron Microscopy                |
| <b>TKD</b>    | Transmission Kikuchi Diffraction                |
| <b>t-EBSB</b> | transmission Electron Backscattered Diffraction |



# Physical Constants

|                        |   |
|------------------------|---|
| Bohr radius            | $a_0 = 5.291\,772\,10 \text{ \AA}$  |
| Electron rest mass     | $m_e = 9.109\,383\,56 \times 10^{-31} \text{ kg}$                         |
| Elementary charge      | $e = 1.602\,176\,62 \times 10^{-19} \text{ C}$                            |
| Permittivity of vacuum | $\epsilon_0 = 8.854\,187\,82 \times 10^{-12} \text{ F m}^{-1}$            |
| Permeability of vacuum | $\mu_0 = 1.256\,637\,06 \times 10^{-6} \text{ V s A}^{-1} \text{ m}^{-1}$ |
| Plank constant         | $h = 6.626\,075 \times 10^{-34} \text{ Js}$                               |



# List of Symbols

| Symbol   | Name                                       | SI Units <sup>1</sup>       |
|--|--|-----------------------------|
| $\mathbf{a}, \mathbf{a}_i, \mathbf{b}, \mathbf{c}$         | Bravais lattice basis vectors              | nm                          |
| $\mathbf{a}^*, \mathbf{a}_i^*, \mathbf{b}^*, \mathbf{c}^*$ | Reciprocal basis vectors                   | nm <sup>-1</sup>            |
| $\mathbf{e}_i$   | Cartesian basis vectors                    | nm                          |
| $\mathbf{r}$   | General position vector                    | nm                          |
| $\mathbf{t}$   | Translation vector                         | nm                          |
| $\mathbf{g}$   | Reciprocal lattice vector                  | nm <sup>-1</sup>            |
| $\mathbf{g}_{hkl}$   | Reciprocal lattice translation vector      | nm <sup>-1</sup>            |
| $\mathbf{k}$   | Wave vector                                | nm <sup>-1</sup>            |
| $\{a, b, c, \alpha, \beta, \gamma\}$                       | Lattice parameters                         | {nm, nm, nm, rad, rad, rad} |
| $d_{hkl}$  | Interplanar spacing for planes ( $h k l$ ) | nm <sup>-1</sup>            |
| $F_{hkl}$  | Structure factor for reflection $h k l$    | ?                           |
| $f(s)$   | Atomic scattering factor                   | V nm                        |
| $\delta_{ij}$  | Kronecker delta                            | -                           |
| $\theta_B$   | Bragg angle                                | rad                         |
| $\lambda$  | Wavelength                                 | nm                          |
| $\rho(\mathbf{r})$   | Charge density                             | ?                           |
| $\Omega$   | Cell volume in real space                  | nm <sup>3</sup>             |
| $(h k i l), (h k . l)$                                     | Miller-Bravais plane indices               |                             |
| $(h k l)$  | Miller indices of a plane                  |                             |
| $\{h k l\}$  | Family of planes                           |                             |
| $[u v t w]$  | Miller-Bravais direction indices           |                             |
| $[u v w]$  | Miller direction indices                   |                             |
| $\langle u v w \rangle$                                    | Family of directions                       |                             |
| $\exists$  | “There exists”                             |                             |
| $\forall$  | “For all”                                  |                             |
| $\therefore$   | “Therefore”                                |                             |

<sup>1</sup> For vectors the units are assigned to their magnitude.



# 1 Introduction

## 1.1 Science as an incremental process

The history of science is all too often taught as a chronological list of discoveries. There is undeniable value in this approach as it underlines the direction of association of ideas; how one big idea brings over the next and so on. On page 62, I too show the history of diffraction as a table of chronological events. These are big shift events, which changed radically and permanently the way future diffraction science was to be done. A good number of names in this table were awarded for their significant contribution with Nobel prizes. Nevertheless, the table is clearly a gross simplification of history, omitting, due to lack of space, the incremental refinement and maintenance work that supported and propelled the bigger ideas. It is quite common for important work of individual voices to be wiped away from science history as we associate a breakthrough to a single name or even to a small group of people. Seeing the bigger picture is, undeniably, worthwhile, but we must not mistake it to be the full picture.

The “unremarkable” work did by the rest of the community which was not awarded prestigious prizes is not less important for the advancement of science, quite the opposite. Science nor culture advance in big steps. In a recent study published in *Nature* [Miu+18] Miu *et al.* looked at the way pieces of software get improved by a community of developers in a simulation of cumulative culture evolution. One of the observations was that the vast majority of advances are of an incremental type and not, as one would naively expect, leaps in knowledge. Observing the strong positive breakthrough bias of scientific publishing one would find it hard to assume that enough credit is given to the “tweakers”.

Another interesting observation was that big changes in the paradigm are more likely to turn out unsuccessful than smaller tweaks. Remember the Nobel prize in medicine awarded for the “discovery” of brain lobotomies? Thankfully, neuroscience moved away from those scientific breakthroughs. Any sort of conversation about the development of science focused only on the leaps of knowledge must ultimately be misrepresenting the scientific process.

The philosopher Daniel C. Dennett in his latest book *From bacteria to Bach and back* [Den17] makes the case that evolution is not only a good protocol for developing the fittest biological organisms but can in fact be successfully applied to a variety of notions, perhaps, he argues, even consciousness and the human mind. For instance, he makes the compelling case that code development ought to follow this protocol, that indeed the power of good code stands in the number of iterations it went through and, perhaps, less in the individual contributions. Each iterative step had the chance to rectify errors or limitations in the code, weed out unnecessary/old lines and replace them with new code capable of new features. We do not expect a sole developer to maintain any significant size code, and we do not expect good code to appear overnight. Why do we then accept it so easily when it comes to scientific or technological breakthrough then?

Of course, we cannot wait around for functional code to “occur” as the results of tens of millions of years of iterations, and, after all, we expect developers to be somewhat wiser than the random processes occurring in nature. But I believe the core idea to be valuable.

I want my thesis work to make a up a positive tweak in the endeavor of making electron diffraction in the SEM a well-understood phenomena in the electron microscopy community. I aim for this work to aid to the understanding of why we can observe and how we can study dislocations in the SEM and I do not expect it to be the definite attempt. For these reasons I tried to make this document as accessible as possible for whoever wants to continue on this journey. I tried to explain in depth the building blocks I used and why I chose them, I provide access to whatever code I ran or wrote and I offer a small collection of extra materials. May your code and science be even a little bit better than mine!

## 1.2 Motivation

## 1.3 Implementations

I will refer throughout this document to supplementary pieces of code most Python and some Fortran95. I will try to describe in detail what they do, sometimes I will include pseudocode and other times I will just state the relevant equations. They can all be found on my, otherwise rather pristine, public GitHub repository [Pas15].

For the smaller scripts I use Jupyter notebooks written in Python. I will assume the reader has Python 2.7 or greater installed. The Anaconda Python distributions ships with Jupyter but if you have just Python installed then you can just use pip:

```
$ pip3 install jupyter
```

To start a Jupyter notebook kernel you just type:

```
$ jupyter notebook
```

And navigate to the desired file. Individual cells are compiled with Shift + Enter.

In some notebooks I use the Plotly for interactive plotting. While entertaining, this package requires an account on the plot.ly website.

## 1.4 Thesis structure



## 2 Background and Basics

I often made the mistake to start talking about diffraction assuming the audience knows exactly what I mean by it. I'd like to rectify that here and introduce the concept and physics of *diffraction* in the SEM. I wrote this chapter as an introduction to theory the first year PhD me would have liked to have read, assuming the wisdom of today.

We cannot even make a dent in diffraction without a working knowledge of crystallography, which is why I will take a good few pages to explore *crystal symmetry* and *point group* analysis. I will limit the examples to the wurtzite system to keep it relevant. I will then talk about the interaction of electrons with the crystal lattice that gives rise to elastic coherent scattering along certain directions and touch on *Bragg's law* and its geometrical form, the *Ewald sphere*. I will also talk about the interaction of the electrons with the unit cell, which affects the intensity of the diffracting beam along chosen direction through the parameter known as the *scattering factor*. There are always these two conditions to take into account when figuring out the diffraction intensity along a certain direction. And both of these parameters (scattering angle from lattice plane and scattering factor) can have values for which the diffraction beam intensity vanishes.

### 2.1 Primer

But first thing first. We need to define terms and notions that we've both seen before but maybe are not quite as within reach as they ought to be in order to comfortably embark on this journey.

#### 2.1.1 Crystal structure

At the atomic level most solids can be described as periodic and rigid arrangements of atoms. It is this periodicity that, as we will see, gives rise to diffraction phenomena which in turn allow us to observe and study very small features in solids. The *periodic arrangements of atoms or molecules* also constitutes the loose definition of a *crystal structure*.

The rigorous definition involves the mathematical construct of crystal *lattice* which characterises its translational symmetry. Figure 2.1 (b) shows an example of a lattice in 2D space (technically known as a *net*). Every point is identical to any other point. When the lattice is populated uniformly by the same fixed structure, or motif, we generate the periodic arrangement we mentioned previously. We show in Fig. 2.1 (a) a  $4 \times 4$  square motif which, when applied to every point in the 2D lattice, generates the tessellation or regular structure in Fig. 2.1 (c)<sup>1</sup>. If the motif is a unit cell made up of atoms or molecules then we can talk about making up a crystal structure.

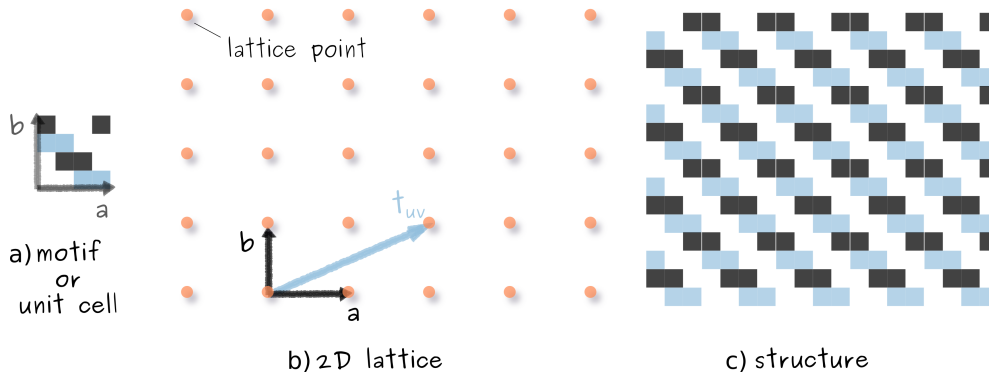


FIGURE 2.1: A periodic structure (c) showing copies of a 2D motif (a) at every lattice point on a 2D lattice. The translation vector  $t_{uv}$  moves the lattice to a position indistinguishable from the original one.

### 2.1.2 Debye-Waller correction factor

When we say that a crystal is rigid structure, we mean that over time the average positions of the atoms/molecules does not change. However, even at room temperature, the atoms exhibit thermal motion, small oscillations around their average “real values”. While this motion does not affect the crystal structure description (*i.e.*, we can ignore small thermal effects when describing the crystal structure), it must be taken into account when the the diffraction measurement is to be interpreted.

Due to these small vibrations, the electron cloud will cover a larger space than a frozen atom would, which will reduce the electron density, and, for our purpose, will reduce or dampen the electron-electron scattering process. An adequate approximation of accounting for atomic thermal vibration is the Debye-Waller (DW) factor  $B(T)$ . We will use this factor to correct the scattering value at a given temperature:

<sup>1</sup>If you want to give 2D tessellation design a play here is a fun website: [link in pdf](#).

$$f_T(s) = f_0(s)e^{-B(T)s^2}, \quad \text{with} \quad s = \frac{\sin \theta_B}{\lambda} \quad (2.1)$$

where the subscripts indicate the temperature at which the scattering factor is calculated. From dimensional analysis we can see that  $B$  is proportional to the mean square displacement of the atom in the direction normal to the Bragg plane. We can also read from this equation that the intensity of the diffracted beam is reduced by a factor  $e^{-B(T)s^2}$  with respect to the intensity of the same beam interacting with the sample at 0 K.

A good approximation, and the one we will use here, is to assume that for close-packed structures the atomic vibration amplitude is isotropic, such that we only require one DW parameters for each element in the crystal structure. This is not a generally valid assumption, however, first principles phonon density calculations for wurtzite-type III-V semiconductors by Schowalter *et al.* [Sch+09] showed that these materials have only small anisotropies of their Debye-Waller factors.

TABLE 2.1: Debye-Waller fitting parameters for cubic elemental crystal from [GP99] and the calculated DW values at 300K.

| Element | $a_0$ | $a_1$                 | $a_2$                 | $a_3$                  | $a_4$                  | ME(%) | $B(\text{\AA}^2)$ |
|---------|-------|-----------------------|-----------------------|------------------------|------------------------|-------|-------------------|
| Al      | 0.19  | $0.16 \times 10^{-2}$ | $0.25 \times 10^{-5}$ | $-0.26 \times 10^{-8}$ | $0.10 \times 10^{-11}$ | 1.31  | 0.83              |
| Ga      | 0.11  | $0.40 \times 10^{-3}$ | $0.66 \times 10^{-5}$ | $-0.18 \times 10^{-7}$ | $0.19 \times 10^{-10}$ | 0.05  | 0.49              |
| In      | 0.08  | $0.77 \times 10^{-2}$ | $0.48 \times 10^{-5}$ | $-0.12 \times 10^{-7}$ | $0.11 \times 10^{-11}$ | 0.08  | 0.43              |

Gao and Peng [GP99] used a fourth degree polynomial regression fit to determine temperature dependent DW for elemental cubic crystal from experimental data. These fit parameters are shown in Table 2.1 for the metal elements Al, Ga and In together with their estimated maximum error (ME) values. The form of the polynomial fit function is shown below:

$$B(T) = a_0 + a_1 T + a_2 T^2 + a_3 T^3 + a_4 T^4$$

We must note here, that the measured Debye-Waller factors for defected materials will be different from that of perfect crystals since defects also scatter electrons. For this reason and the fact that first principles calculations can only be trusted if they predict experimental values, it is always a good rule to use experimental values wherever possible. This being said, the literature on DW factors for Nitrogen is limited and we must turn to theoretical predictions. Schowalter *et al.* [Sch+09] calculated these values

for a number of wurtzite structures. We show below, in Table 2.2, the values predicted for the DW factor of N in AlN, GaN and InN<sup>2</sup>.

The Debye-Waller factor of an element ( $B(el.)$ ) is related to the static correlation function by:

$$B(el.) = \frac{8\pi^2}{3} (2 \langle u_{11}^2(el.) \rangle + \langle u_{33}^2(el.) \rangle),$$

where  $u_\alpha(el.)$  is the displacement of an atom of  $el.$  in the direction  $\alpha$ .

TABLE 2.2: Static correction functions for N in wurtzite materials from DFT LDA calculations [Sch+09] at 300K and the predicted DW factor.

| N in Material | $\langle u_{11}^2(N) \rangle (\text{\AA}^2)$ | $\langle u_{33}^2(N) \rangle (\text{\AA}^2)$ | $B(\text{\AA}^2)$ |
|---------------|--|--|-------------------|
| AlN           | 0.0036                                       | 0.0034                                       | 0.28              |
| GaN           | 0.0039                                       | 0.0037                                       | 0.29              |
| InN           | 0.0065                                       | 0.0062                                       | 0.51              |

The computations that generated the values in the tables in this section can be conveniently found in the Jupyter Notebook titled *Debye-Waller.ipynb*.

### 2.1.3 $hP$ Bravais lattice and the hexagonal crystal system

There are as many lattices as there are possible regular arrangements of lattice points and there are as many possible arrangements as variety of crystal forms observed in nature. In the example above we placed the motifs such that its four corners coincide with four lattice points. In this case the motif maps exactly to one lattice point. In 3D space, we would have had the option to map a 3D motif on one, two or three lattice points, defining lattices known as primitive ( $P$ ), either body-centred ( $I$ ) or base-centred ( $C$ ), and face-centred ( $F$ ), respectively. It is also easy to see that a motif with a very different shape will need a different arrangement of lattice points in order to cover the entire space neatly with no gaps or overlaps. We need, therefore, to unambiguously define both the lattice arrangement and the motif that define a crystal structure.

A specific arrangement of lattice points displays a unique translational symmetry which, in turn, can be characterised by a set of *basis vectors* usually denoted  $\mathbf{a}, \mathbf{b}, \mathbf{c}$  for a 3D lattice. Fig. 2.1 (b) shows the two basis vectors  $\mathbf{a}, \mathbf{b}$  of the 2D lattice we used. We can think of them as having their origin in one of the corners of the motif structure and

<sup>2</sup> We will see later, that since N scatters electrons significantly less than the heavier metallic elements in the system, its DW factors will not carry great importance. However, we did include the computations here for completeness.

running along its edges. Together with the angle between them, the basis vectors can be used to define both the shape of the motif and lattice it can tessellate. We commonly define a unique 3D lattice by its lattice parameters  $\{a, b, c, \alpha, \beta, \gamma\}$  where  $a, b, c$  are the lengths of the vectors  $\mathbf{a}, \mathbf{b}, \mathbf{c}$ ,  $\alpha$  is the angle between  $\mathbf{b}, \mathbf{c}$ ,  $\beta$  is the angle between  $\mathbf{a}, \mathbf{c}$  and  $\gamma$  is the angle between  $\mathbf{a}, \mathbf{b}$ .

The volume described by the lattice parameters is known as the *unit cell* of the lattice. While, for any given lattice, we can always find a *primitive* unit cell, whose volume contains only one lattice point, in practice it is preferred to work with high symmetry cell which reflects the point group symmetry of the crystal structure it describes. We will talk more about point and translation symmetry as applied to crystallographic symmetry in Chap. 2.3 on page 33.

We can now also identify the position of any point on the lattice with the help of the basis vectors. Let us introduce the *translation vector*, defined as the distance between any two points on the lattice. We can write it as  $\mathbf{t}_{uv} = u\mathbf{a} + v\mathbf{b}$  in 2D (shown in Fig. 2.1 (b)), and  $\mathbf{t}_{uvw} = u\mathbf{a} + v\mathbf{b} + w\mathbf{c}$  in 3D, where  $u, v, w$  are integers. Every point on an infinite lattice is equivalent to any other point, such that if one would be to move the structure by  $\mathbf{t}_{uv}$  while we weren't looking, we would not be able to tell anything had changed when we looked back. This means that all lattice points are identical and we can choose any of them as the origin. So that, the position of any lattice point is an integer linear combination of basis vectors independent on the chosen origin.

If the lattice parameters values are chosen with no restriction the resulting lattice has low symmetry. Conversely, let us select a 2D lattice with the two basis vectors equal in length,  $|\mathbf{a}_1| = |\mathbf{a}_2| = a^3$ , and the angle  $\gamma$  between them of  $120^\circ$ , as shown in Fig. 2.2. It is easy to notice that rotating this lattice by  $60^\circ$  around a lattice point picked as origin would produce the same lattice. Another way of saying this is that the lattice is invariant under a  $2\pi/6$  rotation and by definition *hexagonal*. Notably, we could have chosen  $\gamma$  to be  $60^\circ$  and we would have ended up with the exact same lattice.

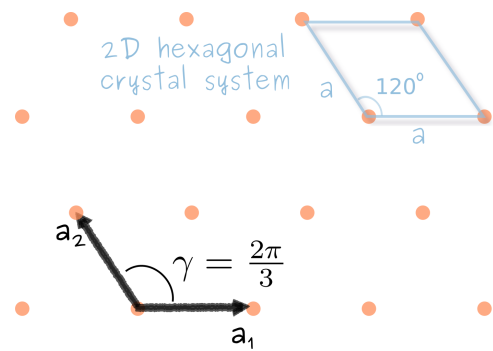


FIGURE 2.2: Hexagonal 2D lattice with basis vectors  $\{\mathbf{a}_1, \mathbf{a}_2, \mathbf{c}\}$ . The lattice parameters can be chosen to be  $\{a, a, 2\pi/3\}$  or  $\{a, a, \pi/3\}$ .

For every lattice with unique symmetry to be decorated with atoms, we talk about a specific *crystal system*. We've seen that the hexagonal 2D crystal system can be described in at least two ways. Similarly, we can construct a  $2\pi/6$  rotation invariant lattice in 3D by selecting the following special values for the lattice parameters:  $|\mathbf{a}| = |\mathbf{b}|$ ,  $\alpha = \beta = 90^\circ$  and  $\gamma = 120^\circ$  as shown in Fig. 2.3 (a). Here all we did was to add a  $\mathbf{c}$  axis normal to the 2D hexagonal lattice and set it as the rotation axis. This is easy to see when comparing the 2D and 3D hexagonal crystal system.

We defined our unit cell as having the edges at lattice points but we did not yet specified which lattice points. It is convenient to opt for a unit cell that is simple and describes the point symmetry of the underlying lattice. It is also useful to work with a small volume and, in practice, the smallest cell that reflects the full symmetry of the system is used. When the unit cell is small enough such that it only contain one full lattice point, *i.e.*, primitive cell, it is denoted by  $P$  as we did in the choice of hexagonal unit cell shown in Fig. 2.3 (b) where  $h$  stands for hexagonal. Otherwise, the choice of unit cell is somewhat arbitrary, so much so that the Wigner-Seitz cell, which is centred on a lattice point and defined as the region of space closer to that lattice point than any other one, does not have edges aligned with lattice points.

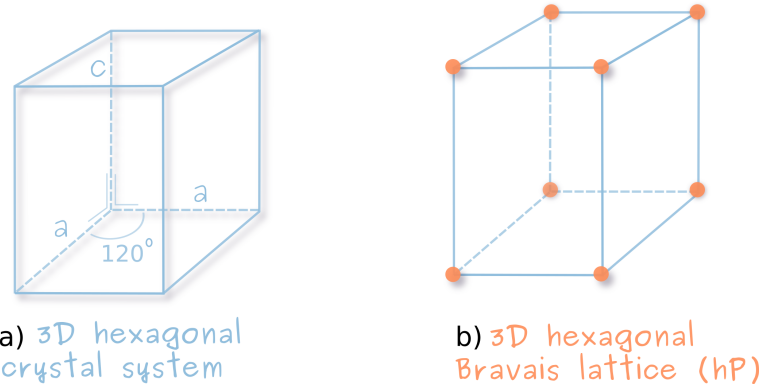


FIGURE 2.3: 3D hexagonal crystal system with lattice parameters  $\{a, a, c, 90^\circ, 90^\circ, 120^\circ\}$  (a) and the 3D hexagonal primitive lattice (b).

The same crystal system can be populated with lattice points in different manners such that it ends up describing different lattices. However, the number of choices of unique lattice points arrangements is limited to 5 for 2D lattices and 14 for 3D lattices. These unique lattice generators are known as *Bravais*. The cubic Bravais lattice ( $c$ ), for instance, comes in three flavours depending on the number of lattice points it contains:

<sup>3</sup> A note about notation consistency. The general basis vectors of a lattice are  $\{\mathbf{a}, \mathbf{b}, \mathbf{c}\}$ . Whenever two or more vectors have the same magnitude we use the same letter and employ indices to differentiate between them such that the hexagonal lattice basis vectors are  $\{\mathbf{a}_1, \mathbf{a}_2, \mathbf{c}\}$ .

one ( $cP$ ), two ( $cI$ ) or three ( $cF$ ). The hexagonal Bravais lattice ( $h$ ) comes only in one type: primitive ( $hP$ ), as shown in Fig. 2.3 (b).

With the notion of a hexagonal crystal system and its cell parameters well laid out, in the following section we will look at how we commonly label a certain plane or direction in this system.

#### 2.1.4 Lattice planes and directions in the hexagonal system

There are in fact two ways we can refer to a given plane or direction in a hexagonal crystal. The usual, or *Miller* notation which applies to all the crystal systems, or the hexagonal symmetry friendly *Miller-Bravais* indexing method. The first is defined by three indices while the latter by four. For planes indexing, going from the four index notation to the three index one means dropping the redundant third index. However, for directions notations things are slightly more involved.

##### Miller indices

Miller wrote and taught extensively about a way to label crystal planes in terms of their intercepts with the crystal reference axes. It was because of this and his choice of  $h, k, l$  letters that the indexing method now bears his name: *Miller indexing*. The method is beautiful in its simplicity: find the intercept with the three basis vectors, invert the intercepts, and last but not least reduce to smallest relative primes. One can also obtain all the equivalent planes belonging to the same family by even permutations of the indices  $h, k, l$ . For the hexagonal system the  $(hkl)$  indices correspond to the  $\{\mathbf{a}_1, \mathbf{a}_2, \mathbf{c}\}$  basis vectors.

For directions, usually labeled  $[uvw]$ , the process is simpler; find the coordinates in the crystal frame of the vector pointing in that direction and reduce them to smallest relative primes. It is this latter step which props us to raise an important observation. The Miller notation for direction does not carry vector length information and should not be used for finding length information. This might sound obvious, yet the temptation to understand direction  $[uvw]$  as vector  $\mathbf{t}_{uvw}$  is significant. The difference between the two becomes more apparent in the hexagonal system.

While the Miller indices notation is tremendously helpful when looking at families of planes in a cubic system, its powers become limited when tackling lower crystal symmetry. For instance in a system with lower than cubic symmetry, the family of planes for a given  $(hkl)$  plane is no longer made up of *all* possible permutations of the Miller indices  $h, k$  and  $l$ .

### Miller-Bravais indices

The hexagonal system indexing is a very different story. Usually treated as a special case in itself, the hexagonal system can keep the permutation equivalence property of Miller indexes as long as an extra, redundant basis vector is added. The new set of basis vectors,  $\{\mathbf{A}_1, \mathbf{A}_2, \mathbf{A}_3, \mathbf{C}\}$ , introduces 4-dimensional type vectors [Fra65] in what is called *Miller-Bravais indexing* [Nic66]. This notation replaces the rhombic prism primitive unit cell with a hexagonal one made up of three primitive hexagonal Bravais lattices ( $hP$ ), as seen in Fig. 2.4. We show here the three-vectors basis set together with the four-vector one.

Three of the Miller-Bravais basis vectors are the Miller basis vectors:  $\mathbf{A}_1 = \mathbf{a}_1$ ,  $\mathbf{A}_2 = \mathbf{a}_2$  and  $\mathbf{C} = \mathbf{c}$ . The extra basis vector is coplanar with the first two and, therefore, linearly dependent on them:

$$\mathbf{A}_3 = -(\mathbf{a}_1 + \mathbf{a}_2) = -(\mathbf{A}_1 + \mathbf{A}_2). \quad (2.2)$$

A vector  $\mathbf{p}$  in this system is defined as  $\mathbf{p} = p_1\mathbf{A}_1 + p_2\mathbf{A}_2 + p'_3\mathbf{A}_3 + p_3\mathbf{C}$ . When coordinates  $\{p_1, p_2, p_3, p'\}$  are integers,  $\mathbf{p}$  becomes the translation vector  $\mathbf{t}$  which shows a common direction in the crystal system. If we take this a step further and reduce the coordinates to relative primes then we obtain the reduced vector  $\mathbf{t}_{uvtw}$  where indices  $u, v, t, w$  form the Miller-Bravais notation.

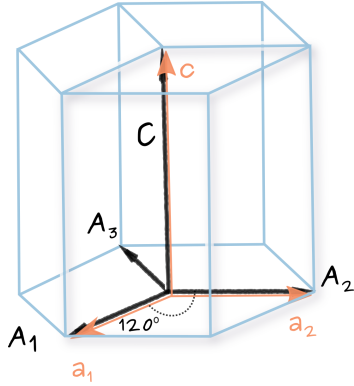


FIGURE 2.4:  
Hexagonal prism  
unit cell and the  
Miller-Bravais  
basis vectors  
 $\{\mathbf{A}_1, \mathbf{A}_2, \mathbf{A}_3, \mathbf{C}\}$ .

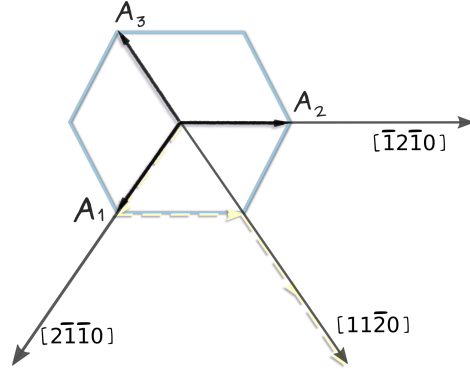


FIGURE 2.5: Directions belonging  
to the  $\langle 2\bar{1}\bar{1}0 \rangle$  family. The yellow  
line shows the formation of the  
vector  $\mathbf{t}_{[11\bar{2}0]}$ .

Directions in the four-index notations are of the form  $u\mathbf{A}_1 + v\mathbf{A}_2 + t\mathbf{A}_3 + w\mathbf{C}$  and

written as  $[u v t w]$ , where  $u, v, t, w \in \mathbb{Z}$  and are relative primes. Comparing this expression to the same direction written with the three Miller basis vectors,  $U\mathbf{a} + V\mathbf{b} + W\mathbf{c}$ , yields the following true relations:

$$U = 2u + v, \quad V = 2v + u, \quad W = w, \quad (2.3)$$

and also

$$t = -(u + v).$$

Because the first three basis vectors are not linearly independent, writing out their Miller-Bravais indices is somewhat awkward as seen in Fig. 2.5. The three coplanar vectors ensure that any given directions will have at least two non-zero components, and the  $\mathbf{A}_i$  basis vectors themselves have three non-zero components. While the Miller direction vectors corresponding to the basis vectors directions have the same lengths as the basis vectors themselves, this is not the case in the Miller-Bravais notation, see vector  $\mathbf{t}_{[11\bar{2}0]}$ . Nevertheless, we can find families of directions through the usual permutations which would not be possible using the Miller notation as we can see from Table 2.3.

TABLE 2.3: Some common directions in hexagonal system given in Miller and Miller-Bravais notation.

| Family                             | Miller-Bravais   | Miller   | Family                             | Miller-Bravais                         | Miller                               |
|------------------------------------|--|--|------------------------------------|--|--------------------------------------|
| $\langle 2\bar{1}\bar{1}0 \rangle$ | $[2\bar{1}\bar{1}0]$<br>$[1\bar{1}\bar{2}0]$<br>$[\bar{1}2\bar{1}0]$<br>$[\bar{2}110]$ | $[100]$<br>$[110]$<br>$[010]$<br>$[\bar{1}00]$ | $\langle 2\bar{1}\bar{1}0 \rangle$ | $[\bar{1}\bar{1}20]$<br>$[1\bar{2}10]$ | $[\bar{1}\bar{1}0]$<br>$[0\bar{1}0]$ |
|                                    |  |  | $\langle 0001 \rangle$             | $[0001]$                               | $[001]$                              |

A plane description in the new basis set will be of the form  $(h k i l)$  where  $i$  can be found from  $i = -(h + k)$  and, bearing no unique information, can be omitted from the notation:  $(h k l)$ . A family of planes is then given by the permutations of the first three Miller-Bravais indices including their negative values:

$$\{h k i l\} = \{(h k i l), (i h k l), (k i h l) (\bar{h} \bar{k} \bar{i} l), (\bar{i} \bar{h} \bar{k} l), (\bar{k} \bar{i} \bar{h} l)\}.$$

Table 2.4 shows a list of commonly used families of planes in a hexagonal system. A graphical representation of these planes is shown in Fig. 2.6. It is clear that the Miller indices are counterintuitive in this system and the Miller-Bravais notation is preferred. We also mention the polarity of each family of planes but we will postpone the explanation of polarity until the point group discussion on page 43.

TABLE 2.4: Common planes in hexagonal system given in Miller and Miller-Bravais notation.

| Family                        | Miller-Bravais | Miller | Family                         | Miller-Bravais | Miller |
|-------------------------------|----------------|--------|--------------------------------|----------------|--------|
| <i>m-plane</i><br>(non-polar) | (1̄100)        | (1̄10) | <i>a-plane</i><br>(non-polar)  | (1̄210)        | (1̄20) |
|                               | (01̄10)        | (010)  |                                | (21̄10)        | (21̄0) |
|                               | (1010)         | (100)  |                                |                |        |
|                               | (1̄100)        | (1̄10) |                                |                |        |
|                               | (01̄10)        | (010)  |                                |                |        |
|                               | (101̄0)        | (100)  |                                |                |        |
| <i>a-plane</i><br>(non-polar) | (11̄20)        | (110)  | <i>r-plane</i><br>(semi-polar) | (1102)         | (112)  |
|                               | (1210)         | (120)  |                                | (0112)         | (012)  |
|                               | (2110)         | (210)  |                                | (1012)         | (102)  |
|                               | (1120)         | (110)  |                                | (1̄102)        | (1̄12) |
|                               |                |        |                                | (01̄12)        | (012)  |
|                               |                |        |                                | (101̄2)        | (102)  |
|                               |                |        | <i>c-plane</i> (polar)         | (0001)         | (001)  |

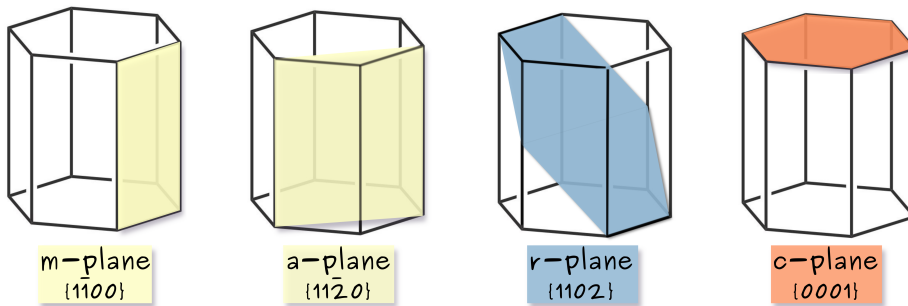


FIGURE 2.6: Common planes in hexagonal crystal structures.

We can also expand the *zone axis* definition, which tells us what planes,  $(h k l)$ , belongs to direction or zone,  $[u v w]$ , given in Miller indices as  $hu + kv + lw = 0$  to the Miller-Bravais notation:

$$hu + kv + it + lw = 0 \quad (2.4)$$

### 2.1.5 The reciprocal space

We have all the Bravais lattice basis set mathematical framework of dealing with vectorial quantities in a crystal frame and yet we had to introduce Miller and Miller-Bravais indices which don't really fit in this vector space. This leads us to why crystallographers like to employ a very different vector space to ease computations, namely the *reciprocal space*. So then, any vectorial quantities in a crystal (*i.e.*, position, direction, strain) can be defined in real space in terms of the basis vectors of its Bravais lattice,

$\{\mathbf{a}, \mathbf{b}, \mathbf{c}\}$ , or, conversely, in the reciprocal space in terms of a new set of basis vectors defined such that the components of a direction vector are the Miller indices,  $(h k l)$ , of the plane normal to that vector,  $\{\mathbf{a}^*, \mathbf{b}^*, \mathbf{c}^*\}$ . To be on the safe side we usually denote vectors defined in the reciprocal space with  $\mathbf{g}$  and the translation vector in reciprocal space by  $\mathbf{g}_{hkl}$ :

$$\mathbf{g}_{hkl} = h\mathbf{a}^* + k\mathbf{b}^* + l\mathbf{c}^*, \quad (2.5)$$

where it must be true that:  $\mathbf{a}^* = \frac{\mathbf{b} \times \mathbf{c}}{\Omega}$ ,  $\mathbf{b}^* = \frac{\mathbf{c} \times \mathbf{a}}{\Omega}$ ,  $\mathbf{c}^* = \frac{\mathbf{a} \times \mathbf{b}}{\Omega}$ .

with  $\Omega$  being the volume of the unit cell,  $\Omega = \mathbf{a} \cdot (\mathbf{b} \times \mathbf{c})$ .

A few observations can be made straight away at this point:

- From dimensional analysis we can tell that the length of a reciprocal space vector,  $|\mathbf{g}|$ , will be measured in units of  $\langle \text{length}^{-1} \rangle$ .
- The reciprocal lattice parameters are going to be  $\{a^*, b^*, c^*, \alpha, \beta, \gamma\}$  with the same angle definition as before.
- The dot product of a real space basis vector with its reciprocal space basis vector will yield zeros except for:  $\mathbf{a} \cdot \mathbf{a}^* = \mathbf{b} \cdot \mathbf{b}^* = \mathbf{c} \cdot \mathbf{c}^* = 1$  or:

$$\mathbf{a}_i \cdot \mathbf{a}_j^* = \delta_{ij} \quad (2.6)$$

A less intuitive observation on this different perspective of the crystal space leads to some upside-down-world-like properties. If we consider a distance vector with components known in relation to a real space basis set, and want to transform it to another real space basis with basis vectors smaller in magnitude, in order to keep the magnitude of the vector we must increase its components values. This property of some vector to counter-vary the change in basis with an inverse change in their components we call *contravariance*. If for the same vector which tells a distance in real space, we do the same exercise in reciprocal space, we find that that a decrease of the basis set gives smaller vector components. This vector behaviour is called *covariance*. The fact that the same vector can have opposite properties in these two different vector spaces tells us that the spaces themselves are reciprocal to each other.

You're welcome reader, you're now an almost crystallographer. The missing bit of information for being a full-fledged one is the Bragg diffraction condition which will be discussed on page 63. It is because the Bragg's diffraction condition depends on the lattice plane orientation with respect to the incident beam and the distance between

the set of planes under scrutiny, that having an easy way of find the normal to a plane ( $hkl$ ) in the reciprocal space vector  $\mathbf{g}_{hkl}$  becomes valuable in crystallography. Not least due to the vector  $\mathbf{g}_{hkl}$  property of having its length equal to the inverse of the distance between the set of planes  $\{hkl\}$ :

$$d_{hkl} = \frac{1}{|\mathbf{g}_{hkl}|}. \quad (2.7)$$

### The reciprocal hexagonal lattice

In the case of the hexagonal structure we find the reciprocal lattice vectors  $\{\mathbf{a}_1^*, \mathbf{a}_2^*, \mathbf{c}^*\}$  to be in terms of the real space hexagonal lattice basis set,  $\{\mathbf{a}_1, \mathbf{a}_2, \mathbf{c}\}$  to be:

$$\mathbf{a}_1^* = \frac{4}{3a^2} \mathbf{a}_1 + \frac{2}{3a^2} \mathbf{a}_2, \quad \mathbf{a}_2^* = \frac{2}{3a^2} \mathbf{a}_1 + \frac{4}{3a^2} \mathbf{a}_2, \quad \mathbf{c}^* = \frac{1}{c^2} \mathbf{c}. \quad (2.8)$$

Where the reciprocal hexagonal lattice translational vector is, from Eq. 2.5:

$${}^{hex} \mathbf{g}_{hkl} = h\mathbf{a}_1^* + k\mathbf{a}_2^* + l\mathbf{c}^*. \quad (2.9)$$

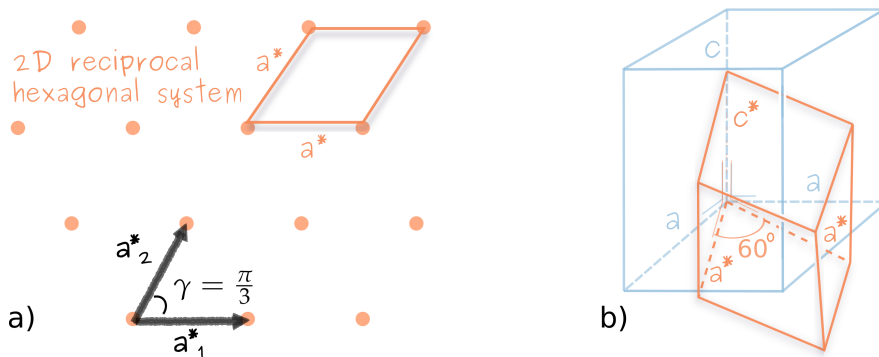


FIGURE 2.7: Reciprocal 2D hexagonal lattice with basis vectors  $\{\mathbf{a}_1^*, \mathbf{a}_2^*\}$  and lattice parameters  $\{a^*, a^*, 60^\circ\}$  (a) and the 3D reciprocal hexagonal crystal system with lattice parameters  $\{a^*, a^*, c^*, 60^\circ, 90^\circ, 90^\circ\}$  over-imposed on the real space one while keeping the same origin (b).

Another noteworthy property of the reciprocal space is that the reciprocal crystal lattice must also be one of the 14 Bravais lattices. We have already seen in the discussion of Fig. 2.2 that the hexagonal lattice can be mapped by two lattice parameters sets. It turns out that the reciprocal hexagonal lattice has the same symmetry as the real space hexagonal lattice mapped by the other set of lattice parameters. Fig. 2.7 (a) shows the reciprocal 2D lattice with parameters  $\{a^*, a^*, 60^\circ\}$  which is comparable to

Fig. 2.2. The 3D reciprocal hexagonal system is the same hexagonal prism as in the real space with the lattice parameters  $\{a^*, a^*, c^*, 60^\circ, 90^\circ, 90^\circ\}$  as can be seen in Fig. 2.7 (b).

The first two vectors in both the real and reciprocal hexagonal system basis sets,  $\{\mathbf{a}_1, \mathbf{a}_2\}$  and  $\{\mathbf{a}_1^*, \mathbf{a}_2^*\}$ , respectively, to not align with each other as Fig. 2.7 indicates and Fig. 2.8 emphasizes. This is the case for the 3-index notation. When the fourth index is added to form the reciprocal basis set  $\{\mathbf{A}_1^*, \mathbf{A}_2^*, \mathbf{A}_3^*, \mathbf{C}^*\}$  defining a lattice with parameters  $\{A^*, A^*, A^*, C^*, 120^\circ, 120^\circ, 120^\circ, 90^\circ, 90^\circ, 90^\circ\}$  things get even more confusing. While the Miller-Bravais real and reciprocal coplanar hexagonal basis vectors,  $\{\mathbf{A}_i\}$  and  $\{\mathbf{A}_i^*\}$ , are parallel to each other, the two reciprocal basis sets,  $\{\mathbf{a}_i^*\}$  and  $\{\mathbf{A}_i^*\}$ , are not. Figure 2.8 should make that somewhat more clear.

The four reciprocal basis vectors can be found in terms of the four real space basis vector to be:

$$\begin{aligned}\mathbf{A}_1^* &= \frac{2}{3a^2}\mathbf{a}_1, & \mathbf{A}_2^* &= \frac{2}{3a^2}\mathbf{a}_2 \\ \mathbf{A}_3^* &= \frac{2}{3a^2}\mathbf{a}_3, & \mathbf{C}^* &= \frac{1}{c^2}\mathbf{c}. \quad (2.10)\end{aligned}$$

Where the four index reciprocal space translation vector is:

$${}^{hex}\mathbf{g}_{hkl} = h\mathbf{A}_1^* + k\mathbf{A}_2^* + l\mathbf{A}_3^* + i\mathbf{C}^* = {}^{hex}\mathbf{g}_{hkl}.$$

The crystallographer must always be extra careful if using both notations. The two reciprocal basis vectors notations are not even describing exactly the same lattice. A closer inspection of Eq. 2.8 and Eq. 2.10, tells us that the four-index reciprocal lattice is three times more dense than the three-index reciprocal one. Nevertheless, all the discussion about Miller-Bravais index notation still hold, *i.e.*, Eq. 2.2 is still valid, and the reciprocal space properties, including Eq. 2.6, still apply.

We will go in more depth about crystallographic computations in a hexagonal system both in the real and reciprocal space in in Section 2.2 on page 22.

### 2.1.6 Wavefunction as physical observable

In the Copenhagen interpretation of quantum mechanics physical quantities are described via operators. The allowed values of the physical quantities are then eigenvalues of these operators. One must find the eigenfunctions of the corresponding

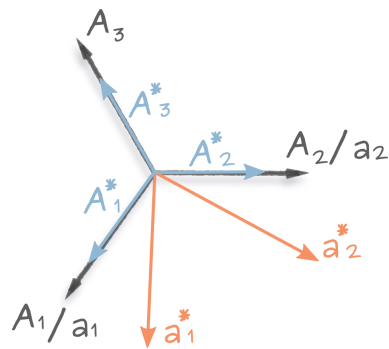


FIGURE 2.8: Relationship between real and reciprocal space hexagonal system basis sets.

operator in order to compute the value of a certain physical observable (*i.e.*, one must solve the equation  $\hat{f}|\Psi\rangle = f|\Psi\rangle$ ).

For a free particle the momentum operator is  $\hat{p} = i\hbar\nabla$  where  $\hbar$  is the reduced Planck's constant ( $\hbar = h/2\pi$ ). The eigenvalues  $\mathbf{p}$  and eigenfunctions  $|\Psi\rangle$  of the momentum operator are defined by the equation:

$$-i\hbar\nabla|\Psi\rangle = \mathbf{p}|\Psi\rangle.$$

Which has solutions of the form:

$$\Psi(\mathbf{r}) = Ce^{\frac{i}{\hbar}\mathbf{p}\cdot\mathbf{r}}$$

We can now use Louis de Broglie's relationship to relate momentum  $p$  of a particle to a wavelength  $\lambda$ :  $\lambda = h/p$ . If the wave number  $k$  is introduced,  $k = 1/\lambda$ , then we can write in vector form  $\mathbf{p} = \hbar\mathbf{k}$ .<sup>4</sup>

We can now rewrite the wave function of a particle as a linear superposition of momentum eigenfunctions:

$$\Psi(\mathbf{r}) = \sum_{\mathbf{k}} c_{\mathbf{k}} e^{2\pi i \mathbf{k}\cdot\mathbf{r}} \quad (2.11)$$

### 2.1.7 Plane waves

Let us explore further the equation above where  $\mathbf{k}$  is the wave vector denoting the direction of travel of the wave and  $\mathbf{r}$  is the position vector a point  $P$  (see Fig. 2.9). Applying dimensional analysis for the exponent, one can show that, if the position vector  $\mathbf{r}$  has components  $\{r_1, r_2, r_3\}$  with respect to the real space basis vectors  $\{\mathbf{a}, \mathbf{b}, \mathbf{c}\}$ :

$$\mathbf{r} = r_1\mathbf{a} + r_2\mathbf{b} + r_3\mathbf{c},$$

then the components of the wave vector  $\mathbf{k}$  must be given with respect to the reciprocal basis vectors and, therefore,  $\mathbf{k}$  must be a reciprocal space vector:

$$\mathbf{k} = k_1\mathbf{a}^* + k_2\mathbf{b}^* + k_3\mathbf{c}^*.$$

---

<sup>4</sup> It is a consequence of the de Broglie formula that the momentum space is equivalent to the reciprocal space, apart from a scaling factor  $\hbar$ .

We will use this opportunity to quickly introduce a useful shorthand notation that allows crystallographers to be economic with their symbols. For this we have to slightly adjust the basis vector notation<sup>5</sup>:

$$\mathbf{r} = r_1 \mathbf{a}_1 + r_2 \mathbf{a}_2 + r_3 \mathbf{a}_3 = \sum_{i=1}^3 r_i \mathbf{a}_i \equiv r_i \mathbf{a}_i$$

Since most of crystallography happens in 3D space we will always assume that the sum goes from  $i = 1$  to  $i = 3$  even when the limits are not written and the sum symbol,  $\sum$ , is dropped altogether. This is known as the *Einstein summation convention* and its rule is that summation is implied over every pair of subscripts which appears on the same side of the equation. Using the Einstein summation convention the dot product  $\mathbf{k} \cdot \mathbf{r}$  can be written as:

$$\mathbf{k} \cdot \mathbf{r} = (k_i \mathbf{a}_i^*) \cdot (r_i \mathbf{a}_i) = k_i r_i \delta_{ij} = k_i r_i,$$

where we made use of the definition of the reciprocal lattice:  $\mathbf{a}_i \cdot \mathbf{a}_j^* = \delta_{ij}$ .

If we now ask the question of where in the real space is the wave going to have constant phase we can easily spot the required condition to be:

$$\begin{aligned} \mathbf{k} \cdot \mathbf{r} &= k_1 r_1 + k_2 r_2 + k_3 r_3 = \text{const.}, \\ \forall \mathbf{r} &= r_1 \mathbf{a}_1 + r_2 \mathbf{a}_2 + r_3 \mathbf{a}_3 \end{aligned}$$

Which looks a lot like the equation of a plane:

$$\mathbf{k}(\mathbf{r} - \mathbf{r}_0) = 0$$

where  $\mathbf{r}_0$  is the position vector of the origin of the wave vector  $\mathbf{k}$  in the real space as shown in the figure to the right. The distance between consecutive planes of same phase values will be given by  $\lambda = 1/|\mathbf{k}|$ .

So then we can say that the totality of points with the same phase form an infinite

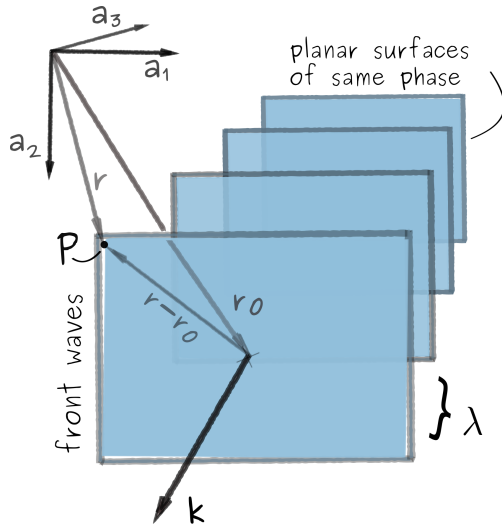


FIGURE 2.9: Schematic drawing of plane waves and the vectors considered in this section.

<sup>5</sup> Another note on basis vector notation. Unfortunately, the letter  $\mathbf{a}$  is overused in crystallography and can bear different meanings. Here we are using  $\mathbf{a}_i$  to denote one component from a generic basis set in which all vectors are labelled with the same symbol but different subscripts. Real space basis in this notation is  $\{\mathbf{a}_i, i \in (1, 2, 3)\}$  and reciprocal space basis vectors are  $\{\mathbf{a}_i^*, i \in (1, 2, 3)\}$ .

plane in the real space. Another way to say this is that the particle wave will exhibit in the real space planar surfaces of same phase, oriented normal to the travelling direction  $\hat{\mathbf{k}}$ . Hence the name of *plane waves* which we will use from now on to refer to expressions of the form:

$$e^{2\pi i \mathbf{k} \cdot \mathbf{r}} \quad (2.12)$$

### 2.1.8 Fourier analysis

We have introduced the notions of crystal lattice and talked about its translational invariance under a translation vector  $\mathbf{t} = u\mathbf{e}_1 + v\mathbf{e}_2 + w\mathbf{e}_3$  where  $u, v, w$  are constants. We have also introduced the reciprocal space and that of plane waves. What is left is to tie everything together through the introduction of Fourier transform which in turn will lead us to the mathematical formulation of diffraction.

Considering the wave function description of a particle as a superposition of momentum eigenfunctions describe by vector  $\mathbf{k}$ , we now want to ask the question: “*What is the relative contribution of a specific wave vector to the total function  $\Psi(\mathbf{r})$ ?*”. This is a very similar question to “*What is the contribution of the basis vector  $\mathbf{e}_1$  to a given vector  $\mathbf{t} = u\mathbf{e}_1 + v\mathbf{e}_2 + w\mathbf{e}_3$ ?*”. We know the answer to that to be  $u$ ; easily derived from the dot product  $\mathbf{t} \cdot \mathbf{e}_1$ . Similarly, we can use the dot product for continuous functions of the plane wave form  $\Phi = e^{2\pi i \mathbf{k} \cdot \mathbf{r}}$  and  $\Phi' = e^{2\pi i \mathbf{k}' \cdot \mathbf{r}}$ . In the bra-ket notation this is defined as:

$$\langle e^{2\pi i \mathbf{k} \cdot \mathbf{r}} | e^{2\pi i \mathbf{k}' \cdot \mathbf{r}} \rangle = \iiint e^{2\pi i (\mathbf{k}' - \mathbf{k}) \cdot \mathbf{r}} d\mathbf{r} = \delta(\mathbf{k}' - \mathbf{k})$$

where the integral is over all 3D space. The delta function form underlines the fact that  $\Phi$  and  $\Phi'$  are orthogonal functions whenever  $\mathbf{k}' \neq \mathbf{k}$  leading to the scalar product of plane wave functions to be zero.

Then, the contribution of a wave vector  $\mathbf{k}$  to the wave function  $\Psi(\mathbf{r})$  is the projection of the wave function on the momentum eigenfunction corresponding to  $\mathbf{k}$ . This also happens to be the definition of the *direct Fourier transform*:

$$\Psi(\mathbf{k}) = \langle e^{2\pi i \mathbf{k} \cdot \mathbf{r}} | \Psi(\mathbf{r}) \rangle = \iiint \Psi(\mathbf{r}) e^{-2\pi i \mathbf{k} \cdot \mathbf{r}} d\mathbf{r} \equiv \mathcal{F}[\Psi(\mathbf{r})] \quad (2.13)$$

The Fourier Transform  $\mathcal{F}$  allows us to transform a wave function from real space,

$\Psi(\mathbf{r})$ , to the momentum space,  $\Psi(\mathbf{k})$ , by using the equation above.<sup>6</sup> The reciprocal relationship is defined by the *inverse Fourier transform*:

$$\Psi(\mathbf{r}) = \mathcal{F}^{-1}[\Psi(\mathbf{k})] \equiv \iiint \Psi(\mathbf{k}) e^{2\pi i \mathbf{k} \cdot \mathbf{r}} d\mathbf{k} \quad (2.14)$$

While the general analytical form of eq. 2.13 does not look overly complicated, it does involve, somewhat inconveniently, a triple integral over the entire space. In the special case when the function to study is periodic, we can simplify this expression and reduce it to a discrete sum, or what is known as a *Fourier series*. Any physical property of the crystal, such as charge density, carries the property of translational invariance under  $\mathbf{t}$ , which means the function for the entire crystal is periodic and can be written as an expansion of complex functions weighted by their Fourier coefficients. For instance, the direct space crystal potential can be written as the discrete inverse Fourier transform version of Eq. 2.14 :

$$V(\mathbf{r}) = \sum_{\mathbf{k}} V_{\mathbf{k}} e^{2\pi i \mathbf{k} \cdot \mathbf{r}}, \quad (2.15)$$

and we will show that the Fourier coefficient  $V_{\mathbf{k}}$  are related to the diffracted wave amplitudes.

---

<sup>6</sup> Note on the sign convention chosen: the sign of Fourier function in eq. 2.13 is due to the order chosen in the bra-ket and it is opposite from the crystallographic sign convention. Also note on the wave vector definition convention used here lacking the factor of  $2\pi$  ( $|\mathbf{k}| = 1/\lambda$ ) which shows up sometimes in solid state physics. Consistent with this choice, the Fourier transform definition used here is missing the  $1/2\pi$  pre-factor and reader should pay attention to the convention used when comparing with the form of these formulas with literature.

## 2.2 Crystallographic computations in the hexagonal system

In the previous chapter we covered the hexagonal crystal system (page 8) together with its basis vectors in both real (page 11) and reciprocal space (page 14). We should be ready now to tackle vectorial computations in these reference frames except for one difficulty. None of the seven crystal systems has Cartesian basis vectors and the hexagonal system is certainly not the exception. Even the cubic system is defined by non-unitary vectors. Therefore none of the usual vector identities applies.

In the following we will use the direct metric tensor to generalize the dot product for a given (non-Cartesian) crystal system both in the real and reciprocal space. We will then cover the equations for distances and angles between directions in a hexagonal system. For a good number of derivations shown here I follow the microscopy friendly textbooks [DG03] and [DGM12].

On page 26 we discuss the real to reciprocal space and vice versa transformations. These are useful manipulations when it comes to combining information defined in the reciprocal space, like the diffraction condition, with information defined in the real space, like position vector in the sample. This applies, indeed, to computations of highly position-dependent diffraction information, like in the case of a polycrystalline material or defected crystal.

The alternative to using the metric tensor is to transform the parameters of interest from the crystal frame to Cartesian frame and, the computations in the usual manner and then translate the result back into the crystal frame if needed. We will use this latter approach for rotation operations which we define in the Cartesian frame on page 27. There is another reason, besides reduction in abstraction, for wanting to move computations in a Cartesian frame or at least orthonormal frame. Regardless of the sample information we are interested in computing, the sample frame, the SEM frame and the detector frame are all at least orthonormal.

### 2.2.1 The direct metric tensor

Let us start by considering a vector  $\mathbf{p}$  defined in a crystal frame with basis vectors  $\{\mathbf{a}_1, \mathbf{a}_2, \mathbf{a}_3\}$  by coordinates  $\{p_1, p_2, p_3\}$ :

$$\mathbf{p} = p_1 \mathbf{a}_1 + p_2 \mathbf{a}_2 + p_3 \mathbf{a}_3$$

Back to the vector  $\mathbf{p}$  this time defined in a crystal system with basis vectors  $\{\mathbf{a}_i, i \in \{1, 2, 3\}\}$  and angles  $\{\alpha, \beta, \gamma\}$  (the list of six lattice parameters). If we are interested in finding its length we know we can use the dot product definition:

$$\mathbf{p} \cdot \mathbf{p} = |\mathbf{p}|^2 \cos(\theta = 0)$$

$$\therefore |\mathbf{p}| = \sqrt{\mathbf{p} \cdot \mathbf{p}} = \sqrt{p_i \mathbf{a}_i \cdot p_j \mathbf{a}_j} = \sqrt{p_i p_j \mathbf{a}_i \cdot \mathbf{a}_j}$$

If we were in a Cartesian frame  $\{\mathbf{e}_1, \mathbf{e}_2, \mathbf{e}_3\}$  we would have known that the result of the last dot product is non-zero only when  $i \neq j$ , i.e.,  $\mathbf{a}_i \cdot \mathbf{a}_j = \mathbf{e}_i \cdot \mathbf{e}_j = \delta_{ij}$ , and therefore  $\mathbf{p} = \sqrt{p_1^2 + p_2^2 + p_3^2}$ . But we are not and we don't (I didn't). Which is why we need to introduce a general result for the dot product between two vectors.

$$\mathbf{a}_i \cdot \mathbf{a}_j = |\mathbf{a}_i| |\mathbf{a}_j| \cos \theta_{ij} \equiv g_{ij},$$

where  $\theta_{ij}$  is the usual angle between basis vectors  $\mathbf{a}_i$  and  $\mathbf{a}_j$  and we introduced component  $ij$  of the the *direct metric tensor*  $g$ . The full  $3 \times 3$  matrix form of the metric tensor can be written in terms of the six lattice parameters of a triclinic system as follows:

$$g = \begin{bmatrix} \mathbf{a}_1 \cdot \mathbf{a}_1 & \mathbf{a}_1 \cdot \mathbf{a}_2 & \mathbf{a}_1 \cdot \mathbf{a}_3 \\ \mathbf{a}_2 \cdot \mathbf{a}_1 & \mathbf{a}_2 \cdot \mathbf{a}_2 & \mathbf{a}_2 \cdot \mathbf{a}_3 \\ \mathbf{a}_3 \cdot \mathbf{a}_1 & \mathbf{a}_3 \cdot \mathbf{a}_2 & \mathbf{a}_3 \cdot \mathbf{a}_3 \end{bmatrix} = \begin{bmatrix} a_1^2 & a_1 a_2 \cos \gamma & a_1 a_3 \cos \beta \\ a_2 a_1 \cos \gamma & a_2^2 & a_2 a_3 \cos \alpha \\ a_3 a_1 \cos \beta & a_3 a_2 \cos \alpha & a_3^2 \end{bmatrix}. \quad (2.16)$$

For a system with higher symmetry, like the hexagonal Bravais lattice,  $hP$ , with lattice parameters  $\{a, a, c, 120^\circ, 90^\circ, 90^\circ\}$ , the form above reduces to:

$${}^{hex}g = \begin{bmatrix} a^2 & -a^2/2 & 0 \\ -a^2/2 & a^2 & 0 \\ 0 & 0 & c^2 \end{bmatrix}. \quad (2.17)$$

We are finally ready to calculate the magnitude of a vector,  $\mathbf{p}$ , defined in a hexagonal crystal system,  $\mathbf{p} = p_1 \mathbf{a}_1 + p_2 \mathbf{a}_2 + p_3 \mathbf{c}$ :

$$|\mathbf{p}| = \sqrt{p_i {}^{hex}g_{ij} p_j} = \sqrt{(a^2(p_1^2 - p_1 p_2 + p_2^2) + c^2 p_3^2)}, \quad (2.18)$$

the general dot product between two vectors,  $\mathbf{p}$  and  $\mathbf{q}$ , defined in the same hexagonal crystal system,  $\mathbf{q} = q_1 \mathbf{a}_1 + q_2 \mathbf{a}_2 + q_3 \mathbf{c}$ :

$$\mathbf{p} \cdot \mathbf{q} = p_i {}^{hex}g_{ij} q_j, \quad (2.19)$$

and the angle  $\theta$  between the same two vectors:

$$\cos \theta = \frac{p_i {}^{hex}g_{ij} q_j}{|\mathbf{p}| |\mathbf{q}|} = \frac{a^2 (p_1 q_1 + p_2 q_2 - \frac{1}{2}(p_1 q_2 + p_2 q_1)) + c^2 p_3 q_3}{|\mathbf{p}| |\mathbf{q}|}. \quad (2.20)$$

It is common to ask about angles between directions rather than specific vectors. In this case it is just a matter of replacing the components  $p_i, q_i$  with the reduced prime integers of the Miller indices of the given directions  $[u v w]$ .

*What about the Miller-Bravais indexing?* I hear you ask. Not to worry, we can apply an identical derivation for the four index notation hexagonal basis set  $\{\mathbf{A}_1, \mathbf{A}_2, \mathbf{A}_3, \mathbf{C}\}$ . We will denote the four-index metric tensor with  $\mathbf{G}$  and follow ref. [OT68] to write:

$$\text{hex } \mathbf{G} = \begin{bmatrix} \mathbf{A}_1 \cdot \mathbf{A}_1 & \mathbf{A}_1 \cdot \mathbf{A}_2 & \mathbf{A}_1 \cdot \mathbf{A}_3 & \mathbf{A}_1 \cdot \mathbf{C} \\ \mathbf{A}_2 \cdot \mathbf{A}_1 & \mathbf{A}_2 \cdot \mathbf{A}_2 & \mathbf{A}_2 \cdot \mathbf{A}_3 & \mathbf{A}_2 \cdot \mathbf{C} \\ \mathbf{A}_3 \cdot \mathbf{A}_1 & \mathbf{A}_3 \cdot \mathbf{A}_2 & \mathbf{A}_3 \cdot \mathbf{A}_3 & \mathbf{A}_3 \cdot \mathbf{C} \\ \mathbf{C} \cdot \mathbf{A}_1 & \mathbf{C} \cdot \mathbf{A}_2 & \mathbf{C} \cdot \mathbf{A}_3 & \mathbf{C} \cdot \mathbf{C} \end{bmatrix} = \frac{a^2}{2} \begin{bmatrix} 2 & -1 & -1 & 0 \\ -1 & 2 & -1 & 0 \\ -1 & -1 & 2 & 0 \\ 0 & 0 & 0 & 2c^2/a^2 \end{bmatrix} \quad (2.21)$$

The magnitude of the same vector  $\mathbf{p}$  this time with components  $\{P_1, P_2, P', P_3\}$  corresponding to the four-vector basis,  $\mathbf{p} = P_1 \mathbf{A}_1 + P_2 \mathbf{A}_2 + P' \mathbf{A}_3 + P_3 \mathbf{C}$  is:

$$|\mathbf{p}| = \sqrt{P_i \text{hex } \mathbf{G}_{ij} P_j} = \sqrt{(3a^2(P_1^2 + P_2^2 + P'^2) + c^2 P_3^2)}, \quad (2.22)$$

which is similar but not the same as Eq. 2.18, note the sign difference. For the same vector the coordinates in four-vector basis are going to be smaller than the coordinates in the three-vector basis, since there are more vectors to contribute. A word of advice for the reader, don't be tempted to apply the vector length derivation to the Miller and Miller-Bravais notation of directions, remember the discussion on page 11.

The angle between two vectors,  $\mathbf{p} = P_i \mathbf{A}_i$  and  $\mathbf{q} = Q_i \mathbf{A}_i$ , defined using the four-vector basis of a hexagonal lattice is then, similarly to Eq. 2.20:

$$\cos \theta = \frac{P_i \text{hex } \mathbf{G}_{ij} G_j}{|\mathbf{p}| |\mathbf{q}|} = \frac{a^2 (3(P_1 Q_1 + P_2 Q_2) + \frac{3}{2}(P_1 Q_2 + P_2 Q_1)) + C^2 P_3 Q_3}{|\mathbf{p}| |\mathbf{q}|}. \quad (2.23)$$

## 2.2.2 The reciprocal metric tensor

On page 16 we covered, to some extent, the reciprocal hexagonal lattice and its basis vectors in both the linearly independent form of  $\{\mathbf{a}_1^*, \mathbf{a}_2^*, \mathbf{c}^*\}$  and the linearly dependent  $\{\mathbf{A}_1^*, \mathbf{A}_2^*, \mathbf{A}_3^*, \mathbf{c}^*\}$ .

The *reciprocal metric tensor*, can be derived in much the same way as the real space one, by dot producting all the pairs of basis vectors:  $\mathbf{g}_{ij}^* = \mathbf{a}_i^* \cdot \mathbf{a}_j^*$ . It is also, quite conveniently, the inverse of the real space metric tensor:  $\mathbf{g}_{ij}^* = (\mathbf{g}_{ij})^{-1}$ , such that for the reciprocal hexagonal lattice with parameters  $\{a^*, a^*, c^*, 60^\circ, 90^\circ, 90^\circ\}$  can easily be written out to be:

$${}^{\text{hex}}\mathbf{g}^* = \begin{bmatrix} \mathbf{a}_1^* \cdot \mathbf{a}_1^* & \mathbf{a}_1^* \cdot \mathbf{a}_2^* & \mathbf{a}_1^* \cdot \mathbf{c}^* \\ \mathbf{a}_2^* \cdot \mathbf{a}_1^* & \mathbf{a}_2^* \cdot \mathbf{a}_2^* & \mathbf{a}_2^* \cdot \mathbf{c}^* \\ \mathbf{c}^* \cdot \mathbf{a}_1^* & \mathbf{c}^* \cdot \mathbf{a}_2^* & \mathbf{c}^* \cdot \mathbf{c}^* \end{bmatrix} = ({}^{\text{hex}}\mathbf{g})^{-1} = \frac{2}{3a^2} \begin{bmatrix} 2 & 1 & 0 \\ 1 & 2 & 0 \\ 0 & 0 & \frac{3a^2}{2c^2} \end{bmatrix}$$

We can write out, similarly to equation 2.18, the length of a generic reciprocal space vector  $\mathbf{g} = g_1\mathbf{a}_1^* + g_2\mathbf{a}_2^* + g_3\mathbf{c}^*$  (written conveniently for Einstein summation) from the dot product with itself:

$$|\mathbf{g}| = \sqrt{g_i g_{ij}^* g_j} \quad (2.24)$$

In terms of the four index notation, the reciprocal metric tensor  $\mathbf{G}^*$  is:

$${}^{\text{hex}}\mathbf{G}^* = \frac{2}{9a^2} \begin{bmatrix} 2 & -1 & -1 & 0 \\ -1 & 2 & -1 & 0 \\ -1 & -1 & 2 & 0 \\ 0 & 0 & 0 & \frac{9a^2}{2c^2} \end{bmatrix} \quad (2.25)$$

Which looks very similar to the real space four-index notation metric tensor  ${}^{\text{hex}}\mathbf{G}$  in Eq. 2.21 with inverse lattice parameters since the real and reciprocal four-basis vectors are parallel to each other.

### 2.2.3 The interplanar spacing

We now have all the tool to calculate the length of the translation vector in the hexagonal system reciprocal lattice,  $\mathbf{g}_{hkl} = h\mathbf{a}_1^* + k\mathbf{a}_2^* + l\mathbf{c}^*$  defined in Eq. 2.5. The identity in eq. 2.24 reduces to:

$$|\mathbf{g}_{hkl}| = \sqrt{\frac{4}{3a^2}(h^2 + k^2 + hk) + \frac{1}{c^2}l^2}$$

Such that we could, finally, derive the expression for distance between a set of planes  $\{hkl\}$  in a hexagonal system defined in Eq. 2.7:

$${}^{\text{hex}}d_{hkl} = \frac{1}{\sqrt{\frac{4}{3a^2}(h^2 + k^2 + hk) + \frac{1}{c^2}l^2}} \quad (2.26)$$

We can also find the distance between a set of hexagonal system planes  $\{hki\}$  given in Miller-Bravais notation:

$${}^{\text{hex}}d_{hki} = \frac{1}{\sqrt{\frac{4}{3a^2}(h^2 + k^2 + i^2 + hk + ki + ih) + \frac{1}{c^2}l^2}} \quad (2.27)$$

Table 2.5 shows a few examples of calculated interplanar distances for common families of planes in wurtzite nitride systems (see Fig. 2.6). Spot that the distance between consecutive *c*-planes is the lattice parameter *c* while the one between *a*-planes is half the lattice parameter *a*.

TABLE 2.5: Calculated interplanar distances in wurtzite nitrides.

| System ( $a[\text{\AA}]$ , $c[\text{\AA}]$ ) | Interplanar spacing for set of planes $\{h k l\}$ |                   |                         |                   |
|--|---|-------------------|-------------------------|-------------------|
|  | r-plane $\{112\}$                                 | a-plane $\{110\}$ | m-plane $\{1\bar{1}0\}$ | c-plane $\{001\}$ |
| AlN (3.11, 4.98)                             | 1.32  | 1.56              | 2.69                    | 4.98              |
| GaN (3.19, 5.19)                             | 1.36  | 1.60              | 2.76                    | 5.19              |
| InN (3.53, 5.70)                             | 1.50  | 1.77              | 3.06                    | 5.70              |

## 2.2.4 To the reciprocal space and back

While the equivalence between reciprocal vector absolute value and inverse of the distance between planes is clear, other transformations between the two vector spaces require a bit more work. Let us start with a vector  $\mathbf{p}$  with components  $\{p_i, i \in (1, 2, 3)\}$  in the real space,  $\mathbf{p} = p_i \mathbf{a}_i$ . This vector must exist independent of the reference frame, so let us give it components  $\{p_i^*, i \in (1, 2, 3)\}$  in the reciprocal space:  $\mathbf{p} = p_i^* \mathbf{a}_i^*$  such that:

$$\mathbf{p} = p_i \mathbf{a}_i = p_i^* \mathbf{a}_i^*. \quad (2.28)$$

If, in the latter equality, we dot product both sides by  $\mathbf{a}_j$  and use both the property of the reciprocal lattice, given in Eq. 2.6, and the definition of the direct metric tensor,  $g_{ij} = \mathbf{a}_i \cdot \mathbf{a}_j$  then we find that:

$$p_j^* = p_i g_{ij} \quad (2.29)$$

Which tells us how to find the components of the vector in the reciprocal space.

Alternatively, if we know the components of the vector in reciprocal space and want to define it in the real space, we dot product the right side of the last equality in Eq. 2.28 by  $\mathbf{a}_j^*$ , and use the definition of the reciprocal metric tensor this time,  $g_{ij}^* = \mathbf{a}_i^* \cdot \mathbf{a}_j^*$ , to find:

$$p_j = p_i^* g_{ij}^* \quad (2.30)$$

Similarly, if we are interested in finding the reciprocal basis vectors,  $\mathbf{a}_i^*$ , knowing the real space basis vectors  $\mathbf{a}_i$ , we replace  $p_i$  with the identity in Eq. 2.30 to find:

$$\mathbf{a}_i^* = \mathbf{g}_{ij}^* \mathbf{a}_j, \quad (2.31)$$

and, inversely,

$$\mathbf{a}_i = \mathbf{g}_{ij} \mathbf{a}_j^*. \quad (2.32)$$

Notice the difference in position of the metric tensor in equations 2.29 and 2.32. Another way to remember this is that the rows of the metric tensor are the components of the direct basis vector in terms of the reciprocal basis vectors, as explained by Marc in *Introduction to CTEM* pg. 17 [DG03], and the columns of the metric tensor contain the reciprocal components of a vector in terms of the real space components.

### 2.2.5 Rotations in Cartesian frame

It is common in crystallographic calculations to want to express a tensor parameter known in one reference in a different reference frame; assuming we can figure out the position of the new reference frame in the old reference frame. For instance, mapping the electron beam scan in the sample frame (a task made especially challenging by the high sample tilt used in electron diffraction techniques which the SEM is not very well designed to account for [Nol07]) involves moving electron scan positions between the beam frame and the sample frame. Assuming the scanning directions  $x$  and  $y$  are truly perpendicular, that the  $x$  scanning direction is indeed parallel to the tilt axis of the sample and that the magnification and spot size are not significantly affected by the tilt (*i.e.*, parallel beam at high magnification) then the relationship between the basis vectors of two frames is a simple rotation. A similar transformation must be done for translating the escaping electron beam positions from the sample frame to the detector frame [Bri+16].

Unfortunately, simply calling an action rotation suffers from many ambiguities. In crystallography, when we talk about rotation we refer to a very well defined transformation. In a right handed system<sup>7</sup> –first source of ambiguity–, a rotation of the coordinate system (CS) around a given axis is the clockwise rotation in the plane normal to that axis as the viewer looks in the direction pointed by the axis. Another way of describing the clockwise rotation is the right hand rule, *i.e.*, holding the thumb in the direction of the chosen axis of rotation, the rest of the fingers point in the direction of rotation.

---

<sup>7</sup>  $(x, y, z)$  follow the thumb, index and middle fingers of the right hand

Another possible ambiguity is whether we refer to a *active* or a *passive* rotation:

- A passive, or alias transformation, like the one above, acts on the coordinate system. It rotates the CS clockwise around a given axis while keeping the position of the object of interest fixed.
- An active, or alibi transformation acts on the object. More explicitly, the active rotation affects the position vector of the object whose coordinates are described in a fixed CS. The direction of rotation is opposite to the passive one and therefore anticlockwise.

It should be obvious that a passive rotation of an object by an angle  $\theta$  around a given axis is equivalent with a passive rotation of its coordinate frame by an angle  $-\theta$  around the same axis.

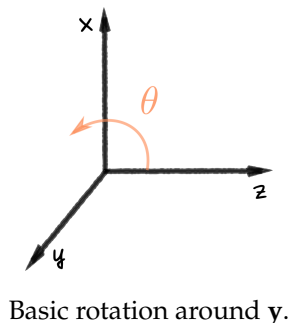
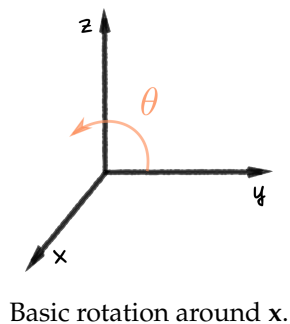
The mathematical form of these transformations in 3D can be written as a  $3 \times 3$  matrices,  $\mathcal{R}$ . In the case in which the axis of rotation is one of the basis vector we call the transformation a basic rotation. The three basic rotation matrices for a right handed Cartesian frame are given below.

The passive rotation of a Cartesian reference frame around the axis  $x$  in the clockwise direction is given in pre-multiplication matrix form as:

$$\mathcal{R}_x(\theta) = \begin{pmatrix} 1 & 0 & 0 \\ 0 & \cos \theta & -\sin \theta \\ 0 & \sin \theta & \cos \theta \end{pmatrix}$$

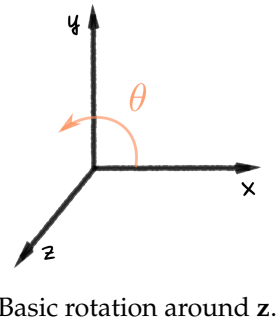
The passive rotation of a Cartesian reference frame around the axis  $y$  in the clockwise direction is given in pre-multiplication matrix form as:

$$\mathcal{R}_y(\theta) = \begin{pmatrix} \cos \theta & 0 & \sin \theta \\ 0 & 1 & 0 \\ -\sin \theta & 0 & \cos \theta \end{pmatrix}$$



The passive rotation of a Cartesian reference frame around the axis  $\mathbf{z}$  in the clockwise direction is given in pre-multiplication matrix form as:

$$\mathcal{R}_z(\theta) = \begin{pmatrix} \cos \theta & -\sin \theta & 0 \\ \sin \theta & \cos \theta & 0 \\ 0 & 0 & 1 \end{pmatrix}$$



Yet another source of ambiguity is the manner in which we apply the rotation matrix. Through this work we pre-multiply the rotation matrix with the position column vector:  $\mathbf{v}' = \mathcal{R}(\theta)\mathbf{v}$ . This leads us to the unambiguous definition of rotation we will use: *The anticlockwise rotation of a position vector in column form,  $\mathbf{v}$ , given in a right handed CS, around the rotation axis  $\mathbf{n}$  leads to a new position which can be calculated by pre-multiplying the rotation matrix  $\mathcal{R}_n$  by the position vector:  $\mathcal{R}_n\mathbf{v}$* . For any property in this definition changed the rotation direction flips. For instance, post-multiplying the rotation matrix with row vector leads to a clockwise rotation.

A useful property of the rotation matrix is that the inverse of a rotation can be calculated by simply transposing the matrix ( $\mathcal{R}\mathcal{R}^\top = \mathcal{I}$ ). Another property is that the product of rotation matrices is yet another rotation matrix. Even in the case in which the rotation axis is not just a basis vector, the rotation can be broken down in maximum tree basic rotations.

This latter scenario describes another rotation formalism known as *Euler rotation* in terms of Euler angles; the rotation is given as a set of tree angles which described tree successive rotations around a combination of the axes  $\{\mathbf{x}, \mathbf{y}, \mathbf{z}\}$ . Since matrix multiplication is not commutative the order of the chosen axis is important and a lack of knowledge of the chosen convention makes the Euler notation ambiguous, in a yet different way. EBSD orientation mapping uses, for instance, the Bunge convention [Bun82], which orders the Euler angles as:  $(\phi_1, \phi_2, \phi_3)$  around  $(\mathbf{x}, \mathbf{z}, \mathbf{x})$ , such that the total rotation is given by:

$${}^{Bunge}\mathcal{R}_{Euler}(\phi_1, \phi_2, \phi_3) = \mathcal{R}_x(\phi_3)\mathcal{R}_z(\phi_2)\mathcal{R}_x(\phi_1).$$

This series of rotations for a coordinate system from one position to another can be read as a rotation of  $\phi_1$  around the basis vector  $\mathbf{x}$  followed by  $\phi_2$  around  $\mathbf{z}$  and, finally,  $\phi_3$  around  $\mathbf{x}$ .

There are application for which neither the rotation matrix nor the Euler angle formalism are fully adequate, not least due to the ambiguities that need to be ironed out. One alternative is the *quaternion representation*. Quaternions are four-dimensional

vectors, or can be seen as complex numbers with two extra imaginary parts of the form  $\hat{\mathbf{q}} = q_i\mathbf{i} + q_j\mathbf{j} + q_k\mathbf{k} + q_r = [q_i, q_j, q_k, q_r]$ . A quaternion of this form describes a rotation around a rotation axis  $\mathbf{n} = [n_x, n_y, n_z]$  by an angle  $\theta$  such that  $q_i = n_x \sin(\theta/2)$ ,  $q_j = n_y \sin(\theta/2)$ ,  $q_k = n_z \sin(\theta/2)$  and  $q_r = \cos(\theta/2)$ . Quaternion maths will be faster on a computer compared to rotation matrices since the trigonometric functions are absent.

Rowenhost *et al.* [Row+15] worked out the complete conversions between the rotation formalisms used in material science (including the Rodrigue-Frank vectors and homochronic vectors) and provided extensive open source Fortran-90 libraries with the implementations. Marc's GitHub repository [DG14] contains Fortran95, IDL, MatLab, and C++ implementations for the rotations and conversions as well.

Now that we covered how to do rotations in a Cartesian frame we will go over transformations to and from the crystal frame.

## 2.2.6 Crystal to Cartesian frame and the structure matrix

While computations in the crystal frame conserves the symmetry of the crystal and keeps the equations somewhat intuitive, there are undeniable benefits to bringing the calculations into the Cartesian frame as well. If only because implementing non Cartesian vectorial manipulation requires extra work but ultimately because we want to project the information on a square detector or screen. We are interested in writing out the path of transforming from both the real and reciprocal hexagonal space to the Cartesian system.

The easiest and most common way of defining a Cartesian frame with basis vectors  $\mathbf{e}_i$  with respect to the crystal frame with basis vectors  $\mathbf{a}_i$  and corresponding reciprocal space vectors  $\mathbf{a}_i^*$  is as follows:

- $\mathbf{e}_1$  is the unit vector parallel to  $\mathbf{a}_1$ :

$$\mathbf{e}_1 = \frac{\mathbf{a}_1}{|\mathbf{a}_1|} \quad (2.33)$$

- $\mathbf{e}_3$  is the unit vector parallel to  $\mathbf{a}_3^*$ :

$$\mathbf{e}_3 = \frac{\mathbf{a}_3^*}{|\mathbf{a}_3^*|} \quad (2.34)$$

- and  $\mathbf{e}_2$  completes the right handed Cartesian reference frame:

$$\mathbf{e}_2 = \mathbf{e}_3 \times \mathbf{e}_1. \quad (2.35)$$

Let us consider a vector  $\mathbf{p} = p_i \mathbf{a}_i$ , whose components in the Cartesian frame are  $x_i^p$ . Since  $\mathbf{p} = p_i \mathbf{a}_i = x_i^p \mathbf{e}_i$  it means that we could find a coordinate transformation matrix  $a_{ij}$  which relates the components  $p_i$  and  $x_i^p$ :

$$x_i^p = a_{ij} p_i \quad (2.36)$$

The components of the matrix  $a_{ij}$  can be found by rewriting the lengths of the lattice vectors in Eq.'s 2.33 to 2.35 in terms of the direct and reciprocal matrix tensors. For instance,  $|\mathbf{a}_1| = \sqrt{g_{11}}$  (see Eq. 2.16). For the rest of the beautiful derivation we send the reader to page 140 of ref [DGM12]. The final matrix will have elements containing both the direct and reciprocal metric tensor. We give here the form of matrix  $a_{ij}$ , also known as the *direct structure matrix*, for a hexagonal lattice:

$${}^{hex}a_{ij} = \begin{bmatrix} a & \frac{-a}{2} & 0 \\ 0 & \frac{\sqrt{3}a}{2} & 0 \\ 0 & 0 & c \end{bmatrix} \quad (2.37)$$

If we want to translate a reciprocal space vector to the same Cartesian frame, we have to introduce a second matrix  $b_{ij}$  known as the *reciprocal structure matrix*. We start now with a vector  $\mathbf{g}$  with components  $g_i$  in the reciprocal space:  $\mathbf{g} = g_i \mathbf{a}_i^*$ . The same vector will have components  $x_i^g$  in the Cartesian frame:  $\mathbf{g} = x_i^g \mathbf{e}_i = g_i \mathbf{a}_i^*$  such that  $x_i^g = b_{ij} g_i$ . We can use the reciprocal structure matrix  $g_{ij}^*$  (Eq. 2.31) to rewrite the reciprocal basis vectors  $\mathbf{a}_i^*$  in terms of the real ones  $\mathbf{a}_j$  such that:

$$\mathbf{g} = x_i^g \mathbf{e}_i = g_i g_{ij}^* \mathbf{a}_j,$$

where we can now use the direct structure matrix  $a_{ij}$  (Eq. 2.36) to relate the quantities  $x_i^g$  and  $g_i g_{ij}^*$ :

$$x_i^g = a_{ij} g_i g_{jl}^* = a_{ij} g_{jl}^* g_l.$$

We can now define the reciprocal structure matrix for a hexagonal lattice,  ${}^{hex}b_{ij}$ :

$${}^{hex}b_{ij} = {}^{hex}a_{ij} {}^{hex}g_{jl}^* = \begin{bmatrix} \frac{1}{3a} & 0 & 0 \\ \frac{\sqrt{3}}{3a} & \frac{2\sqrt{3}}{3a} & 0 \\ 0 & 0 & \frac{1}{c} \end{bmatrix}. \quad (2.38)$$

### 2.2.7 Metric tensor implementations

I took the time to write out a good number of equations in this section. While these are well established and, probably, well understood vectorial manipulation in the world of X-ray diffraction, many electron microscopists are quite resistant to applying them on a daily basis. I make this claim based on the observation that, while the implementation would be trivial, there is a lack of mature, accessible and easy to plug-and-play (ideally open) software out there to answer some of the crystallographic questions the material scientists might ask when using an SEM as a characterization tool.

Until a *Python* library will be available and documented for crystallographic basis sets computations I leave the reader with a [web tool](#)<sup>8</sup>, albeit limited in capabilities, written by Albes Koxhaj, an excellent summer project student who implemented a few of the equations here, and revised by me. The last two blocks of calculators in this tool were written to find the coordinates, in the crystal frame, of the normal direction on a given plane ( $hkl$ ) or ( $hkil$ ). For a hexagonal plane, we show that there are two special conditions in which the normal to a plane can be reduced to Miller indices  $[uvw]$ . The first case is when the  $\mathbf{c}$ -direction is parallel to the plane ( $l = 0$ ) such that the lattice parameters can be removed from the indices and we are left with integer numbers. The second case is when the  $\mathbf{c}$ -direction is normal to the plane ( $h = l = 0$  or  $h = l = i = 0$ ), when the normal is along  $\mathbf{c}$  in both the real and reciprocal space. Any other case will keep coordinates dependent on the lattice parameters  $a, c$  which would make them unlikely to be reduced to integers.

I also wrote a few Python lines in the Jupyter notebook `grainNormal.ipynb`, showing the steps needed to calculate the surface normal in the crystal frame of individual grains from the Euler angles of an EBSD map by applying the identities in this section.

*EMsoft* [DG13] contains Fortran90 implementations of the metric tensor tensor formalism. The source code can be found in the `crystal.f90` and `symmetry.f90` modules in Source/EMsoftLib path on the GitHub page.

---

<sup>8</sup> Link address is: <http://ssd.phys.strath.ac.uk/resources/crystallography/crystallographic-direction-calculator/>.

## 2.3 Symmetry in crystallography

Many objects in nature exhibit symmetry of some sort. The human body has approximate mirror symmetry. A shamrock (the species of clover or trefoil used as the symbol of Ireland) has three-fold rotational symmetry (trefoil) and, and here's a bit of trivia to make you a star at the next British party, not four-fold symmetry as U.S. advertisements sometimes wrongly represents it. The reader might have noticed that the way we talk about object symmetry involves a motion action, which made upon the object would leave it unchanged. Indeed, the symmetry of an object will be defined by its *symmetry operations* that map the object onto itself. While for any motion one can find an object for which this is a symmetry motion, if we start with the object it is easy to start with these three basic actions to test its symmetry<sup>9</sup>:

1. rotate
2. reflect
3. translate

If after any or a combination of 1. 2. and 3. the object looks the same as it originally looked than we talk about the object as being symmetric. There is a nuanced distinction between these operations since 1. and 3. can be physically realised and known as *proper* or first kind operations. Operations that involve 2. are *improper* or of second kind. Inversion is yet another improper operation that can be reduced in three dimensions to a rotation plus a reflection.

We will see that all this can be written in mathematical form with only minor adjustments. First, operation 3. can only truly be a symmetry operator for infinite objects which are not very common in everyday life. Second, the identity operator is also introduced as symmetry operator, such that, in the mathematical sense, all objects hold at least one symmetry property. Now there's nothing stopping you from being the soul of the party.

We will spend some time exploring a subset of symmetry operations chosen such that when combined can generate the entire symmetry of a wurtzite crystal. We will follow closely the notation used in *International Tables for Crystallography, Volume A* [Hah96] described in some detail on page 46. We will use the two most common

---

<sup>9</sup> Assuming we are to leave the metric properties of space undisturbed, *i.e.*, no stretching, bending, twisting, which should be easy to achieve in the physical world.

shorthand notations to write down symmetry operations: the *Hermann-Mauguin notation* also known as the *international notation* which is the standard one, and the *Schoenflies notation* which is widely used in Physics and Chemistry. We will also show the graphical symbols for the operations discussed.

### 2.3.1 Symmetry operations

The set of symmetry operations of a given object have noteworthy properties:

1. the application of two symmetry operations results in a third symmetry operator of that object
2. the inverse of an operation is also an operation of that object
3. all objects exhibit the identity operation
4. the associative law is valid when combining three or more operations.

These four properties are also the group axioms and tell us that the set of symmetry operations of a given object form a mathematical group. This will come in handy in the next section. For now it is worthwhile to look at how to write these operation in mathematical form.

In the following we will explore a non-exhaustive list of symmetry operations. We choose our examples such that they are relevant for generating the wurtzite crystal structure symmetry. Note that the basis vectors of a hexagonal lattice do not form a Cartesian frame. This means that the usual algebraic formulas used for transformation operations must be revised. We do expect the form of rotation, translation and reflection matrices to be therefore not as familiar, which is why we take the time to explore them here.

#### Operation of first kind: pure rotation

A pure rotation is fully determined by a rotation axis and a rotation angle which is chosen to be positive in the counter-clockwise direction. The rotation axis is given as a vector  $[u\ v\ w]$  and the rotation angle is given as fraction of  $2\pi$ . For instance a rotation of order three or three-fold rotation is a rotation by angle  $2\pi/3$ . In general an  $n$ -fold rotation is represented by symbol  $n$  ( $C_n$ ) and Table 2.7 shows examples for three-fold and six-fold rotations together with their graphical symbols which are filled polygons with  $n$  sides.

TABLE 2.7: Examples of pure rotation symbols.

| Name                | Graphical | Hermann-Mauguin | Schoenflies |
|---------------------|-----------|-----------------|-------------|
| Three-fold rotation | ▲         | 3               | $C_3$       |
| Six-fold rotation   | ◆         | 6               | $C_6$       |

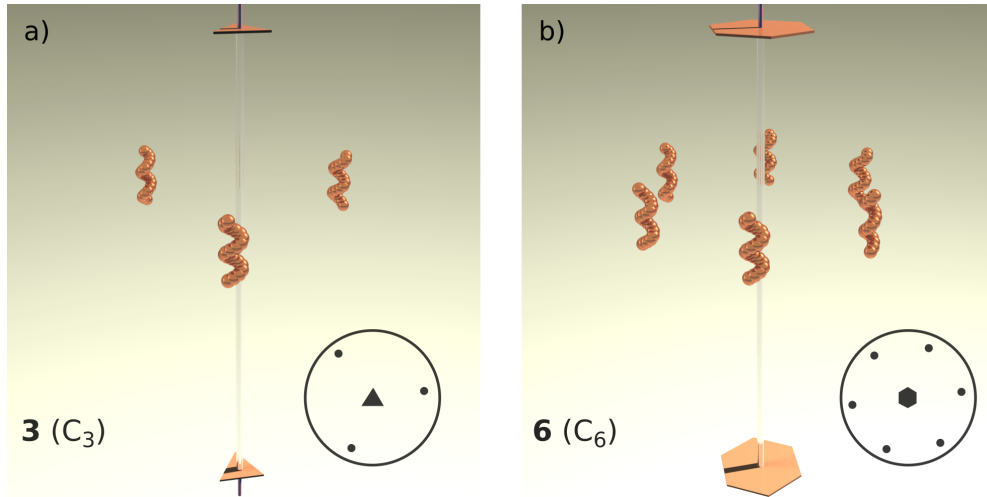


FIGURE 2.10: Rendered 3D graphical representations of a) three-fold and b) six-fold pure rotations. The circles in the bottom right of the images represent the stereographic projections of the operators.

3D representations of the rotation operator are shown in Figure 2.10 for rotations of order 3 in (a) and 6 in (b), respectively. The images have been rendered with the public domain software Rayshade 4.0.9 software<sup>10</sup>. The input files I used are very closely based on the input \*.ray files<sup>11</sup> developed by Marc De Graef [DG98] with the purpose of teaching the crystallography group symmetry[DG08]. My scripts can be found at this BitBucket repository<sup>12</sup>. The relevant files for this example are 3FoldPureRotationPNG.ray and 6FoldPureRotationPNG.ray and can be compiled on a Linux machine after the installation of Rayshade software (and making sure ImageMagick is available on the machine) by typing:

```
rayshade [filePNG].ray > [filePNG].mtv
convert [filePNG].mtv [file].png
```

where [file] is the name of the file used. \*.mtv files can also be converted to \*.png or \*.gif with ImageMagick. All the input scripts and resulting images and animated files

<sup>10</sup> Link is <https://sourceforge.net/projects/rayshade/>.

<sup>11</sup> Link is <http://som.web.cmu.edu/frames2.html>.

<sup>12</sup> Link is [https://bitbucket.org/elenapascal/\\_wurtzite-symmetry/src/master/](https://bitbucket.org/elenapascal/_wurtzite-symmetry/src/master/).

can be found in the extra materials. To render the \*.gifs one need more patience and has to do:

```
rayshade [fileGIF].ray > [fileGIF].mtv
convert [fileGIF].mtv [file].gif
```

The small helix object used by Marc in these images (made up of a helical string of spheres) was chosen such that it holds no rotational symmetry. The object also exhibits handedness and its mirror reflection will look different from the original object. Despite this, the entire system, the three objects in Fig. 2.10 (a) or six objects in Fig. 2.10 (b), looks indistinguishable from original when rotated  $2\pi/3 = 120^\circ$  and  $2\pi/6 = 60^\circ$ , respectively, around the rotation axis. Similarly, a triangle prism will look the same after being rotated around the central axis by  $120^\circ$  and a hexagonal prism will look indistinguishable after being rotated  $60^\circ$ , respectively.

It is common that the axis of rotation to be the third basis vector *i.e.*, parallel to the crystallographic **c**-axis and, in those cases, the rotation axis to not be explicitly stated. In any other case, the rotation axis must be given, either in vector form  $[uvw]$  or as the equation of the line coinciding with the axis. The latter notation method is the one used in the *International Tables for Crystallography*. As an example we can look at *Symmetry operation* (2) of a hexagonal lattice point group shown in Fig. 2.16.  $3^+(0,0,z)$  is a three-fold pure rotation around the  $[001]$  direction given here in line equation form. The  $^+$  sign informs us that the position of the point is elevated with respect to the drawing plane.

A three fold symmetry of a lattice tells us that for every “motif” at position  $(x,y,z)$  we will find the same motif at the equivalent position  $(x',y',z')$  obtained through a  $120^\circ$  rotation around the central axis, here  $\mathbf{e}_z$ . In order to represent the rotation operation in mathematical form we must turn to rotation matrices. Unlike the intuitive form when used in an everyday orthonormal system (HREF TO WHERE INTRODUCED), when derived for a general, nonorthonormal lattice the rotation matrices can become cumbersome and will obscure the symmetry(see ref. [Dav73]). Luckily, we can avoid that by considering the passive rotation of the system instead of the active rotation of the motif.

We want to find the rotation matrix  $D(\theta)$  which, when applied to a set of (not necessary orthonormal) basis vectors  $(\mathbf{e}_x, \mathbf{e}_y, \mathbf{e}_z)$  rotates them once around  $\mathbf{e}_z$  by an angle  $\theta$  to a new configuration  $(\mathbf{e}'_x, \mathbf{e}'_y, \mathbf{e}'_z)$ . This passive rotation is defined in crystallography by the right hand rule<sup>13</sup>. It should be clear that this is equivalent to an active

---

<sup>13</sup> The right thumb points towards the direction line and the fingers indicate the positive rotation.

rotation (*i.e.*, rotating a vector defined in this basis) by the same angle anticlockwise around  $\mathbf{e}_z$  when looking in the direction of  $\mathbf{e}_z$ .

If the set of basis vectors describes a hexagonal lattice<sup>14</sup> and the angle of rotation is  $120^\circ$  then the matrix  $D^{\text{hex}}(120^\circ)[001] \equiv D^{(n)}$  is a three-fold rotation and can be derived by geometry as shown in Fig. 2.11.

$$\begin{aligned} (\mathbf{e}'_x & \quad \mathbf{e}'_y & \quad \mathbf{e}'_z) = (\mathbf{e}_y & -\mathbf{e}_x - \mathbf{e}_y & \quad \mathbf{e}_z) \\ & = (\mathbf{e}_x & \quad \mathbf{e}_y & \quad \mathbf{e}_z) D^{(n)} \end{aligned}$$

Which completely determines the matrix  $D^{(n)}$  to be:

$$D^{(n)} = \begin{pmatrix} 0 & -1 & 0 \\ 1 & -1 & 0 \\ 0 & 0 & 1 \end{pmatrix} \quad (2.39)$$

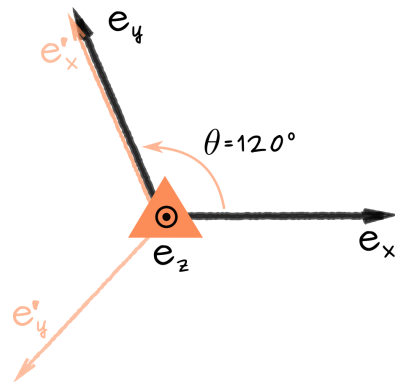


FIGURE 2.11: Three-fold rotation around the third axis of a hexagonal basis set.

It is not only rotations that can be expressed in matrix form, reflections as well as any combination of reflection and rotation can be written down as matrix operations. Every possible symmetry operation a crystal holds, if it excludes translation, will part of a finite and well determined group of  $3 \times 3$  matrices. Only of subset of these matrices is really necessary to determine the entire group and these are known as *generators*. There are only 14 matrices  $D^{(x)}$  that can act as generators, where  $(x)$  spans from  $(a)$  to  $(n)$ . Talking in detail about groups and space groups is beyond the purpose of this thesis, but a good introduction to crystallography for the electron microscopist can be found in *Structure of Materials; an introduction to crystallography, diffraction and symmetry* [DGM12] while an in-depth overview is given in the introduction to the *International Tables for Crystallography, Volume A* [Hah96] both of which we will reference throughout this section.

### Operation of first kind: pure translation

A pure translation is fully determined by translation vector  $\mathbf{t} = u_1 \mathbf{e}_1 + u_2 \mathbf{e}_2 + u_3 \mathbf{e}_3$ . The lattice translation vector was introduced on page 8 and to this can be added lattice centring vectors if present. The latter are useful for describing non-primitive lattices

<sup>14</sup> We have not explicitly shown that the hexagonal lattice is compatible with this symmetry operation but perhaps the reader will not be too suspicious of a hexagon showing tree fold rotation symmetry.

where lattice points exists not only at the corners of the crystal structure. The international symbol for translation is  $t(u_1, u_2, u_3)$  as can be observed in the representation of the basis vectors given in the *Generators* list in Fig. 2.16:  $t(1, 0, 0), t(0, 1, 0), t(0, 0, 1)$ .

Mathematically, a translation is just a vector addition:

$$\mathbf{r}' = \mathbf{r} + \mathbf{t}. \quad (2.40)$$

However, we want to integrate this into the matrix formulation we developed for the rotation operation. To achieve this we introduce a 4D vector. By adding a trivial equation in the form of a fourth component which is just:  $1 (x_1, x_2, x_3) \rightarrow (x_1, x_2, x_3, 1)$ . We also upgrade the Einstein notation to go from  $i = 1$  to  $i = 4$ , such that Eq. 2.40 becomes:  $x'_i = x_i + u_i$  or in matrix form:

$$\begin{pmatrix} x'_1 \\ x'_2 \\ x'_3 \\ 1 \end{pmatrix} = \begin{pmatrix} 1 & 0 & 0 & u_1 \\ 0 & 1 & 0 & u_2 \\ 0 & 0 & 1 & u_3 \\ 0 & 0 & 0 & 1 \end{pmatrix} \begin{pmatrix} x_1 \\ x_2 \\ x_3 \\ 1 \end{pmatrix} \quad (2.41)$$

The  $4 \times 4$  matrix consists of the  $3 \times 3$  rotation matrix  $D_{ij}^{(i)}$  in the upper left corner, a  $3 \times 1$  column vector containing the translation vector components on the right and a  $1 \times 4$  row at the bottom,  $(0\ 0\ 0\ 1)$ , containing no useful information. We will introduce the symbol  $\mathcal{W}$  for the  $4 \times 4$  matrix such that:

$$x'_i = \mathcal{W}_{ij} x_j.$$

In practice, it is more useful to denote the rotation matrix and translation vector that are implied, which is why the *Seitz symbol*, written as  $(D|\mathbf{t})$ , is more commonly used. For instance, the  $\mathcal{W}$  matrix in Eq. 2.41 has the Seitz symbol  $(E|\mathbf{t})$ , where  $E$  is the identity matrix  $D$ . The  $\mathcal{W}$  matrix for a rotation plus translation is:

$$\mathcal{W} = (D|\mathbf{t}) = \begin{pmatrix} D_{11} & D_{12} & D_{13} & u_1 \\ D_{21} & D_{22} & D_{23} & u_2 \\ D_{31} & D_{32} & D_{33} & u_3 \\ 0 & 0 & 0 & 1 \end{pmatrix}. \quad (2.42)$$

The pure rotation in Eq. 2.39 has the Seitz symbol  $(D^{(n)}|\mathbf{0})$  and as a  $4 \times 4$  matrix becomes:

$$\mathcal{W}_\Delta = \begin{pmatrix} 0 & -1 & 0 & 0 \\ 1 & -1 & 0 & 0 \\ 0 & 0 & 1 & 0 \\ 0 & 0 & 0 & 1 \end{pmatrix}.$$

### Operation of second kind: pure reflection

A pure reflection operation, more commonly known as a *mirror*, is characterised by a plane, schematically indicated by a solid line, as shown in Table 2.8 when it does not coincide with the plane of drawing. The international notation for mirror plane provides also information on the orientation of the plane, usually by writing down the equation of the plane. For instance, the plane parallel to  $(110)$  is written as  $m(x, -x, z)$ .

TABLE 2.8: Example of pure reflection symbols.

| Name         | Graphical | Hermann-Mauguin | Schoenflies |
|--------------|-----------|-----------------|-------------|
| Mirror plane | —         | m               | $\sigma$    |

Mirror operations can be represented by a matrix  $D(m)$ , which, analogous to the rotation matrix, can be determined from geometry. For the reflection operation in Fig. 2.12:

$$\begin{pmatrix} \mathbf{e}'_x & \mathbf{e}'_y & \mathbf{e}'_z \end{pmatrix} = (-\mathbf{e}_y \quad -\mathbf{e}_x \quad \mathbf{e}_z) \\ = (\mathbf{e}_x \quad \mathbf{e}_y \quad \mathbf{e}_z) D(m)$$

From which we find the set operation  $D^{hex}(m_{(x,-x,z)}) \equiv D^{(k)}$  to be:

$$D^{(k)} = \begin{pmatrix} 0 & -1 & 0 \\ -1 & 0 & 0 \\ 0 & 0 & 1 \end{pmatrix}. \quad (2.43)$$

Which, in turn, completely determines the matrix  $\mathcal{W}_m$  with Seitz symbol  $(D^{(k)}|0)$ .

### Combination of rotation and translation

Combining translation with rotation yields a new type of symmetry operation, known as a *screw axis*. While applying a pure rotation of order  $n$  to an object we recover the original position after  $n$  successive operations, the extra translation operation in the screw axis renders this observation invalid. During a screw axis operation, the object is translated after every rotation step by a certain vector  $\tau$  parallel to the rotation axis. We can see that in Fig. 2.13. Input files used are `2_1PNG.ray` and `6_1PNG.ray` (see how

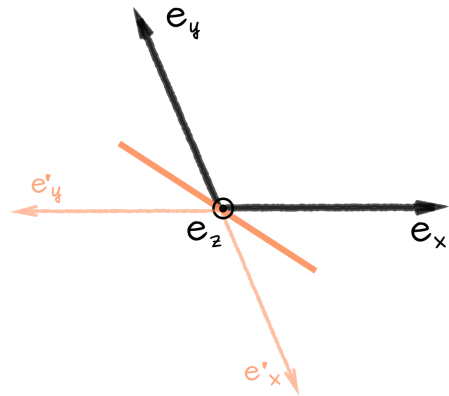


FIGURE 2.12:  
 $m(x, -x, z)$  mirror  
plane operation in a  
hexagonal basis set.

to use them in the *Pure Rotation* subsection on page 35). For a  $2_1$  screw axis shown in Fig. 2.13 a), after a two-fold ( $2\pi/2 = 180^\circ$ ) rotation, the object is also translated by a vector  $\tau$  from point **0** to point **1**. After  $n = 2$  rotations it is translated  $2\tau$  in the direction of the screw axis to the point **2**. This position is identical to the original one except for a translation vector  $m\mathbf{t}$  where  $\mathbf{t}$  is the smallest possible translation vector in the given direction and, in this case,  $m = 1$ . This is where the subscript <sub>1</sub> comes from in the notation  $2_1$ .

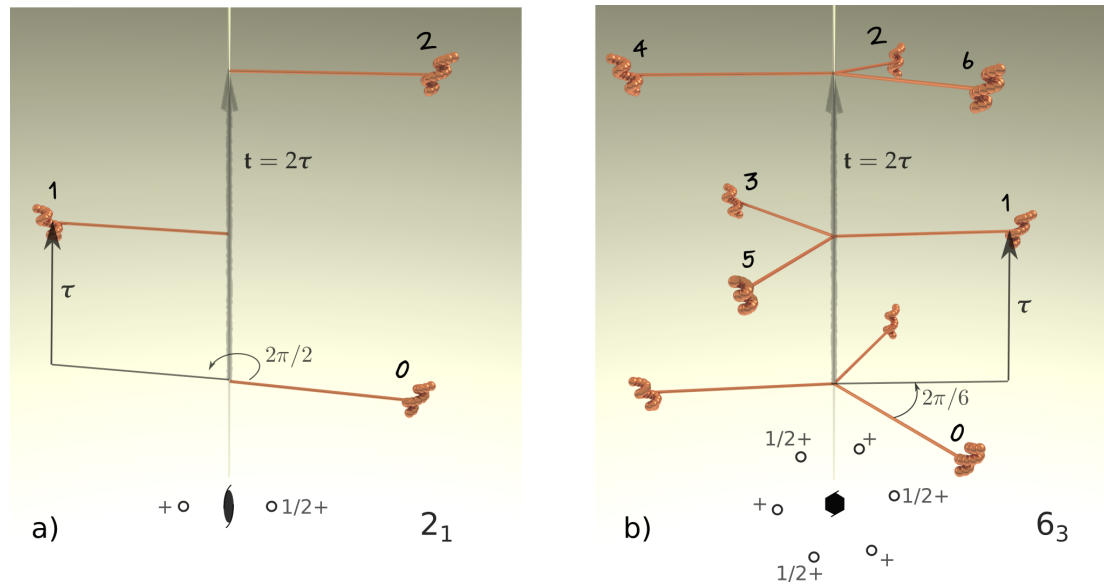


FIGURE 2.13: Rendered 3D graphical representations and (sequentially numbered) operations involved in the construction of screw axis a)  $2_1$  and b)  $6_3$ . Standard 2D graphical projections are included at the bottom.

Generally, the notation for a screw axis is  $n_m$  where  $n\tau = m\mathbf{t}$ , which tells us that after  $n$  screw axis operations the original point is translated  $m$  lattice translation vectors in the direction of the screw axis. One screw axis operation involves an  $n$ -fold rotation plus a  $\tau = m\mathbf{t}/n$  translation. Table 2.9 shows the graphical and notation symbols for the relevant screw axis operations of the wurtzite crystal:  $2_1$  and  $6_3$ . The  $6_3$  operation, shown in Fig. 2.13 b), involves a  $\tau = 3\mathbf{t}/6 = \mathbf{t}/2$  translation after each six-fold rotation, which takes the object on which it operates from point **0** to point **1**. After two  $6_3$  operations the object has been translated by a total vector equal to the lattice translation vector  $\mathbf{t}$ . To obtain the next points, **3**, **4** and **6**, we must leave the unit cell in which we started. Because all unit cells must be the same, the screw rotation in the cell below dictates equivalent points in this cell corresponding to the position of points **3-6**.

The bottom of the images in Fig. 2.13 contain standard graphical representation of the corresponding symmetry operations such that the axis of rotation are normal to

the page. The open circles indicate that the object are above the plane of drawing and the numbers next to the circle refer to the height of their positions.

TABLE 2.9: Examples of screw axis symbols.

| Name                | Graphical | Printed | Screw vector $\tau$ in units of $t$ |
|---------------------|-----------|---------|-------------------------------------|
| Two-fold screw axis |           | $2_1$   | $1/2$                               |
| Six-fold screw axis |           | $6_3$   | $1/2$                               |

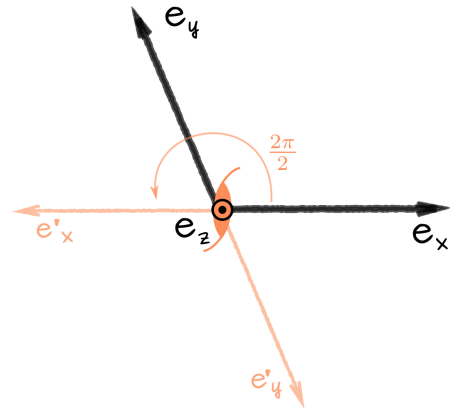
The *International Tables for Crystallography* denote the screw axis operations by the order of the rotation together with the translation vector  $\tau$ :  $n(\tau)$ . The axis of rotation is also added as it can be seen in the symmetry operations list on page 48. Operation (4), for instance, denotes a  $2_1$  screw axis around the c-axis in a hexagonal unit cell.

Mathematically, we can write this operation from geometry (see Fig. 2.14) as:

$$\begin{aligned} (\mathbf{e}'_x \quad \mathbf{e}'_y \quad \mathbf{e}'_z) &= (-\mathbf{e}_x \quad -\mathbf{e}_y \quad \mathbf{e}_z) \\ &= (\mathbf{e}_x \quad \mathbf{e}_y \quad \mathbf{e}_z) D^{(b)} \end{aligned}$$

From which we find the set operation  $D^{(b)}$  to be:

$$D^{(b)} = \begin{pmatrix} -1 & 0 & 0 \\ 0 & -1 & 0 \\ 0 & 0 & 1 \end{pmatrix}. \quad (2.44)$$

FIGURE 2.14:  $2_1$  screw axis operation in a hexagonal basis set.

Which completely determines the matrix  $\mathcal{W}$ , with Seitz symbol  $(D^{(b)} | \tau_{(0,0,1/2)})$ :

$$\mathcal{W} = \begin{pmatrix} -1 & 0 & 0 & 0 \\ 0 & -1 & 0 & 0 \\ 0 & 0 & 1 & 1/2 \\ 0 & 0 & 0 & 1 \end{pmatrix}.$$

Now that we have written out the mathematical framework necessary for studying a number of different symmetries we can take a closer look at how to describe a crystal structure starting from the symmetry it manifests. More importantly, we want to answer the question “What is the minimum number of symmetry operations from which a specific structure can be recovered?”.

### 2.3.2 Point groups

It turns out maths already has the answer to that question and it can easily be applied to crystallography. If we forget for a moment about translations, then any of the remaining symmetry operators can be applied to an object and leave exactly one point invariant, namely the origin. For all the symmetry operations we talked about, the choice of the origin (a plane for reflection, an axis for rotation ...) was non-ambiguous. Another way of saying this is that all symmetry operators except translation overlap in exactly one point. All these operators can be expressed as  $3 \times 3$  matrices  $D$  and carry the name of *point symmetries*. The total point symmetries of an object must also form a *group* with the properties given on page 34. If the object under consideration is a crystal structure, then those symmetry operations are selected such that they are compatible with the translational periodicity of its lattice. Starting, then, from a *point* one can derive 32 sets of consistent symmetry operations compatible with the Bravais lattices also known as crystallographic point groups (see Chapter 9 in [DGM12]).

Groups have several useful properties, including the fact that one can generate all elements of a group starting with a list of operations and constructing a multiplication table. The minimum symmetry operations needed to construct a full point group is known as a set of *generators*. There are only 14 total generators, a subset of which will produce any possible crystal symmetry. We have encountered three of them so far, denoted as  $D^{(b)}$ ,  $D^{(k)}$  and  $D^{(n)}$ . The matrices  $D^{(i)}$  form the set of generators where ( $i$ ) can go from ( $a$ ) to ( $n$ ),  $D^{(a)}$  being the identity matrix, which, as previously discussed, describes the symmetry of all systems and is always implied.

We keep on following the Hermann-Mauguin and Schoenflies notations for crystallographic point groups, with the latter shown in brackets. The Hermann-Mauguin notation for point groups has a maximum of three symbols, each corresponding to a particular direction in the Bravais lattice. Since the choice of origin is very specific when we consider the possible symmetries a crystal would exhibit, the possible axes of symmetry for a given crystal will be the directions used to describe the point group of a particular system.

Table 2.10 shows the three directions for the three possible set of symbols describing the point group of a hexagonal crystal system. For instance, we can consider a group made up of only the identity operation and all powers<sup>15</sup> of the rotation operator, we talked about rotation operations on page 34. The notation of this simple group will follow the notation of the operators, therefore, a six-fold rotational point group (also known as cyclic) is **6** or  $C_6$  (C for cyclic).<sup>16</sup> If a hexagonal crystal is known to be

<sup>15</sup> An operator to power 2 simply means applying that operator twice in succession.

<sup>16</sup> Note that we use the Sans Serif font for operators symbols and the Bold font for group notation.

part of the crystallographic point group 6 then we can conclude it has six-fold rotational symmetry and can read from Table 2.10 that the rotation axis must be [00.1].

TABLE 2.10: Primary, secondary and tertiary symmetry directions (Miller-Bravais) of the point group notation for the hexagonal crystal.

| Crystal system | Primary[u v . w] | Secondary[u v . w] | Tertiary[u v . w] |
|----------------|------------------|--------------------|-------------------|
| Hexagonal      | [00.1]           | {10.0}             | {12.0}            |

Now that we set the rules with the simplest of examples let's take a look at something a bit more involved. (1) *What happens if we combine the proper rotation group with reflection operations? and (2) How do we generate the full symmetry of such a group?*

### 6mm point group from generators

If we give a mirror plane (m) a six-fold rotation axis (6) then we end up with the point group shown in Fig. 2.15. Notice the change of handedness (chirality) of the orange object as an indication of the reflection symmetry. The generating file is `6mmPNG.ray`. It turns out that, for even rotation orders, an extra mirror symmetry appears. One can easily see that in the stereographic projection at the bottom of the image. Every second mirror is not generated by the rotation operation, however the structure clearly displays the extra reflections. This is why the group **6mm** has two 'm's in its notation. From Table 2.10 we can read that the first set of mirrors have the normals {10.0} while the second set of mirrors have the normals {12.0}. Similarly, the **v** in the Schoenflies notation **C<sub>6v</sub>** indicates the vertical orientation of the mirror planes.

The generators matrices of point group are:  $D^{(a)}$ ,  $D^{(b)}$ ,  $D^{(k)}$ ,  $D^{(n)}$ ; where we denoted the identity operator with the label  $D^{(a)}$ . Conveniently, we have already derived the three  $3 \times 3$  matrices corresponding to the last three of these operators:  $D^{(b)}$  (Eq. 2.44),  $D^{(k)}$  (Eq. 2.43),  $D^{(n)}$  (Eq. 2.39). We can find these matrices in the *International Tables for Crystallography, Volume A* [Hah96] in the *Generators* list of the space group (pages 584-585 shown here on page 48) as operations (1), (2), (4), (7). In order to find the full list of symmetry operators of the space group, we can read the *Symmetry operations* section from the *Tables* or we can multiply the generators among themselves until we find the full list of 12. We'll show here the hard way for the reader to use as a reference but also to somewhat demystify the origin of these matrices.

Before that we want to add a few notes on point group characteristics. The number 12 represents the size of the set of points in this group which have equivalent position. That is to say, if we start with an arbitrary position  $(x, y, z)$  how many new positions are generated when the full set of symmetry operations are applied. This is also known

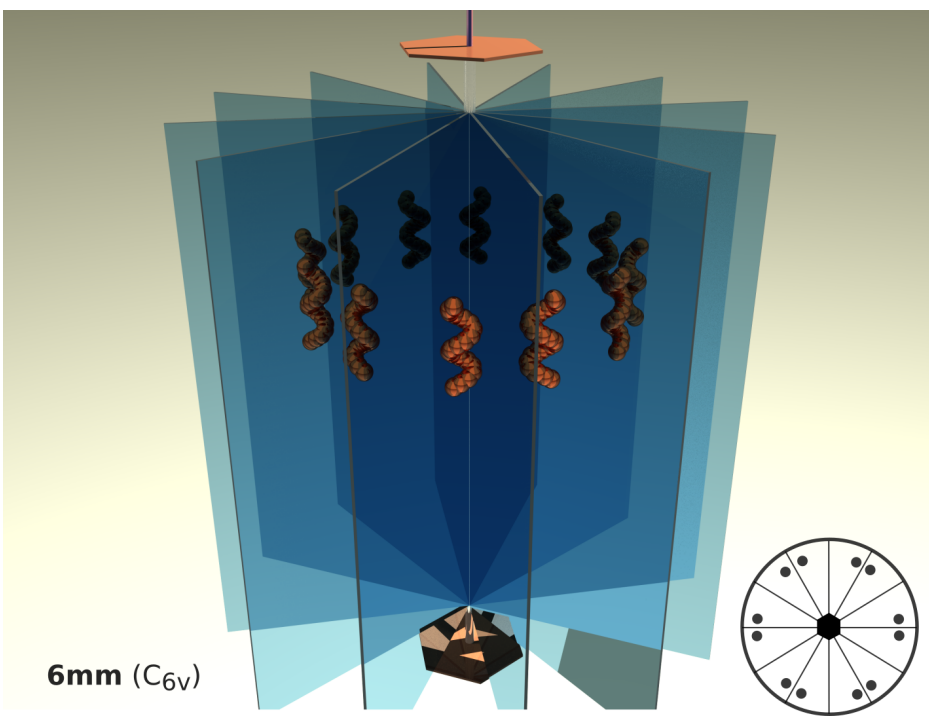


FIGURE 2.15: Graphical 3D representation of **6mm** point group together with its stereographic projection in the bottom corner right.

as the *order* of the group. We can then say that the **6mm** point group has order 12. Another point group property is that of *centrosymmetry*. If we define polarity as the property of a group in which directions  $\mathbf{t}$  and  $-\mathbf{t}$  are not related to each other by any symmetry operation, then we can note that this group is only polar along the rotation axis. We can also conclude that this point group is not centrosymmetric.

To find the full symmetry of a point group starting with the list of generator matrices, we multiply each operator with itself and the others, remembering that matrix multiplication is not commutative. For every resulting matrix that is not the identity matrix we check if we already have it in the set. If not then we can add it and start the matrix multiplications again. When we did all the possible operations in a set without finding any new matrices we can stop looking and declare we found the full symmetry operations group. The *Python* style pseudocode for this is shown below in Algorithm 1. This function is implemented in the Jupyter notebook `Symmetry_matrices.ipynb`.

```

def findSymMat(knownMat, *newMat):
    input : List of  $3 \times 3$  generator matrices
    output: Entire list of symmetry operators as  $3 \times 3$  matrices

    while still finding new matrices do
        for matrix_i in newMat do
            for matrix_j in knownMat do
                isThisNew = matrix_i  $\times$  matrix_j
                if isThisNew is not Identity Matrix and is not in knownMat then
                    add isThisNew to newMat
                    add isThisNew to knownMat
                else
                    stop looking
                end
            end
        end
        if new matrix is found then
            | findSymMat (knownMat, newMat)
        end
    end
end

```

ALGORITHM 1: Recursive function to find the symmetry matrices of a space group starting from the list of generators.

Using this implementation<sup>17</sup> we find the following 12 symmetry matrices of the **P6<sub>3</sub>mc** point group:  $D^{(a)}$ ,  $D^{(b)}$ ,  $D^{(k)}$ ,  $D^{(n)}$ ,  $D^{(nn)}$ ,  $D^{(nb)}$ ,  $D^{(nk)}$ ,  $D^{(kn)}$ ,  $D^{(kb)}$ ,  $D^{(bnk)}$ ,  $D^{(nkk)}$ ,  $D^{(knk)}$  (not necessary in the same order as in the *Tables*). Here we used the notation:  $D^{(nb)} = D^{(n)} \times D^{(b)}$  to represent a combination of operations applied in a specific order. For instance,  $D^{(nn)}$  is a 3-fold rotation applied twice and it should come as no surprise that a 3-fold rotation applied tree times is the identity operator:  $D^{(nnn)} = D^{(a)}$ . Similarly,  $D^{(kk)}$  is a double reflection and, again, equals to the identity operator.

The equivalent positions in the space group can then be easily determined by simply applying these operators to a general position  $(x, y, z)$ .

<sup>17</sup> Luckily, there is a good selection of mature or novel open software available to do these type of computations as well. Here are a few examples:

- **GAP** - provides an extensive computational group theory algebra library and tools.
- **Mantid** - available as a *Python* package, can handle crystallographic point and space group maths.
- **EMsoft** - the routine `CalcPositions` in the module `symmetry.f90` should do a generalised version of the implementation shown here.

### 2.3.3 Space groups

So far we have explored some possible symmetries of a system (motif) that are compatible with the hexagonal Bravais lattice of a crystal structure. It is time to add these point group symmetries on the crystal lattice points and observe what new symmetries emerge. This simply involves combining the point group operators the Bravais lattice translational vectors of a given crystal system. Every time this combination yields a new unique system then we can talk about a different symmetry group this time known as a *space group*.

There are 230 three dimensional space groups which might sound like a formidable result when we considered that we only combine 32 point groups with 14 Bravais lattices. However, bear in mind that there are more than one way of adding the point group symmetries at the lattice points. Additionally, combining symmetry operation can yield extra symmetries, just like the extra mirror planes “popped up” in the 6mm point group. Screw axes and glide planes<sup>18</sup> are symmetry operators containing a translation vector and therefore not forming point groups. However, when used to point group symmetries, in combination with Bravais lattices, these operators will form new space groups.

The space group symbol is formed by combining the centring information of the Bravais lattice with the point group Hermann-Mauguin notation symbol. The information about the symmetry of the crystal system can be dropped since it will be implied in the point group symmetry. One can predict extra symmetry operations describing a unique space group by replacing one or more operations in the Hermann-Mauguin point group notation with a screw rotation or glide plane. It is entirely possible to end up with a situation in which the point group of a space group contains operations which do not occur in the space group at all.

Depending on whether or not the space group contains any glide planes or screw axis symmetry operations we differentiate between *non-symmorphic* and *symmorphic* space groups. Symmorphic space groups contain then only the point group operations and are easy to spot from their Hermann-Mauguin symbols.

#### **The International Tables for Crystallography, Volume A**

The series of volumes constituting the *International Tables for Crystallography* are a comprehensive database of crystallographic information relevant in the studies of the

---

<sup>18</sup> We haven't explicitly talked about glide planes, but these are symmetry operations obtained by combining a mirror plane with translation over half the lattice vector parallel to the mirror plane. The symbol for a glide plane is  $a$ ,  $b$  or  $c$  if the glide vector is  $\mathbf{a}/2$ ,  $\mathbf{b}/2$  or  $\mathbf{c}/2$ , respectively.

structure or properties of materials. *Volume A* [Hah96], specifically tackles the space groups. We have already referenced a few times to a specific page in *Volume A* which shows all the information needed for the study of the space group symmetry **P6<sub>3</sub>mc** in tabulated form. It is a useful skill for a crystallographer to be able to read these pages.

- The top of the page holds the crystal system (hexagonal), the Patterson symmetry definition<sup>19</sup>, the point group symmetry (6mm), the Schoenflies symbol ( $C_{6v}^4$ ), the complete space group symbol ( $P6_3mc$ ), the space group shorthand symbol **P6<sub>3</sub>mc** and the space group number (186).
- Below, there is a drawing of the relative positions of the symmetry elements in the group, projected along the main direction (c), on the right. On the left, the equivalent positions are shown in the same projection.
- While the *Origin* of the group can be chosen arbitrarily, it is customary to choose the position with the highest symmetry of the group; here  $6_3mc^{20}$ . The symmetry is given in the usual point group notation following the system's symmetry directions (seen in Table 2.10). To clarify the ambiguity a second set of symmetries is given  $3m1$ , where the 1 is a place-holder for no more than identity symmetry for this direction, to establish the origin in the upper left corner of the unit cell.
- The *Asymmetric unit* is the smallest volume of the unit cell that will completely and exactly fill the space when the group's symmetry operators are applied to it. It is defined in terms of the sides and vertices containing the volume, which in terms are the result of the intersecting symmetry planes bounding the cell. The volume of the asymmetric cell has the property of being the volume of the full unit cell divided by the product of the order of the point group,  $n$ , (for 6mm  $n = 12$ ) and the number of centering operations plus one. For **P6<sub>3</sub>mc** then, the volume of the asymmetric cell is  $V_a = V / (12 \times 1) = V/12$ .
- Below, the full list of *Symmetry operations* together with their positions is given and we have already shown how to read some of these operations. There are a total of 12 symmetry operators including the identity operator.
- From these operators only 4 make it to the list of *Generators*, (1), (2), (4), and (7), together with the basis translation vectors. Starting with these list of 4 operators the full previous list can be generated by matrix multiplication.

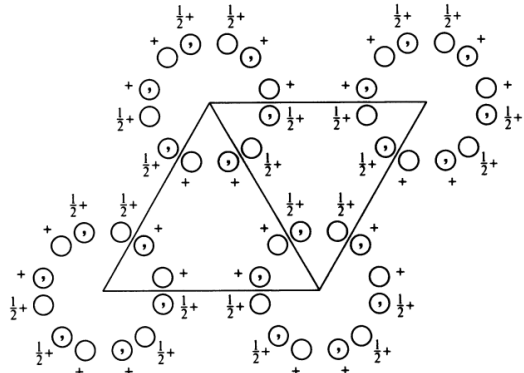
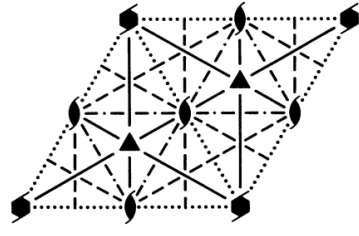
<sup>19</sup> The Patterson function is a mathematical construct of higher symmetry than the electron density function which it replaces in order to solve the phase problem in X-ray crystallography.

<sup>20</sup> Note that, while the notation is point group like, the origin position symmetries do not need to form a group and we do not keep the point group symbol notation.

Hexagonal

 $6mm$ Patterson symmetry  $P6/mmm$  $C_{6v}^4$  $P6_3mc$  $P6_3mc$ 

No. 186

Origin on  $3m$  1 on  $6_3mc$ 

**Asymmetric unit**     $0 \leq x \leq \frac{2}{3}; \quad 0 \leq y \leq \frac{1}{3}; \quad 0 \leq z \leq 1; \quad x \leq (1+y)/2; \quad y \leq x/2$   
**Vertices**     $(0,0,0) \quad \frac{1}{2}, 0, 0 \quad \frac{2}{3}, \frac{1}{3}, 0$   
                     $0, 0, 1 \quad \frac{1}{2}, 0, 1 \quad \frac{2}{3}, \frac{1}{3}, 1$

**Symmetry operations**

- |                          |                 |                            |         |                            |         |
|--------------------------|-----------------|----------------------------|---------|----------------------------|---------|
| (1) 1                    | (2) $3^+ 0,0,z$ | (3) $3^- 0,0,z$            |         |                            |         |
| (4) $2(0,0,\frac{1}{2})$ | $0,0,z$         | (5) $6^-(0,0,\frac{1}{2})$ | $0,0,z$ | (6) $6^+(0,0,\frac{1}{2})$ | $0,0,z$ |
| (7) $m \ x, \bar{x}, z$  |                 | (8) $m \ x, 2x, z$         |         | (9) $m \ 2x, x, z$         |         |
| (10) $c \ x, x, z$       |                 | (11) $c \ x, 0, z$         |         | (12) $c \ 0, y, z$         |         |

**Generators selected** (1);  $t(1,0,0)$ ;  $t(0,1,0)$ ;  $t(0,0,1)$ ; (2); (4); (7)**Positions**

| Multiplicity,<br>Wyckoff letter,<br>Site symmetry | Coordinates                             |   |  |                               |                                      |                          | Reflection conditions  |
|---|---|---|--|-------------------------------|--------------------------------------|--------------------------|--|
| 12 $d$ 1  | (1) $x, y, z$                           | (2) $\bar{y}, x - y, z$                     | (3) $\bar{x} + y, \bar{x}, z$                |                               |                                      |                          |  |
|   | (4) $\bar{x}, \bar{y}, z + \frac{1}{2}$ | (5) $y, \bar{x} + y, z + \frac{1}{2}$       | (6) $x - y, x, z + \frac{1}{2}$              |                               |                                      |                          | $hh\bar{2}\bar{h}l: l = 2n$                                  |
|   | (7) $\bar{y}, \bar{x}, z$               | (8) $\bar{x} + y, y, z$                     | (9) $x, x - y, z$                            |                               |                                      |                          | $000l: l = 2n$   |
|   | (10) $y, x, z + \frac{1}{2}$            | (11) $x - y, \bar{y}, z + \frac{1}{2}$      | (12) $\bar{x}, \bar{x} + y, z + \frac{1}{2}$ |                               |                                      |                          |  |
| 6 $c$ . $m$ .                                     | $x, \bar{x}, z$                         | $x, 2x, z$                                  | $2\bar{x}, \bar{x}, z$                       | $\bar{x}, x, z + \frac{1}{2}$ | $\bar{x}, 2\bar{x}, z + \frac{1}{2}$ | $2x, x, z + \frac{1}{2}$ | General:<br>no extra conditions                              |
| 2 $b$ $3m$ .                                      | $\frac{1}{3}, \frac{2}{3}, z$           | $\frac{2}{3}, \frac{1}{3}, z + \frac{1}{2}$ |  |                               |                                      |                          | $hkil: l = 2n$<br>or $h - k = 3n + 1$<br>or $h - k = 3n + 2$ |
| 2 $a$ $3m$ .                                      | $0, 0, z$                               | $0, 0, z + \frac{1}{2}$                     |  |                               |                                      |                          | $hkil: l = 2n$   |

**Symmetry of special projections**Along [001]  $p6mm$ 

$$\mathbf{a}' = \mathbf{a} \quad \mathbf{b}' = \mathbf{b}$$

Origin at  $0, 0, z$ Along [100]  $p1g1$ 

$$\mathbf{a}' = \frac{1}{2}(\mathbf{a} + 2\mathbf{b}) \quad \mathbf{b}' = \mathbf{c}$$

Origin at  $x, 0, 0$ Along [210]  $p1m1$ 

$$\mathbf{a}' = \frac{1}{2}\mathbf{b} \quad \mathbf{b}' = \frac{1}{2}\mathbf{c}$$

Origin at  $x, \frac{1}{2}x, 0$ FIGURE 2.16: Pages 584-585 (compressed here) of *International Tables for Crystallography, Volume A* [Hah96] describing the space group  $P6_3mc$ .

- The *Position* tables contains the symmetrically equivalent points in the crystal system divided between the general positions in the first block followed by the special positions blocks underneath. The general position is left invariant by the identity operator but no other symmetry operation of the space group, while the special positions are left invariant by at least one other symmetry operation in addition to the identity. All the symmetry operations that map a point onto itself form together a *site symmetry* group for that position given in the third column of the table. The coordinates for the general position,  $(i)x', y', z'$ , are the result of a symmetry operation  $(i)$  on the most general position  $x, y, z$ . These can also be viewed as a shorthand notation of the symmetry matrices of the group. The numbers in the first column indicate the number of equivalent points per unit cell or the *multiplicity* of the position. For the general position the multiplicity is the number of symmetry operators, while for the special positions each added site symmetry reduces the multiplicity by the order of symmetry. For instance, the second positions entry shows a mirror site symmetry which halves the multiplicity of the point to 6. The *Wyckoff letters* are labels for the Wyckoff positions, which in turn are a way of describing the positions of the atoms in the asymmetric unit. The last column in this table, entitled *reflection conditions*, is a list of diffraction information given as requirements for the structure factor to not be zero (conditions of occurrence) for the given position.
- The last section shown here is the *Symmetry of special projections* which contains two dimensional projection information of the unit cell along lattice directions. If the wurtzite unit cell is projected along the  $[100]$  direction, then the resulting 2D object will have **p6mm** plane group symmetry and will be defined by the unit vectors  $\mathbf{a}'$  and  $\mathbf{b}'$  which in general are expected to be fractions of linear combinations of the original basis vectors. The origin of the 2D unit cell is also specified.

An account of crystal symmetry would be incomplete without referencing the *International Tables for Crystallography*. Now that we know how to read the *Tables* we can just read out the results of many of the derivations we've done in the *Symmetry in Crystallography* section. In the following, we will explore the symmetries of **P6<sub>3</sub>mc** space group starting from the information tabulated in these pages.

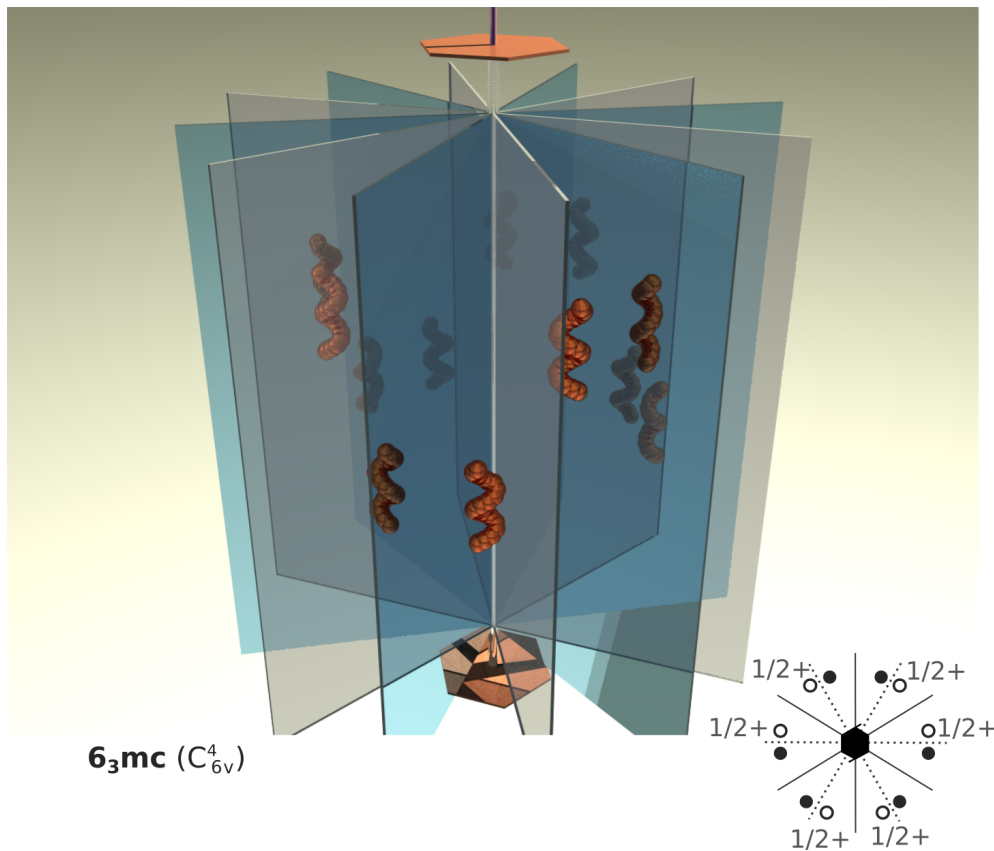


FIGURE 2.17: Graphical 3D representation of the **6<sub>3</sub>mc** symmetry combination together with the 2D projection in the bottom right corner (filled circles indicate the object is in the plane of the drawing, open circles indicate the object is above the plane at the indicated height).

### The P<sub>6</sub><sub>3</sub>mc space group

Let us consider the space group **P<sub>6</sub><sub>3</sub>mc**. If we start with the primitive hexagonal Bravais lattice *hP* and add the **6mm** point group at every lattice point we obtain the **P6mm** space group. But we can generate a group with a different symmetry if we replace the **6** symbol in the point group with a  $6_3$  screw axis operation and the second **m** with a glide plane **c** in the direction of basis vector **c**. The resulting symmetry group **6<sub>3</sub>mc** is shown in Fig. 2.17. The blue planes are the mirror planes and the white planes represent the glide planes. As before, the generating files can be found in **6\_3mcPNG.ray** for the **\*.png** image and **6\_3mcGIF.ray** for the **\*.gif** animation. The dotted lines represent a glide plane with translation normal to the drawing plane.

Note that this combination does not make up a point group as it does not present unique symmetry. However, when combining the **6<sub>3</sub>mc** symmetry with the hexagonal

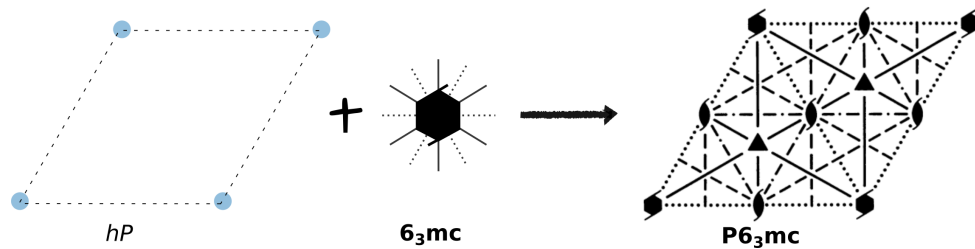


FIGURE 2.18: Top view construction of space group **P6<sub>3</sub>mc** from the Bravais lattice **hP** combined with the symmetry combination **6<sub>3</sub>mc**. [Right image taken from Fig. 2.16.]

TABLE 2.11: The **P6<sub>3</sub>mc** space group with its corresponding number and crystallographic point group.

| Space group # | Point group | Symbol                  |
|---------------|-------------|-------------------------|
| 186           | 6mm         | <b>P6<sub>3</sub>mc</b> |

primitive Bravais lattice it generate the brand new space group **P6<sub>3</sub>mc** as illustrated in Fig. 2.18. One can find the corresponding point group of a space group containing glide planes or screw axes (non-symmorphic) by simply replacing the glide planes by mirrors and the screw axes by regular rotations. We show in Table 2.11 the corresponding crystallographic point group together with the space group number as it is indexed in the *International Tables for Crystallography*. It is interesting to note that the external shape of a **6<sub>3</sub>mc** space group crystal is given by its corresponding point group symmetry.

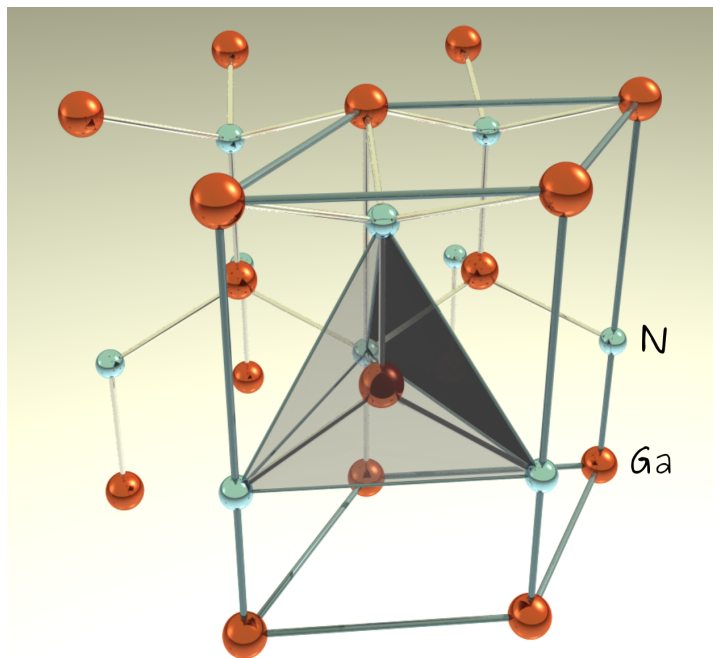


FIGURE 2.19: 3D render of wurtzite crystal structure hexagonal unit cell, together with the hexagonal primitive cell ( $hP$ ) enclosed by blue edges and the tetrahedral asymmetric unit cell enclosed by glass faces.

## 2.4 Wurtzite crystal structure

It is customary to describe a crystal structure by its space group, lattice parameters and atom positions in the asymmetric unit cell.

## 2.5 Electron scattering

Before we can talk about diffraction we need to address the phenomena of scattering. Classically, the collision of particles is fully defined by their velocities and interaction parameters. However, high energy electrons are quantum mechanical objects. The notion of defined path for particles with known velocity is meaningless in the quantum mechanical world. Instead, we are interested in defining the probability that, as a result of the collision, the particle will deviate by a given angle. We call this *scattering*.

Electrons are small charged particles that will suffer multiple scattering events even in thin samples in contrast to X-ray and neutron interactions with matter. Electron scattering in a solid is a complex multi dimensional problem. For practical considerations it is common to classify the interaction of electrons with a crystal in two distinct processes:

- *Elastic scattering*, defined as a process which does not change the state of the crystal. Mostly made up by interactions with the nucleus: Rutherford scattering taking into account just Coulomb forces between the charged electron and the nucleus. This account for most of the angular scattering.
- *Inelastic scattering*, defined as the process in which the state of the crystal is modified by the interaction. Important contribution here is made by the electron-electron scattering which cause the incident beam electron to loose small amounts of energy but cause relatively little angular deflections.

### 2.5.1 Elastic scattering

Elastic collision reduces, in the quantum mechanical world, to the interaction of a free particle interacting with a fixed potential field  $U(\mathbf{r})$ .

#### Rutherford scattering

### 2.5.2 Inelastic scattering

#### Bethe's equation

### 2.5.3 The rest of the story

To be very technical we have to make the disclaimer that no electron scattering event is ever purely zero energy. Any interaction will transfer some energy from the electron to the atom. However since the mass ratio is small, the energy transfer is very small as

well and quantum mechanically if the energy to be transferred is below the first excited energy level of the atom then no energy is transfer and the scattering is truly elastic.

## 2.6 The scanning electron microscope

# 3 Diffraction

## 3.1 A word on *channelling*

Centuries after the decline of the Western Roman Empire, the allure of power and honour brought by the title of Roman Emperor was undiminished. While Irene of Athens, a female, was occupying the Roman throne, the pope crowned the king of Franks, Charlemagne, as Holy Roman Emperor – a new title Charlemagne found nifty enough to add to his already significant collection. But, as Voltaire reflected later on, the title, while maintained for an impressive span of a thousand years, bared little practical significance: “[...] *the Holy Roman Empire was neither holy, nor Roman, nor an Empire*”. The title persisted even though the territory was not unified in religion and one of the emperors was even excommunicated by the pope. Rome was not by any stretch of imagination the centre of the *Holy Roman Empire*, in fact Italy eventually stopped being part of the empire with no effect on the Empire designation. While its border continued to change, the Holy Roman Empire was consistently made up of Germanic nations. Additionally, Latin was not a popular language across the territories. Finally, unlike the Roman Empire, the Holy Roman Empire was hardly an empire in the sense of unitary legal entity and the absolute power the emperor would hold over its territories. Yet, the name prevailed, despite it being a gross misnomer<sup>1</sup>, perhaps even an anachronism.

When it comes to the SEM techniques, their labels are also not terribly accurate. Some keep insisting calling the transmission diffraction mode in the SEM - transmission electron backscattered diffraction (t-EBSD), apparently oblivious to the oxymoron in the association. But, perhaps even more confusing, is the fact that, while some techniques carry in their name the type of electron interaction that generates the signal, EBS-Diffraction, TK-Diffraction, others do not. Electron channelling patterns (ECP) and electron channelling contrast imaging (ECP) misleads the inexperienced reader to assume that the source of signal is fundamentally different, that in fact *channelling*

---

<sup>1</sup>Here is another classic example: the Jerusalem artichoke is the root of a North American plant, in the sunflower family – the name is probably a corruption of the Italian for “sunflower”, *girasole*.

might be the type of interaction to blame. These labels are the “Holy Roman Empire” of electron microscopy.

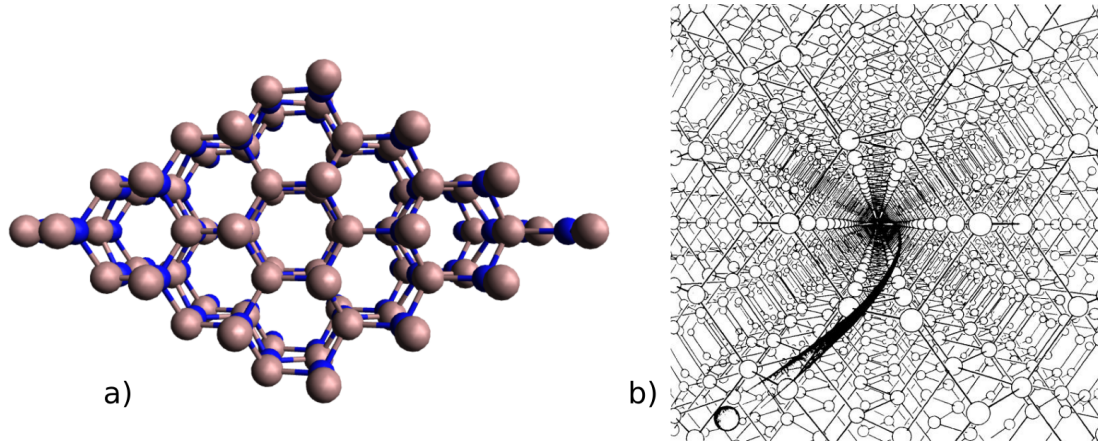


FIGURE 3.1: a) Open “channels” between rows of atoms along the main direction [0 0 1] in GaN – *not* responsible for what is sometimes called electron “channelling”. b) Artist’s impression of channelling of heavy charged particles, from [Bra68].

These two SEM techniques carry the word *channelling* for historical reasons. In early 1960s, before electrons became widely used in high resolution microscopy, it was observed that the penetration depth of ions in crystalline materials would depend on their incident direction [Dav83]. It became apparent that an incident ion beam aligned along any of the major axes of the crystal would yield longer penetration depths [Pie+63]. This was initially explained as simple geometrical transparency, *i.e.*, columns of empty space along major axes as shown in Fig. 3.1 a), such that the ions would simply suffer less scattering on their path as shown in the beautiful artist render in Fig. 3.1 b) hence the name *channelling*.

Based on these observations, Linhard [Lin65] developed a classical mechanics explanation that required the incident particles to have small and incoherent wavelengths such that interference patterns would be absent. He then went on to establish an upper limit for stable channelling for the incidence angle relative to a major direction he called the *critical channelling angle*:

$$\phi_{chan} \leq \sqrt{\frac{2Ze^2}{Ed}} \quad (3.1)$$

It was soon observed that the channelling extends to other charged particles like high energy protons [Dea+68].

## 3.2 Introduction

In the previous chapter we have dusted up the tool-kit we'll need to tackle diffraction. This section deals with the theoretical formalism of electron diffraction and its predictions when applied to group III nitride compounds.

Historically, diffraction is associated with X-rays, and we will end up using the parts of the theories developed for X-rays diffraction when talking about electron diffraction. While the phenomenon is described by the same Physics regardless of the type of particles used, the way individual diffracting particles interact with matter can differ. While X-rays diffract from the electron density in the crystal, electrons are scattered elastically by the Coulomb potential. The latter is related to the electron density via the Poisson equation and, additionally, it also includes the nuclear contributions. Similarly, neutron interact only with the nuclear potentials in the crystal sample. Table 3.1 shows the properties of the most common types of particles used in diffraction experiments together with their scattering sources.

TABLE 3.1: Particles used in diffraction experiments together with their scattering properties.

| Particle     | $\lambda$ [nm] | Charged? | Scattering object             |
|--------------|----------------|----------|-------------------------------|
| X-ray photon | 0.01 – 1.0     | no       | electron density distribution |
| neutron      | $\sim 0.1$     | no       | atomic nuclei distribution    |
| electron     | 0.1 – 0.001    | yes      | atomic potential distribution |

Compared to X-rays, electrons are scattered much more strongly by matter and have shorter wavelengths. This means that electrons convey information about much smaller crystal volumes than conventional X-ray microscopy, in other words better spatial resolution. It also means that while we can ignore a good portion of the interaction of X-rays with matter, resulting in a relatively straightforward geometrical understanding of diffraction intensities, we need to take into account the fact that electrons will lose energy and coherence on their paths through the sample leading us to the usage of the dynamical theory for the prediction of scattered intensities.

We have already made the note that diffraction is chiefly related to the wave behaviour of small particles like photons, electrons or neutrons. This behaviour is mathematically written in the form of a Bloch wave  $\psi(\mathbf{r})$  whose squared amplitude,  $|\psi(\mathbf{r})|^2$ , describes the probability density of finding the particle at position  $\mathbf{r}$ . In layman terms, diffraction is the phenomena of directional scattering arising as constructive interference along certain directions and destructive interference along others. From the intensity of the interfering waves one can derive information on the spatial distribution

of the scattering centres and we will see how that relates to directional elastic scattering. We will talk chiefly about the crystal planes which dictate the Bragg scattering direction, or as we will call it here, the *geometrical diffraction factor*. However, it will always be implied, that in addition to Bragg diffraction, we must take into account diffraction from individual atoms, which in turn will favour certain directions more than others.

We will be covering some of the theoretical aspects of diffraction in this section. For a thorough and in-depth description of diffraction and its application in crystallography we suggest the reader to find a copy of the *International Tables of Crystallography Volume B: Reciprocal space* [Aut06; Cow+06].

### 3.3 Short historical overview

Soon after systematically experimenting with generating what will end up being known in the English languages as *X-rays*, the German physicist Wilhelm Röntgen used this new form of high energy radiation to “take a picture” of his wife’s hand. To everyone’s amazement the picture taken in 1895 showed the bones of her hand wearing her wedding ring. While the medical applications of X-rays are impressive in their own right, a material scientist will claim that the best application of X-rays was yet to come.

Not even twenty years later, another German physicist, Max von Laue, decided to use this new radiation, which he’d probably called Röntgen rays, to “take a picture” of a crystal. He actually had a good reason to try that. Von Laue expected the wavelength of these radiations to be of the same order of magnitude as the distance between atoms in matter. If this criterion is met then the wave behaviour of the radiation will suffer constructive interference along directions dictated by the crystal lattice planes. What he observed in his image was a series of ordered spots which would end up telling a story about the particular ordered arrangement of the crystal atoms. From here on things move rather quickly. Table 3.3 shows a quick overview over about a hundred years of historical events building to the development of electron diffraction techniques.

It is interesting to notice the interplay between experimental observations and theoretical predictions in the development of diffraction as a field. The observation of X-ray diffraction supported, first of all, the controversial wave-like behaviour of particles narrative, and, second of all, the description of crystalline materials as periodic lattice structures. It also lead to the development of Bragg’s law. Moreover, since the

theory of space group symmetry had already been developed by the Russian crystallographer E. S. Fedorov, X-ray diffraction quickly became the structure analysis tool of choice of crystallography.

While Bragg's law was good enough to explain the geometry of the diffraction spots, it proved inconsistent in predicting experimental X-ray diffraction intensities. This lead C. G. Darwin to develop a first form of dynamical diffraction theory. He took into account the interaction of X-rays with matter as partially transmitted and partially reflected amplitudes at each lattice plane. His theory predicted correct values for the reflected intensities. Later, in 1917, P. P. Ewald [Ewa17] introduced a new form of dynamical theory in which he considered the crystal to be a periodic distribution of dipoles excited by the incident wave. The new theory predicted both transmitted and reflected intensities.

There were still limitations in the dynamical theories. In 1930, J. A. Prins [Pri30] modified Darwin's theory to take into account the fact that the crystal is an absorbing medium. Just a year later, in 1931, von Laue [Lau31] showed that the interaction in Ewald's theory can be described by solving Maxwell's equations in a continuous medium with dielectric susceptibility distributed periodically in three dimensions. It is in this form that the dynamical diffraction theory is most used today and also the one we will use in this work.

The inverse effect was triggered by de Broglie's doctoral thesis in which he speculates that all particles ought to also behave as waves. The discovery of the remarkable phenomena that is electron diffraction provided the experimental means for the development of quantum mechanics. It soon became apparent that the diffraction theory must again be expanded to account for the more complex electron interaction with matter. Indeed, a number of dynamical theories for electrons have been developed over the years all carrying the legacy of X-ray diffraction theoretical interpretations.

Electrons diffracting through crystals proved to give access to a plethora of information. That access was made widely available with the development of the electron microscope; first the direct mode in which the electron penetrated through a sample and the image was collected on the other side (TEM) and, later, the scanning mode, in which the incident electron beam scans over the sample in a raster manner and the image is recorded one "pixel" at a time (SEM). The diffraction spots observed in the TEM or when at a grazing incidence angle in the SEM (both conditions in which the crystal volume with which the electron beam interacts is small enough to approximate the behaviour to kinematical diffraction) were identified to be related to the crystal structure. The electron channelling patterns (ECP) observed in the SEM could tell about the bulk crystal orientation. If the detector is placed in the SEM such that mostly forward

TABLE 3.2: Partial chronology of the history of diffraction.

| Year   | Event  |
|--------|--|
| 1912   | First X-ray diffraction experiments by W. Friedrich, P. Knipping and M. von Laue [FKL12].  |
| 1913   | Bragg family derives their name bearing law [BB13] to describe the geometry of diffraction spots.  |
| 1914   | C. G. Darwin [Dar14] derives the first dynamical theory for the intensities of the diffraction spots.  |
| 1924   | L. de Broglie hypothesises that particles should also behave as waves.   |
| 1927   | Independently, G. P. Thomson [TR27] at the University of Aberdeen and C. J. Davisson and L. H Germer [DG27] at the Bell Labs, observe low energy electron diffraction spots through thin films.  |
| 1928   | H. Bethe [Bet28] use eigenvalue equations to explain and predict intensities in electron diffraction images.   |
| 1928   | First electron diffraction patterns is recorded by S. Nishikawa and S. Kikuchi [NK28] from grazing incidence geometry and is described as “black and white lines in pairs due to multiple scattering and selective reflection”.  |
| 1931-4 | E. Ruska and M. Knoll [KR32] build the first electron microscope (EM), later known as a direct or transmission EM (TEM).   |
| 1935-8 | M. Knoll suggests the idea of a scanning EM (SEM). M. von Ardenne [Ard38] constructs the first one.  |
| 1961   | A. Howie and M. J. Whelan [HW61] expands Darwin’s theory to develop a simultaneous differential equation form for electron diffraction applicable for predicting diffraction contrast.   |
| 1960-5 | P. B. Hirsch and co-workers at Cambridge [HHW60; Hir+65] develop the theory of electron diffraction contrast which can be used to identify line and planar defects in thin films in TEM images.  |
| 1967   | D. G. Coates [Coa67] observes electron diffraction patterns in the SEM later labelled electron channelling patterns ( <b>ECPs</b> ).   |
| 1967   | G. R. Booker [Boo+67] provides a theoretical interpretation for the phenomena based on the Darwin-Howie-Whelan theory. He also notices that the backscattered intensity varies rapidly with orientation close to Bragg condition, which will develop in a new technique of its own known as electron channelling contrast imaging ( <b>ECCI</b> ). |
| 1973   | J. A. Venables and C. J. Harland [VH73] describe another diffraction technique capable of providing local crystallographic information termed electron backscattering patterns ( <b>EBSP</b> ) or latter electron backscattered diffraction ( <b>EBSD</b> ).   |
| 2012   | The latest diffraction technique in the SEM with improved spatial resolution compared to EBSD is reported as transmission EBSD ( <b>t-EBSD</b> ) by R. R. Keller and R. H. Geiss [KG12] and Transmission Kikuchi Diffraction ( <b>TKD</b> ) by P. W. Trimby [Tri12].   |

scattered electrons are collected, then one can obtain Kikuchi lines (EBSD) from a very small crystal volume or, in the language of microscopy, high spatial resolution.

If the geometry was such that the incident beam was close to a Bragg condition, high contrast around small crystallographic defects could be observed in the recorded images, a technique which will be known as electron channelling contrast imaging (ECCI). The theories developed by this point could be extended to even take into account such small phase perturbations and predict correct contrast profiles for dislocations observed in ECCI.

Even for far from perfect crystals electron diffraction could provide great insight. By scanning over a micro-granular crystal in the SEM and recording the EBSD image for each pixel, one could pick up the orientation of individual grains using orientation indexing techniques. In the world of material science this was extremely powerful as tool of mapping the quality of a new material. A number of companies focused on developing modern SEMs packaged with indexing software appeared and experienced reasonable success catering to the industry's requirements. Unfortunately, it also marked the steady decline of academic interest in open electron diffraction software.

### 3.4 Kinematical versus dynamical theory

The geometrical or kinematical diffraction theory, developed for X-rays, assumes that each incident wave is scattered only once in the sample and all other interactions can be ignored. This, in turn, implies that 1) the amplitude incident on each of the diffraction centres is the same and 2) the sum of the diffracted amplitude is the sum of individual amplitudes diffracted by each diffraction centre. Therefore, the geometrical phase difference between diffracted beams is the main contributor to the diffraction pattern and the distribution of diffracted amplitudes in reciprocal space is the Fourier Transform of diffraction centres in real space.

The integrated elastically scattered intensities predicted by the kinematical theory are proportional to the square of the structure factor and also with the crystal volume with which the incident wave interacts. Because no loss of amplitude is taken into account, the kinematical theory predicts that as the interaction crystal volume increases to infinity so would the intensity of the diffracted beam. This is obviously nonsensical for anything but very small crystals. We can conclude that kinematical approach holds well only for relatively weak interactions (X-ray interaction with matter) and/or small crystals. Darwin [Dar22] extended this theory and showed it can also be applied to large but defected crystals. Additionally, there is no phase information tracked in the kinematical theory and this becomes important for multiple reflections.

TABLE 3.3: Kinematical vs. dynamical diffraction theories.

| Kinematical theory                      | Dynamical theory                   |
|---|------------------------------------|
| weak interaction                        | strong interaction                 |
| small crystal OR large defected crystal | infinite crystal                   |
| single scattering                       | multiple scattering “pendellösung” |
| assumes no loss                         | takes loss into account            |
| no phase information                    | carries information about phase    |
| intensity $\propto  F_{hkl} ^2$         | intensity $\propto  \psi_g ^2$     |

Electrons manifest wave properties similar to those of X-ray and their diffraction behaviour in crystals is in many ways analogous to that of X-rays. Nevertheless, it should be obvious by now to the careful reader that the single scattering approximation of the kinematical theory will not be suitable for the strong interactions of electrons in crystals composed of more than a few layers. For this reasons the dynamical diffraction theory for fast electrons has been developed and applied to qualitatively interpret electron diffraction patterns.

## 3.5 Applications and limitations

X-ray diffraction intensity is conveniently described the Fourier transform of the electron density of the crystal. This makes X-rays a great tool for structural determination. [other x-rays application]

1929 The younger W. L. Bragg was responsible for the first crystal structural determination using X-rays diffraction. The Bragg family used X-ray diffraction to infer electron density maps of crystalline solids.

While, in theory, electron diffraction is not completely unlike that of X-rays and electrons can be used for crystal structure determination, in practice X-rays diffraction dominate this field. [LEED]

## 3.6 Diffraction geometry

Having set the context of diffraction as a means of identifying the crystal structures of elements and compounds, we will explore the governing rule of the phenomena, that of the Bragg's law. In this section we are going to make use of the mathematical form of plane waves and their Fourier transform.

### 3.6.1 Bragg's law in real space

Consider the drawing in Fig. 3.2. A plane wave of wavelength  $\lambda$  and wave vector  $\mathbf{k}$  is incident with incidence angle  $\theta$  on a set of parallel plane with Miller indices  $(h k l)$ . The planes are partially transparent and partially reflective, such that the reflected beams together with the incident ones and the normal to the planes are coplanar. We ask the question: “*What is the condition that two reflected plane waves (1) and (2) will be in phase?*”. The answer is straightforward. The path difference between waves (1) and (2), shown in orange, must equal an integer number of wavelengths [BB13]:

$$2d_{hkl} \sin \theta = n\lambda.$$

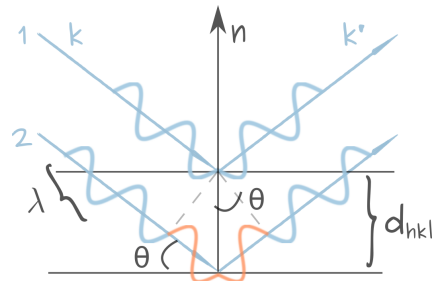


FIGURE 3.2: Geometrical representation of Bragg's equation in real space. The path difference of the reflected plane wave (2) with respect to (1) is shown in orange.

Please note that Fig. 3.2 is a planar section of the diffraction geometry. The diffracted beam  $\mathbf{k}'$  will travel in a direction contained by a conical surface of opening angle  $\pi/2 - \theta$  centred around the plane normal. For every plane  $(hkl)$  in a crystal there will be a conical surface of diffracted beams, with parameters determined by the inter-planar spacing  $d_{hkl}$  and the radiation wavelength  $\lambda$ .

In common practice we will only consider first order diffraction; instead of talking about  $n$  order diffraction from planes  $(hkl)$  we will talk about first order diffraction from planes  $(nhnl)$ . The reader will recall that the planes with Miller indices  $(nhnl)$  are parallel to the planes  $(hkl)$  but with an inter-planar spacing given by  $d_{nhnl} = d_{hkl}/n$ . The version of Bragg law used in diffraction is then:

$$2d_{hkl} \sin \theta_B = \lambda. \quad (3.2)$$

The angle  $\theta$  for which constructive interference occurs is known as *Bragg angle*,  $\theta_B$ . Table 3.4 shows the Bragg angles for 20 kV electrons diffracting from common wurtzite crystal planes (shown in Fig. 2.9). Recall that the formula for inter-planar spacing in hexagonal unit cells is given in Eq. 2.26.

TABLE 3.4: Bragg angles for the most common planes in wurtzite materials for 20 keV incident electrons.

| planes  | (hkl) | $d_{hkl}$     | $AlN\theta_B$ | $GaN\theta_B$ | $InN\theta_B$ |
|---------|-------|---------------|---------------|---------------|---------------|
| m-plane | (100) | $\sqrt{3}a/2$ | $2.74^\circ$  | $2.67^\circ$  | $2.42^\circ$  |
| c-plane | (001) | $c$           | $0.49^\circ$  | $0.47^\circ$  | $0.43^\circ$  |
| a-plane | (110) | $a/2$         | $1.58^\circ$  | $1.54^\circ$  | $1.39^\circ$  |

Note that while the Bragg equation describes the geometric condition for diffraction, as constructive interference, to occur it does not, however, provide any information on the intensity (if any) of the diffracted beam. The real space form of this equation is only useful in determining the Bragg angles for a given wavelength and crystal structure as we have done here. More useful is the study of the direction of the diffracted beam for a given crystal structure which require the expression of some reference frame. In order to tackle this problem, it is common to express the Bragg equation to the reciprocal reference frame and introduce the Ewald sphere as we will do in the next section.

### 3.6.2 Bragg's law in reciprocal space

## 3.7 Diffraction intensity

We have explored the relationship between the geometry of the diffraction pattern and the crystal planes responsible for diffracting the beam of particles. Bragg's law remains the same for photons, electrons or neutrons even if the Bragg angles can vary greatly depending on the energy of the incoming beam. We will now introduce the scattering physics that is highly sensitive to the type of particle interaction and the precise geometry arrangement of atoms in the lattice. Clearly, very different unit cells made of different atoms can exhibit similar lattice planes geometries and we could naively predict similar diffraction pattern geometries. However, we will see that even when Bragg's conditions are satisfied the intensity of diffraction beam can be zero.

When it comes to studying the intensity distribution on the diffraction pattern, things get a bit more involved. In order to understand how a lattice potential scatters a beam of electrons we must first take a closer look at how the electron cloud, then a single atom and then a unit cell scatter the incident beam. In the process we will introduce the useful mathematical concept of *structure factor* which describes how the positions of the atoms in the unit cell affect the intensity of the diffracted beam.

### 3.7.1 Electrostatic lattice potential

We have previously talked about the interaction of a beam of high energy electrons with a crystalline sample as being mathematically represented in the Schrödinger's equation by the electron interaction with the sample's electrostatic Coulomb potential  $V(\mathbf{r})$ . Finding the correct potential for a given crystalline structure is a fundamental problem in solid-state physics usually tackled by so-called first principles methods. These methods are notoriously expensive when solving even small systems since they aim to provide a solution for the many body problem that is the electron-electron interaction of the crystal structure. Fortunately for electron microscopists, the high energy of the incoming beam simplifies the crystal to the behaviour of isolated spherical point scatterers, represented by *atomic scattering factor*  $f^e(\mathbf{s})$ .

#### X-ray scattering by electron charge density and the X-ray scattering factor

When a linearly polarised, monochromatic plane-wave X-ray beam is incident upon a stationary atom of atomic number  $Z$ , each of its  $Z$  electrons will scatter the X-ray

waves. The oscillating electric field of the incident X-ray excites the individual electrons of mass  $m$  and charge  $e$  causing them to oscillate at the same frequency as the incident radiation. In turn, the individual electrons, now in the form of accelerated charge, will become a source of spherically radiated X-rays of frequency equal to the incident one. Multiple scattering processes can occur including incoherent scattering or Compton processes but for now we will only consider coherent scattering.

The intensity of a scattered radiation at a distance  $r$  from the scattering site of the individual electrons in terms of the incident radiation intensity  $I_0$  and the scattering angle  $\theta$  is well described by Thomson's equation:

$$I = I_0 \frac{K}{r^2} \sin^2 \theta, \quad (3.3)$$

which highlights the high directionality of coherent scattering. That is to say, most of the intensity of scattered X-rays will be in the forward direction. In the above equation  $K$  is a very small constant given by:

$$K = \left( \frac{\mu_0}{4\pi} \right)^2 \times \left( \frac{e^4}{m^2} \right) = 7.9 \times 10^{-30} \text{ m}^2$$

indicating that in practice scattering effects can become measurable only when a large number of electrons ( $> 10^{23}$ ) are scattering.

In the forward direction, each of the  $Z$  electrons will scatter the X-rays beam with an identical phase change of  $\pi$  and no destructive interference (see Fig. 3.3 a)). Scattering in any other direction,  $\theta \neq 0$ , will result in pathway differences between X-rays scattered by different electrons. The loss of intensity due to destructive interference will translate to a reduced scattered intensity when compared to the forward scattered case (see Fig. 3.3 b)).

It is now time to introduce the atomic scattering factor,  $f^X$ , for a given direction  $\theta$  and wavelength  $\lambda$  as the ratio of amplitude scattered by an entire atom to the amplitude scattered by only one electron in the same direction. Equivalently, the atomic scattering factor can be thought of as the probability amplitude that the atomic potential of an atom will scatter an incident wave with wave vector  $\mathbf{k}_0$  into the direction  $\mathbf{k}'$ .

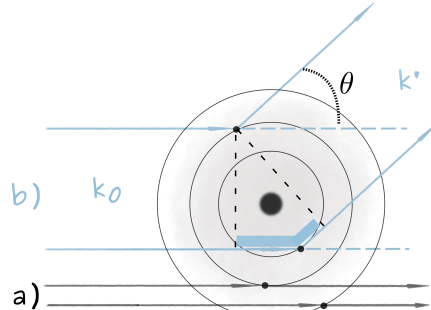


FIGURE 3.3: Schematic diagram of a) forward scattering and b) scattering by an angle  $\theta$ . Note the pathway difference marked by thick blue line in b).

But this probability is the Fourier transform of the atomic potential that does the scattering, which in the case of incident X-rays is the electron charge density [Aut06]. The “International Tables of Crystallography” contain tabulated calculated scattering intensity values for all atoms. Since it would be tedious to list the scattering factor values for all possible  $\theta$  and  $\lambda$ , it is often more convenient to list them as curve fitting parameters. The scattering factor fitted function as a function of the variable  $s = \sin \theta / \lambda$  is then given by:

$$f^X(s) = Z - 41.78214 s^2 \sum_{i=1}^N a_i e^{-b_i s^2} \quad (3.4)$$

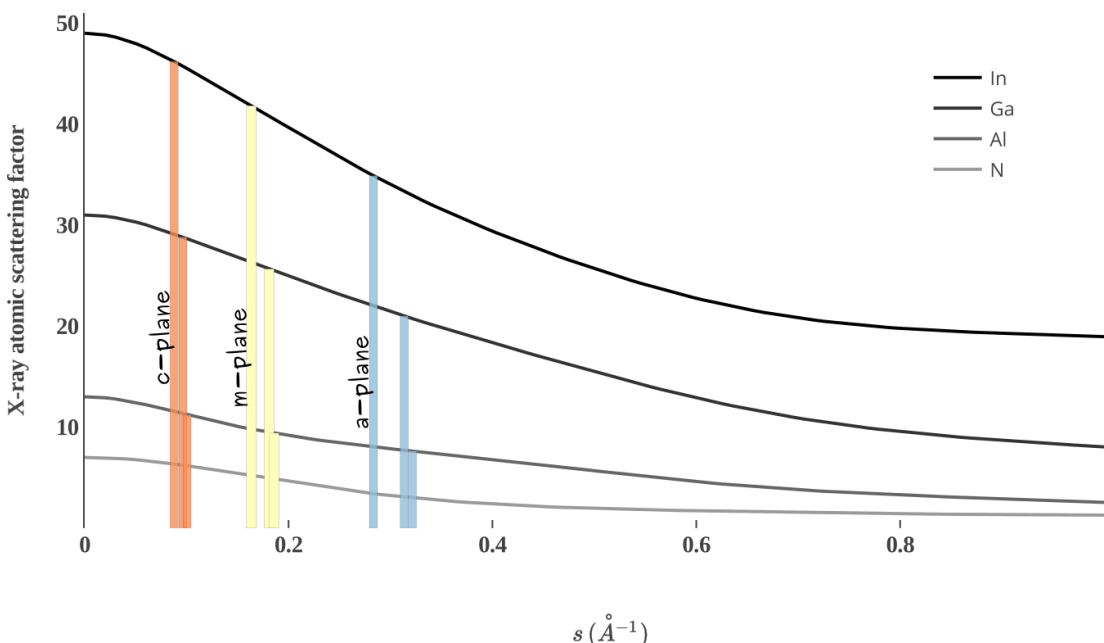


FIGURE 3.4: Atomic X-ray scattering factors for In, Ga, Al, N with superimposed coloured lines indicating the most common planes for InN, GaN and AlN. Each coloured line reaches to the group III element which makes up the compound for which the computation was carried out. For instance, the first vertical line (orange), reaching the In line, represent the  $s$  value for the c-plane in InN.

Table 3.5 lists the Doyle-Turner [DT68]  $a_i, b_i$  parameters values ( $N = 4$ ) for a few group III-nitrides semiconductor elements: N, Al, Ga and In. Note that the values in the table are given assuming  $s$  is expressed in  $\text{\AA}^{-1}$  and  $\lambda$  is expressed in  $\text{\AA}$ .

The behaviour of the X-ray scattering factor is shown in Figure 3.4. The coloured lines indicate the  $s$  values for the most common planes in wurtzite materials (see Fig. 2.6). Note in the figure that the value for  $\theta = 0$  is indeed the atomic number, and

TABLE 3.5: Doyle & Turner atomic scattering parameters [DT68] for a few elements. These values were calculated assuming that  $s$  is expressed in  $\text{\AA}^{-1}$ .

| Element | Z  | $a_1$ | $b_1$  | $a_2$ | $b_2$  | $a_3$ | $b_3$ | $a_4$ | $b_4$ |
|---------|----|-------|--------|-------|--------|-------|-------|-------|-------|
| N       | 7  | 0.572 | 28.847 | 1.043 | 9.052  | 0.465 | 2.421 | 0.131 | 0.317 |
| Al      | 13 | 2.276 | 72.322 | 2.428 | 19.773 | 0.858 | 3.080 | 0.317 | 0.408 |
| Ga      | 31 | 2.321 | 65.602 | 2.486 | 15.458 | 1.688 | 2.581 | 0.599 | 0.351 |
| In      | 49 | 3.153 | 66.649 | 3.557 | 14.449 | 2.818 | 2.976 | 0.884 | 0.335 |

as expected, the curve decreases rapidly with increasing scattering angle (or decreasing wavelength). The code used for this plot can be found in the Jupyter notebook `scatterFactor.ipynb`.

### Electron scattering by individual atom and the electron scattering factor

As far as the incoming electron beam is concerned, the electrostatic potential  $V_{atom}(\mathbf{r})$  of one atom in the specimen is related to its spherically symmetric charge distribution through Poisson's equation:

$$\Delta V_{atom}(\mathbf{r}) = -\frac{|e|}{\epsilon_0} (\rho_n(\mathbf{r}) - \rho_e(\mathbf{r})), \quad (3.5)$$

where  $\Delta$  is the Laplacian (second order differential) operator. It will contain a contribution from the point charge nucleus  $\rho_n$  and a contribution from the electron cloud charge distribution  $\rho_e$ .

This does not take us very far since analytical solutions for the electron charge density can only be written for hydrogen. Luckily, the X-ray scattering amplitude calculated on the previous page (Eq. 3.4) is the Fourier transform of the electron charge density  $\rho_r(\mathbf{r})$  so all that is left to do is to calculate the inverse Fourier transform of the X-ray diffraction amplitude.

We are now ready to define the atomic scattering factor for an electron beam  $f^e(\Delta\mathbf{k})$ , similarly to the case of an incident X-ray beam, as the probability that an incident plane wave with wave vector  $\mathbf{k}_0$  is scattered by the atomic potential  $V_{atom}(\mathbf{r})$  in the direction  $\mathbf{k}'$ . Where we introduced the momentum transfer vector  $\Delta\mathbf{k} = \mathbf{k}' - \mathbf{k}_0$ . Or, equivalently, we can write the probability as the Fourier transform of the atomic potential distribution  $V_{atom}(\mathbf{r})$ :

$$f^e(\Delta\mathbf{k}) \equiv \iiint V_{atom}(\mathbf{r}) e^{-2\pi i \Delta\mathbf{k} \cdot \mathbf{r}} d\mathbf{r} \quad (3.6)$$

Since the atoms studied are part of crystals we can use Bragg's condition,  $\mathbf{k}' = \mathbf{k}_0 + g$ . We will again make use of the useful variable transformation  $s = \sin\theta/\lambda$ , which at the Bragg angle has the magnitude:

$$|\mathbf{s}| = \frac{\sin\theta}{\lambda} = \frac{|\mathbf{g}_{hkl}|}{2} = \frac{1}{2d_{hkl}}. \quad (3.7)$$

Making the approximation that the nuclear charge density can be mathematically written as a delta function of weight  $Z$ , we are now ready to inverse Fourier transform all the quantities in Eq. 3.5 to obtain:

$$f^e(s) = \frac{|e|}{16\pi^2\epsilon_0|s|^2} [Z - f^e(s)]. \quad (3.8)$$

The reader might recognise equation 3.8 to be the Mott-Bethe formula. The use of the variable  $s$  defined in Eq. 3.7 means that for a given crystal structure the atomic scattering factor is only “sampled” at scattering vectors corresponding to half the reciprocal lattice vectors  $\mathbf{g}_{hkl}$ . It also means that, since for a given crystal structure the magnitude of  $\mathbf{s}$  is independent of the wavelength of electrons, the electron scattering factor is independent on the experimental conditions.

If we use the convenient Doyle-Turner parametrised form of the X-ray scattering factor given in Eq. 3.4 we can rewrite the Mott-Bethe formula to be:

$$f^e(s) = 0.04787801 \sum_{i=1}^{N=4} a_i e^{-b_i s^2}, \quad (3.9)$$

This expansion is accurate for values of  $s$  up to  $20 \text{ nm}^{-1}$ . Figure 3.5 plots the equation above and shows the electron scattering factor for the same elements as before. See the description for Fig. 3.4 on how to read the information in the figure. The code used for this plot can be found, as well, in the Jupyter notebook `scatterFactor.ipynb`.

### Scattering by the unit cell and the structure factor

#### Scattering by an infinite crystal

One way to write out an infinite lattice in math form is as a set of unit-weight delta functions located at the lattice points:

$$\mathcal{L}(\mathbf{r}) = \sum_{u,v,w} \delta(\mathbf{r} - \mathbf{t}_{uvw}) = \begin{cases} 1 & \text{if } \exists u, v, w \in \mathbb{Z} \text{ such that } \mathbf{r} = \mathbf{t}_{uvw} \\ 0 & \text{otherwise} \end{cases} \quad (3.10)$$

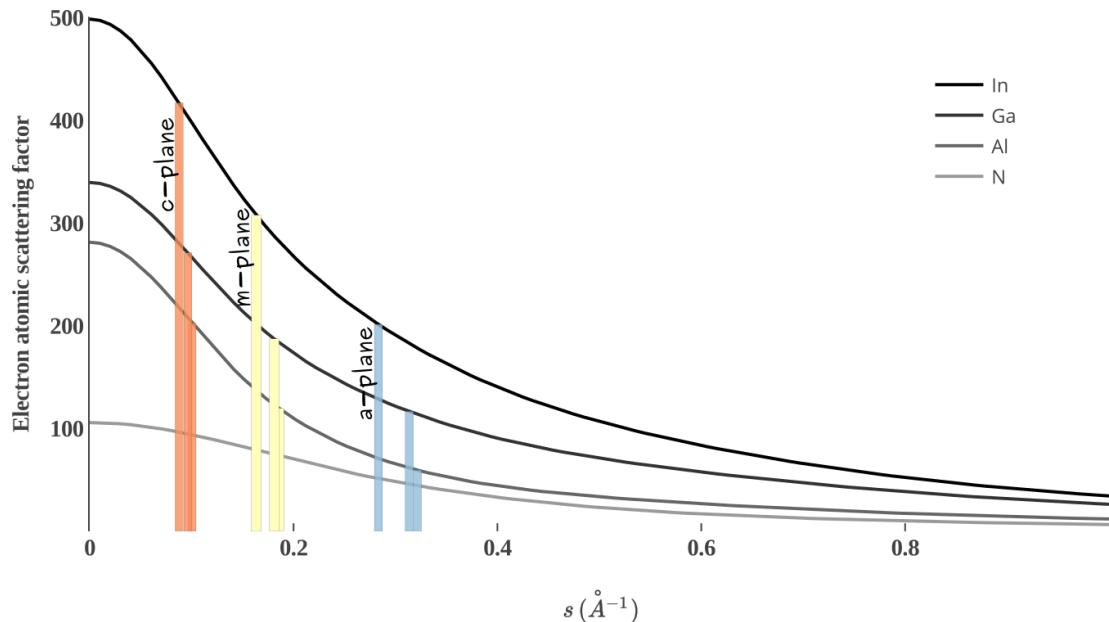


FIGURE 3.5: Atomic electron scattering factors for In, Ga, Al, N with superimposed coloured lines indicating the most common planes for InN, GaN and AlN (see Fig. 2.6). The scattering factor units are V Å<sup>3</sup>.

where  $\mathbf{t}_{uvw} = u\mathbf{a} + v\mathbf{b} + w\mathbf{c}$  is a lattice vector defined as a linear combination of the three lattice basis vectors  $\mathbf{a}, \mathbf{b}, \mathbf{c}$ .

The lattice points themselves correspond to single unit cells and their own potential is described by the N atoms in the unit cell located at positions  $\mathbf{r}_i$ :

$$V_{\text{unit cell}}(\mathbf{r}) = \sum_{i=1}^N V_{\text{atom}_i}(\mathbf{r} - \mathbf{r}_i) \quad (3.11)$$

The full lattice potential of an infinite crystal is an instance of the unit cell potential at each lattice point. This can be written as the convolution<sup>2</sup> of the single unit cell potential with the delta functions potential of the crystal lattice:

$$V_{\text{IC}}(\mathbf{r}) = V_{\text{unit cell}}(\mathbf{r}) \circledast \mathcal{L}(\mathbf{r}) \quad (3.12)$$

By construction,  $\mathcal{V}(\mathbf{r})$  has the periodicity of the underlying Bravais lattice:

$$V_{\text{IC}}(\mathbf{r}) = V_{\text{unit cell}}(\mathbf{r} + \mathbf{t}_{uvw}), \forall \text{ Bravais lattice vectors } \mathbf{t}_{uvw} = u\mathbf{a} + v\mathbf{b} + w\mathbf{c}. \quad (3.13)$$

<sup>2</sup> Convolution with a delta function means “copying” the unit cell potential at the position of the delta function which, here, is every lattice site.

This allows us to conveniently expand the potential as a discrete Fourier series.

$$V(\mathbf{r}) = \sum_{\mathbf{g}} V_{\mathbf{g}} e^{2\pi i \mathbf{g} \cdot \mathbf{r}} \quad (3.14)$$

where  $V_{\mathbf{g}}$  are the Fourier coefficients of the electrostatic lattice potential corresponding to each set of planes  $\mathbf{g}$  in the crystal. In the absence of absorption the potential of the crystal will be a real value. In order to account for loss of electrons from the diffraction signal to inelastic scattering processes a complex optical potential can be introduced.

$$V_c(\mathbf{r}) = V + iW = \sum_{\mathbf{g}} V_{\mathbf{g}} e^{2\pi i \mathbf{g} \cdot \mathbf{r}} + i \sum_{\mathbf{g}} W_{\mathbf{g}} e^{2\pi i \mathbf{g} \cdot \mathbf{r}} \quad (3.15)$$

### 3.7.2 The structure factor

**Numerical computation of the Fourier coefficients of the lattice potential**

**Symmetry**

**systematic absences**

## 3.8 General derivation of the Darwin-Howie-Whelan equations

The time independent Schrödinger equation can be written for an electron wavefunction  $\Psi$  of energy  $eE$  in a periodic crystal potential  $V(\mathbf{r})$  in the form known as the Helmholtz equation as:

$$\Delta\Psi(\mathbf{r}) + \frac{8\pi^2 me}{h^2} [E + V(\mathbf{r})] \Psi(\mathbf{r}) = 0, \quad (3.16)$$

where  $m, e, h$  are the usual constants and  $\Delta$  is the Laplace operator standing for:

$$\Delta\Psi = \frac{\partial^2\Psi}{\partial x^2} + \frac{\partial^2\Psi}{\partial y^2} + \frac{\partial^2\Psi}{\partial z^2}.$$

The meaning of  $\Psi$  is taken here to be that the value  $\Psi\Psi^* d\tau$  is the probability of finding the electron in the volume  $d\tau$ .

The crystal potential  $V(\mathbf{r})$  presents the periodicity of the underlying lattice and can, therefore, be written as a Fourier expansion :

$$V(\mathbf{r}) = \sum_{\mathbf{q}} V_{\mathbf{q}} e^{2\pi i \mathbf{q} \cdot \mathbf{r}}. \quad (3.17)$$

When absorption is taken into account the potential  $V(\mathbf{r})$  will be replaced by a complex value  $V(\mathbf{r}) \rightarrow V(\mathbf{r}) + iV'(\mathbf{r})$  with complex Fourier coefficients.

$$V(\mathbf{r}) + iV'(\mathbf{r}) = \sum_{\mathbf{q}} V_{\mathbf{q}} e^{2\pi i \mathbf{q} \cdot \mathbf{r}} + iV'_{\mathbf{q}} e^{2\pi i \mathbf{q} \cdot \mathbf{r}}. \quad (3.18)$$

It is useful at this point to separate the zero-frequency real component  $V_0$  out of the Fourier series as it represents the crystal's mean inner potential and a constant independent on the diffracting planes. This positive potential accelerates the electrons as they enter the crystal in a phenomenon known as *refraction*<sup>3</sup>.

$$V(\mathbf{r}) + iV'(\mathbf{r}) = V_0 + \sum_{\mathbf{q} \neq 0} V_{\mathbf{q}} e^{2\pi i \mathbf{q} \cdot \mathbf{r}} + i \sum_{\mathbf{q}} V'_{\mathbf{q}} e^{2\pi i \mathbf{q} \cdot \mathbf{r}}. \quad (3.19)$$

We can then write out the wavefunction of the incident electron beam corrected for refraction by the mean inner potential  $V_0$ :

$$\mathbf{K}^2 = K^2 = 2me(E + V_0)/h^2$$

In preparation for the substitution of Eq. 3.19 in Eq. 3.16 the following shorthand notation is also introduced:

$$U(\mathbf{r}) + iU'(\mathbf{r}) = \frac{2me}{h^2} \left\{ \sum_{\mathbf{q} \neq 0} V_{\mathbf{q}} e^{2\pi i \mathbf{q} \cdot \mathbf{r}} + \sum_{\mathbf{q}} V'_{\mathbf{q}} e^{2\pi i \mathbf{q} \cdot \mathbf{r}} \right\}$$

Howie and Whelan [HW61] followed Bethe's approach [Bet28] developed for the Bragg case in a perfect crystal with no absorption and generalised it. The Bragg's law predicts that electrons travelling in direction  $\mathbf{k}_0$  before diffraction will travel in direction  $\mathbf{k}'$  after diffraction, where  $\mathbf{k}' = \mathbf{k}_0 + \mathbf{g}$  for any lattice point  $\mathbf{g}$  on the Ewald sphere. It makes sense, then, to write the total wavefunction of those electrons contributing to diffraction as a superposition of plane waves, one for each direction predicted by Bragg's law and to investigate a solution to the above equation of this form.

$$\Psi(\mathbf{r}) = \sum_{\mathbf{g}} \psi_{\mathbf{g}} e^{2\pi i (\mathbf{k}_0 + \mathbf{g}) \cdot \mathbf{r}}. \quad (3.20)$$

Where  $\psi_{\mathbf{g}}$  is the complex amplitude of the Bragg plane wave  $\mathbf{g}$  and is the unknown to be determined.

Substituting 3.19 and 3.20 in the master equation 3.16:

$$\sum_{\mathbf{g}} \left\{ i(\mathbf{k}_0 + \mathbf{g}) \cdot \nabla \psi_{\mathbf{g}} + \pi [K^2 - (\mathbf{k}_0 + \mathbf{g})^2] \psi_{\mathbf{g}} \right\} e^{2\pi i (\mathbf{k}_0 + \mathbf{g}) \cdot \mathbf{r}} + \pi \sum_{\mathbf{q}} \sum_{\mathbf{g}} U_{\mathbf{q}} \psi_{\mathbf{g}} e^{2\pi i (\mathbf{q} + \mathbf{k}_0 + \mathbf{g}) \cdot \mathbf{r}} = 0$$

---

<sup>3</sup> This is equivalent to the decrease in the speed of light as it enters a medium with a refractive index larger than that of vacuum.

Van Dyck [VD76] has shown that the Laplacian term in Eq. 3.16 is negligible for high energy electrons and we have dropped it here. This is known the *high-energy approximation* and Van Dyck showed that it holds for penetration depths of a few hundred nanometres, depending on the average atomic number of the crystal. Howie and Whelan [HW61] ignore the first derivative as well for the high energy electrons in TEM, but we shall keep it[ ??].

We will assign  $\mathbf{e}_z^{\text{beam}}$  in the electron beam propagation direction, so the wave vector is  $\mathbf{k}_0 = |\mathbf{k}_0| \mathbf{e}_z^{\text{beam}}$ . The amplitude of a Bragg plane wave  $\psi_g$  can only be dependent on  $\mathbf{e}_z^{\text{beam}}$  direction. In the TEM geometry the beam interacts normally with a somewhat perfectly planar thin film. Here the  $z$ -direction of the sample, that which is normal to its surface, coincides with the beam's  $z$ -direction such that the two frames can be used interchangeably. TEM literature [DG03] offers the following simplification:

$$\nabla \psi_g = \frac{d\psi_g}{dz_{\text{sample}}},$$

and, therefore, from the definition of the dot product:

$$(\mathbf{k}_0 + \mathbf{g}) \cdot \nabla \psi_g = |\mathbf{k}_0 + \mathbf{g}| \cos \alpha \frac{d\psi_g}{dz_{\text{sample}}}.$$

For a more general geometry, the coordinate system of the incidence beam needs to be explicitly introduced in order to account for its  $z$ -direction not necessarily coinciding with the sample's  $z$ -direction. Then, for a general incidence angle we can keep the simplification above if we replace  $z_{\text{sample}}$  by  $z_{\text{beam}}$ :

$$\nabla \psi_g = \frac{d\psi_g}{dz_{\text{beam}}}.$$

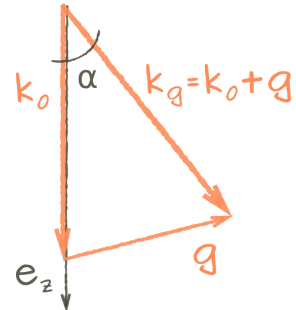


FIGURE 3.6: Diagram of incident and diffracted wave vector geometry.

### 3.9 The two beam case: DHW formalism

### 3.10 Electron channelling modelling

Diffraction of high energy electrons traditionally is taken to imply elastic scattering from the understanding of diffraction in TEM. Defect characterisation in TEM is relatively well established. Both qualitative models such as the kinematical theory [HHW60] which only assumes a single scattering process to occur from the direct beam of electrons into the diffracted one, and more quantitative models – the dynamical theory – which takes into account multiple scatterings between the two beams [HW61] have been developed and broadly applied [HHW60; CH71; SHH72].

However, for thicker samples than the ones valid for the approximations implied in the above theories, inelastic scattering of electrons also becomes important. This has a twofold implication. On one hand, electrons are “absorbed” from the diffracted beam(s) through inelastic scattering, and this loss must be accounted for. On the other hand, these inelastically scattered electrons are also responsible for some of the features in the patterns observed in the SEM. If we are to study these features, we require a separate dynamical formulation of the inelastic interactions. If we are interested in a quantitative description of defect contrast for different beam orientations as observed in the ECCI (or over many outgoing beams as in EBSD), we ought to couple the dynamical descriptions of the two electron scattering mechanisms. This has previously been achieved by matching the dynamical theory solution, which accounts for elastic effects, at the entrance surface of the crystal to a multiple scattering theory, developed to account for the inelastic processes, at greater depths inside the crystal[BCH73; How+78].

The dynamical theory solves the Schrödinger equation for the high energy electrons inside a crystal. The electrons see the perfect crystal as a periodic potential and their wavefunction is perturbed in such a way that if we consider a forward scattered electron wavefunction and a backwards scattered one, the amplitude will be dynamically transferred between these two waves as they travel through the crystal in a manner similar to the transfer of energy in the coupled pendulum oscillations. Figure 3.7 shows exactly this periodic variation in the direct wave intensity (bright field) with depth in crystal by plotting the measured intensity of the transmitted beam along the bottom of wedge crystal. These thickness fringes are a direct result of the fact that the direct and diffracted electron wave intensities oscillate with depth in the crystal.

Two equivalent quantum mechanical descriptions of the electron wavefunction behaviour inside a crystal are given below:

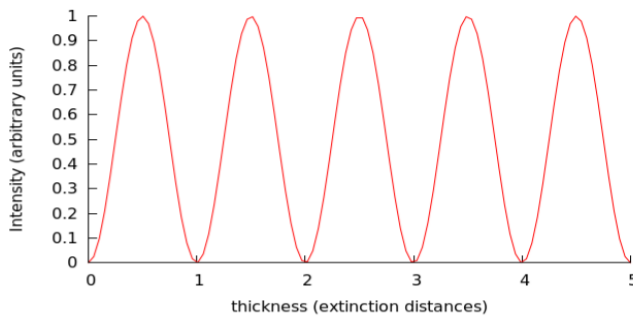


FIGURE 3.7: Dynamical profile of thickness fringes as seen in transmission mode with absorption ignored from a wedge crystal. Profile is calculated in bright field condition [Hir+65].

- First, we can treat electrons as optical waves (or beams)  $\{\Phi(\mathbf{g})\}$ <sup>4</sup> where we consider the incident wave of complex amplitude  $\phi_0(z)$  and at least one diffracted beam of complex amplitude  $\phi_g(z)$  both of which vary with depth  $z$  into the crystal. We usually set the boundary conditions of  $\phi_0 = 1$  and  $\phi_g = 0$  at the entry surface of the crystal. If the crystal is thin enough we can ignore scattering from the diffracted beam back into the incident one, but if the crystal is thicker we must link together the amplitudes  $\phi_0$  and  $\phi_g$  through a coupled differential equation of the form [HW61]:

$$\frac{d\phi_0}{dz} = \frac{\pi i}{\xi_0} \phi_0 + \frac{\pi i}{\xi_g} \phi_g \exp(2\pi i s z) \frac{d\phi_g}{dz} = \frac{\pi i}{\xi_0} \phi_g + \frac{\pi i}{\xi_g} \phi_0 \exp(-2\pi i s z) \quad (3.21)$$

where  $\xi$  is an important parameter known as the “extinction distance” which measures the physical distance over which the beam amplitude is scattered back and forth between the beams and  $s$  measures the deviation from exact Bragg diffraction<sup>5</sup>.

The equations above are valid for a perfect crystal and also ignores any absorption due to inelastic scattering. However, they can easily be generalised to account for imperfections by adding a vector  $\mathbf{R}(\mathbf{r})$  which measures the deviation from a perfect lattice. The theoretical profile in Figure 3.7 is not something we would observe in the real microscope where the effect of absorption is important. In reality, the oscillations would also die out with the thickness of the crystal as more and more electrons are removed from the diffracting beam. Nevertheless, we can phenomenologically account for this effect as well. Using an idea

<sup>4</sup> $\mathbf{g}$  is the usual reciprocal lattice vector.

<sup>5</sup>In reciprocal space the exact Bragg condition requires the lattice points to lie on the Ewald sphere.

borrowed from x-ray diffraction, namely that adding an imaginary part to the electrostatic lattice potential has essentially the same effect as accounting for the electrons lost to inelastic scattering.

2. The second description of the electron wavefunction has to do with the periodicity of the crystal potential. It seems straightforward to take advantage of this periodicity in writing out the description of the electron's wave. In this description the steady state solutions of the wavefunction of the electron inside a periodic potential of the crystal are known as Bloch waves  $\{\psi(\mathbf{r})\}$ . The electron wavefunction inside the crystal obeys the non-relativistic Schrödinger's equation<sup>6</sup>:

$$\frac{-\hbar^2}{2m} \nabla^2 \psi(\mathbf{r}) + [E + V(\mathbf{r})] \psi(\mathbf{r}) = 0 \quad (3.22)$$

where the kinetic energy of the electron is related to the wave vector in the usual manner:  $E_{kin} = \hbar^2 k^2 / 2m_e$  and  $V(\mathbf{r})$  has the periodicity of the crystal lattice (i.e.  $V(\mathbf{r}) = V(\mathbf{r} + \mathbf{a})$  where  $\mathbf{a}$  is any lattice vector). The solution of this equation in the form of Bloch waves of wave vector  $\mathbf{k}$  is of the form:

$$\psi(\mathbf{r})^{(i)} = \sum_g C_g^{(i)}(\mathbf{k}^{(i)}) \exp\left(2\pi i(\mathbf{k}^{(i)} + \mathbf{g}) \cdot \mathbf{r}\right) \quad (3.23)$$

where  $C_g(\mathbf{k})$  denotes the wave amplitude of the Bloch wave of wave vector  $\mathbf{k}$ .

The minimum number of Bloch waves we can choose is also two. The first Bloch wave is defined such that its maxima are at interstices, while the second Bloch wave's maxima occur on atom columns. We can also offer a more intuitive picture of the anomalous absorption in this frame since it is to be expected that the electrons from the second Bloch waves, that spend more time near the atomic nuclei will be more readily scattered than the ones contained in the first Bloch wave.

The two descriptions above are equivalent [Hir+65], such that we can write, after some manipulation:

$$\phi_0(\mathbf{r}) = C_0^{(1)} \psi^{(1)}(\mathbf{r}) + C_0^{(2)} \psi^{(2)}(\mathbf{r}) \phi_g(\mathbf{r}) = C_g^{(1)} \psi^{(1)}(\mathbf{r}) \exp(i\mathbf{g} \cdot \mathbf{r}) + C_g^{(2)} \psi^{(2)}(\mathbf{r}) \exp(i\mathbf{g} \cdot \mathbf{r}) \quad (3.24)$$

---

<sup>6</sup>For an electron beam under an accelerating voltage of 30 kV we can calculate the speed of the electrons to be  $\sim (0.1 \times \text{speed of light})$ , far outside any important relativistic effects.

with the boundary conditions:

$$\phi_0(0) = \sum_{i=1,2} \phi^{(i)} C_0^{(i)} = 1 \quad \phi_g(0) = \sum_{i=1,2} \phi^{(i)} C_g^{(i)} = 0 \quad (3.25)$$

In the case of crystal subject to a deformation that moves an atom from the point  $\mathbf{r}$  to a point  $\mathbf{r} + \mathbf{R}(\mathbf{r})$  the potential of the crystal changes by a factor  $\{\exp(-2\pi i \mathbf{g} \cdot \mathbf{R}(\mathbf{r}))\}$ . The derivation of the displacement field  $\mathbf{R}(\mathbf{r})$  is the subject of the Section ??.

So far we have discussed diffraction, but as previously mentioned, if we are interested in backscattered electrons we must also consider the behaviour of the inelastically scattered electrons. Approaches including multiple inelastic scattering calculated out of transport type equations[SHH72; SH80] have been incorporated into diffraction theories in order to produce a more quantitative description of the backscattered electrons intensities. This type of approach has then been implemented in order to predict contrast profiles for dislocation lines running parallel to the crystal surface (i.e. misfit type dislocations) for both screw [SHH72] and edge dislocations [WH95]. However, no attempts had been made so far to apply this approach to threading dislocation and more importantly to threading dislocations reaching the surface.



# Bibliography

- [Ard38] M. von Ardenne. "The Electron Scanning Microscope". In: *Journal of Physics* 109.9-10 (1938), pp. 553–572.
- [Aut06] A. Authier. "Dynamical theory of X-ray diffraction". In: *International Tables for Crystallography Volume B: Reciprocal space*. Springer, 2006, pp. 534–551.
- [BB13] W. H. Bragg and B.A. WL. Bragg. "The reflection of X-rays by crystals". In: *Proceedings of the Royal Society of London A* 88.605 (1913), pp. 428–438.
- [BCH73] M. Baines, D. R. Clarke, and A. Howie. "Backscattered images of dislocations and crystal defects". In: *Scanning Electron Microscopy Systems and Applications* 18 (1973).
- [Bet28] H. Bethe. "Theory on the diffraction of electrons in crystals". In: *Annalen der Physik* 392.17 (1928), pp. 55–129.
- [Boo+67] G. R. Booker et al. "Some comments on the interpretation of the 'kikuchi-like reflection patterns' observed by scanning electron microscopy". In: *Philosophical magazine* 16.144 (1967), pp. 1185–1191.
- [Bra68] Werner Brandt. "Channeling in crystals". In: *Scientific American* 218.3 (1968), pp. 90–101.
- [Bri+16] T. B. Britton et al. "Tutorial: Crystal orientations and EBSD—Or which way is up?" In: *Materials Characterization* 117 (2016), pp. 113–126.
- [Bun82] H. J. Bunge. *Texture analysis in materials science: mathematical methods*. Butterworths, 1982.
- [CH71] D. R. Clarke and A. Howie. "Calculations of lattice defect images for scanning electron microscopy". In: *Philosophical Magazine* 24.190 (1971).
- [Coa67] D. G. Coates. "Kikuchi-like reflection patterns obtained with the scanning electron microscope". In: *Philosophical magazine* 16.144 (1967), pp. 1179–1184.

- [Cow+06] J. M. Cowley et al. "Electron diffraction and electron microscopy in structure determination". In: *International Tables for Crystallography Volume B: Reciprocal space*. Springer, 2006, pp. 276–345.
- [Dar14] C. G. Darwin. "The theory of X-ray reflexion". In: *The London, Edinburgh, and Dublin Philosophical Magazine and Journal of Science* 27.158 (1914), pp. 315–333.
- [Dar22] C. G. Darwin. "XCII. The reflexion of X-rays from imperfect crystals". In: *The London, Edinburgh, and Dublin Philosophical Magazine and Journal of Science* 43.257 (1922), pp. 800–829.
- [Dav73] P. B. Davenport. "Rotation about nonorthogonal axes". In: *American institute of Aeronautics and Astronautics* 11.6 (1973).
- [Dav83] J.A. Davies. "The channeling phenomenon-and some of its applications". In: *Physica Scripta* 28.3 (1983), p. 294.
- [Dea+68] G. Dearnaley et al. "Proton channelling through thin crystals". In: *Philosophical Magazine* 18.155 (1968), pp. 985–1016.
- [Den17] D. C. Dennett. *From bacteria to Bach and back: The evolution of minds*. WW Norton & Company, 2017.
- [DG03] M. De Graef. *Introduction to transmission electron microscopy*. Cambridge university Press, New York, 2003.
- [DG08] M. De Graef. *Teaching crystallographic and magnetic point group symmetry using three-dimensional rendered visualizations*. International Union of Crystallography. <https://www.iucr.org/education/pamphlets/23/full-text>. 2008.
- [DG13] M. De Graef. *EMsoft*. <https://github.com/marcdegraef/EMsoft>. Carnegie Mellon University, 2013-2017.
- [DG14] M. De Graef. *3Drotations*. <https://github.com/marcdegraef/3Drotations>. Carnegie Mellon University, 2014-2017.
- [DG27] C. Davisson and L. H. Germer. "Diffraction of electrons by a crystal of nickel". In: *Physical review* 30.6 (1927), p. 705.
- [DG98] M. De Graef. "A novel way to represent the 32 crystallographic point groups". In: *J. Matter: Educ* 20 (1998).
- [DGM12] M. De Graef and M. E. McHenry. *Structure of Materials; an introduction to crystallography, diffraction and symmetry*. second. Cambridge University Press, 2012.

- [DT68] P. A. Doyle and P. S. Turner. "Relativistic Hartree-Fock X-ray and electron scattering factors". In: *Acta Crystallographica* 24 (1968).
- [Ewa17] P. P. Ewald. "Zur begründung der kristalloptik". In: *Annalen der Physik* 359.23 (1917), pp. 519–556.
- [FKL12] W. Friedrich, P. Knipping, and M. V. Laue. "Interference phenomena with Röntgen rays". In: *Sitzber. Math-phys. Kl. bayer. Akad. Wiss. Manche* 22 (1912), p. 303.
- [Fra65] F. C. Frank. "On Miller-Bravais Indices and four-dimensional Vectors". In: *Acta Crystallographica* 18.862 (1965).
- [GP99] H. X. Gao and L. M. Peng. "Parametrization of the temperature dependence of the Debye-Waller factor". In: *Acta Crystallographica* A.55 (1999).
- [Hah96] T. Hahn. *International tables for crystallography: Brief teaching edition of volume A, Space-group symmetry*. Vol. 1. Kluwer Academic Pub, 1996.
- [HHW60] P. B. Hirsch, A. Howie, and M. J. Whelan. "A kinematical theory of diffraction contrast of electrons transmission microscope images of dislocations and other defects". In: *Philosophical Transactions A* 252 (1960).
- [Hir+65] P. B. Hirsch et al. *Electron microscopy of thin crystals*. London Butterworths, 1965.
- [How+78] A. Howie et al. "Electron Diffraction (1927–1977)". In: *Eds., P. J. Dobson, J. B. Pendry and C. J. Humphreys. IOP Conf. Series*. Vol. 41. 1978.
- [HW61] A. Howie and M. J. Whelan. "Diffraction contrast of electron microscope images of crystal lattice defects - II. The development of a dynamical theory". In: *Proceedings of Royal Society of London A*. Vol. 263. 1961.
- [KG12] R. R. Keller and R. H. Geiss. "Transmission EBSD from 10 nm domains in a scanning electron microscope". In: *Journal of Microscopy* 245.3 (2012), pp. 245–251.
- [KR32] M. Knoll and E. Ruska. "Das elektronenmikroskop". In: *Zeitschrift für Physik* 78.5-6 (1932), pp. 318–339.
- [Lau31] M. von Laue. "Die dynamische Theorie der Röntgenstrahlinterferenzen in neuer Form". In: *Ergebnisse der exakten naturwissenschaften*. Springer, 1931, pp. 133–158.
- [Lin65] J. Lindhard. "Influence of Crystal Lattice on Motion of energetic charged particle". In: *Kgl. Danske Vidensk. Selskab. Mat. Fys. Medd* 34.14 (1965).

- [Miu+18] E. Miu et al. "Innovation and cumulative culture through tweaks and leaps in online programming contests". In: *Nature Communications* 9.2321 (2018).
- [Nic66] J. F. Nicholas. "The simplicity of Miller-Bravais indexing". In: *Acta Crystallographica* 21.880 (1966).
- [NK28] S. Nishikawa and S. Kikuchi. "Diffraction of cathode rays by calcite". In: *Nature* 122.3080 (1928), p. 726.
- [Nol07] Gert Nolze. "Image distortions in SEM and their influences on EBSD measurements". In: *Ultramicroscopy* 107.2-3 (2007), pp. 172–183.
- [OT68] P.R. Okamoto and G Thomas. "On the Four-Axis Hexagonal Reciprocal Lattice and its use in Indexing of Transmission Electron Diffraction Patterns". In: *phys. stat. sol.* 25 (1968).
- [Pas15] E. Pascal. *SEM-diffraction*. <https://github.com/elenapascal/SEM-diffraction>. University of Strathclyde, 2015-2018.
- [Pie+63] G. R. Piercy et al. "Experimental evidence for the increase of heavy ion ranges by channeling in crystalline structure". In: *Physical Review Letters* 10.9 (1963), p. 399.
- [Pri30] J.A. Prins. "Die Reflexion von Röntgenstrahlen an absorbierenden idealen Kristallen". In: *Zeitschrift für Physik* 63.7-8 (1930), pp. 477–493.
- [Row+15] D. Rowenhorst et al. "Tutorial: Consistent representations of and conversions between 3D rotations". In: *Modelling and Simulation in Materials Science and Engineering* 23.8 (2015), p. 083501.
- [Sch+09] M. Schowalter et al. "Temperature-dependent Debye-Waller factors for semiconductors with wurtzite-type structure". In: *Acta Crystallographica* A.65 (2009).
- [SH80] J. P. Spencer and C. J. Humphreys. "A multiple scattering transport theory for electron". In: *Philosophical Magazine A* 42.4 (1980).
- [SHH72] J. P. Spencer, C. J. Humphreys, and P. B. Hirsch. "A dynamical theory for the contrast of perfect and imperfect crystals in the scanning electron microscope using backscattered electrons". In: *Philosophical Magazine* 26.1 (1972).
- [TR27] G. P. Thomson and A. Reid. "Diffraction of cathode rays by a thin film". In: *Nature* 119.3007 (1927), p. 890.

- [Tri12] P. W. Trimby. "Orientation mapping of nanostructured materials using transmission Kikuchi diffraction in the scanning electron microscope". In: *Ultramicroscopy* 120 (2012), pp. 16–24.
- [VD76] D. Van Dyck. "The importance of backscattering in high-energy electron diffraction calculations". In: *physica status solidi (b)* 77.1 (1976), pp. 301–308.
- [VH73] J. A. Venables and C. J. Harland. "Electron back-scattering patterns—A new technique for obtaining crystallographic information in the scanning electron microscope". In: *Philosophical Magazine* 27.5 (1973), pp. 1193–1200.
- [WH95] A. J. Wilkinson and P. B. Hirsch. "The effects of surface stress relaxation on electron channelling contrast images of dislocations". In: *Philosophical Magazine A* 72.1 (1995).